William R. Wiley
EMSL
Environmental Molecular Sciences Laboratory

Annual Report 1997

Chemical Structure and Dynamics

March 1998

Pacific Northwest National Laboratory
Operated by Battelle for the U.S. Department of Energy

DISCLAIMER

PACIFIC NORTHWEST LABORATORY
operated by
BATTELLE MEMORIAL INSTITUTE
for the
UNITED STATES DEPARTMENT OF ENERGY
under Contract DE-AC06-76RLO 1830

PNNL--11863

PNL-11863
UC-400

Annual Report 1997
Chemical Structure and Dynamics

Steven D. Colson, Associate Director
Robin S. McDowell, Program Manager
and the Staff of the Chemical Structure and Dynamics Program

March 1998

Prepared for the U.S. Department of Energy under Contract DE-AC06-76RLO 1830

Pacific Northwest National Laboratory
Operated by Battelle for the U.S. Department of Energy

DISCLAIMER

Contents

4. Cluster Models of the Condensed Phase

5. Miscellaneous

6. Appendix

Funding Support

[a]DOE Office of Basic Energy Sciences, Chemical Sciences Division, Fundamental Interactions Branch.
[b]Instrument development under the Environmental Molecular Sciences Laboratory (EMSL) Project.
[c]Pacific Northwest National Laboratory (PNNL) Laboratory Directed Research and Development (LDRD).
[d]DOE Environmental Management Science Program (EMSP).
[e]DOE Office of Basic Energy Sciences, Material Sciences Division.
[f]National Science Foundation.
[g]Strategic Environmental Research and Development Program (SERDP).
[h]Cooperative Research and Development Agreement (CRADA).
[i]Medical Technology Initiative.
[j]DOE Office of Nonproliferation and National Security.
[k]DOE Office of Biological and Environmental Research under the Atmospheric Radiation Measurement (ARM) Program.

1. Introduction

Purpose

The Chemical Structure and Dynamics (CS&D) program is a major component of the William R. Wiley Environmental Molecular Sciences Laboratory (EMSL), developed by Pacific Northwest National Laboratory (PNNL) to provide a state-of-the-art collaborative facility for studies of chemical structure and dynamics. We respond to the need for a fundamental, molecular-level understanding of chemistry at a wide variety of environmentally important interfaces by (1) extending the experimental characterization and theoretical description of chemical reactions to encompass the effects of condensed media and interfaces; (2) developing a multidisciplinary capability for describing interfacial chemical processes within which the new knowledge generated can be brought to bear on complex phenomena in environmental chemistry and in nuclear waste processing and storage; and (3) developing state-of-the-art analytical methods for characterizing complex materials of the types found in stored wastes and contaminated soils, and for detecting and monitoring trace atmospheric species.

This research effort was initiated in 1989 as a program of rigorous studies of fundamental molecular processes in model systems, such as well-characterized surfaces, single-component solutions, clusters, and biological molecules; and studies of complex systems found in the environment (multispecies, multiphase solutions; solid/liquid, liquid/liquid, and gas/surface interfaces; colloidal dispersions; ultrafine aerosols; and functioning biological systems).

Our program aims at achieving a quantitative understanding of chemical reactions at interfaces and, more generally, in condensed media, comparable to that currently available for gas-phase reactions. This understanding will form the basis for the development of *a priori* theories for predicting macroscopic chemical behavior in condensed and heterogeneous media, which will add significantly to the value of field-scale environmental models, predictions of short- and long-term nuclear waste storage stabilities, and other areas related to the primary missions of the U.S. Department of Energy (DOE).

The CS&D group has particular expertise in the preparation and spectroscopic analysis of molecular clusters (S. D. Colson, D. Ray, S. W. Sharpe, and L. S. Wang); ultrafast and nonlinear optical spectroscopies (D. Ray, G. R. Holtom, and X. Xie); ultrahigh resolution spectroscopy for measurements of electronic and geometric structures and dynamics (S. W. Sharpe and R. S. McDowell); surface and interface structure, chemical reaction dynamics, and kinetics (J. P. Cowin, W. P. Hess, S. A. Joyce, B. D. Kay, and T. M. Orlando); ion-molecule traps and storage technology (S. E. Barlow); and specialized chambers and instruments for chemical reactivity and analysis of atmospheric aerosols (S. E. Barlow and R. S. Disselkamp).

Environmental Problems

Pollution prevention and remediation and restoration of contaminated environments present major scientific challenges because they require information about the relevant chemistry and physics at many scales: from spatial scales of meters to kilometers and temporal scales of days to hundreds of years that are important in the field, to distances of 10^{-10} meters and times on the order of 10^{-12} seconds that are important for processes at the molecular level. Developing the knowledge base needed to address the environmental restoration issues of the DOE, as well as aiding industry in minimizing its environmental impact, requires understanding of the problems at the field scale, identification of the important processes at macroscopic scales, and more detailed insight into mechanisms at microscopic scales (from grain to colloid size) and molecular scales. Our research is focused on the molecular scale in order to develop a fundamental understanding of molecules and their interactions in isolation and in liquids, on surfaces, and at interfaces (condensed media).

The focus of our research is defined primarily by DOE's environmental problems: fate and transport of contaminants in the subsurface environment, processing and storage of waste materials, cellular effects of chemical and radiological insult, and atmospheric chemistry as it relates to air quality and global change. The CS&D program is part of a broader response by EMSL staff and programs to the following problem areas:

Fate and Transport of Contaminants in the Subsurface Environment. Past practices of DOE have resulted in the discharge of chemical and radioactive materials into the environment at many DOE sites, which has resulted in extensive contamination of soils and groundwater. The use of conventional technology to remediate the unique mix of chemical and radioactive wastes at the DOE sites are cost prohibitive, and new technologies are sought to reduce the expense of remediation.

The development of improved technologies for remediating subsurface contamination requires an understanding of the factors that control how fast the contaminants move (mass transport) and their fate (degradation or reaction). At the macroscopic level, hydrologic processes (e.g., fluid flow through porous media) and geologic processes (e.g., sorption on soil particles) play important roles. At this scale, soil composition and heterogeneity have a profound influence on contaminant fate and transport. At the microscopic level it is important to know the speciation of contaminants, that is, the chemical form of the contaminant (e.g., the oxidation state of a metal and whether it is complexed, or whether a contaminant is adsorbed to a surface or not), the mechanisms for changing between different species (adsorption/desorption, redox chemistry, etc.), and the influence of colloidal particles on transport and transformation. Molecular-level studies can provide fundamental understanding and critical information about microscopic mechanisms and macroscopic processes. For example, molecular approaches can provide equilibrium constants, reaction rate coefficients, and transport coefficients that determine the partitioning of contaminants between different phases, their speciation, and the microscopic rates at which equilibrium is attained.

Processing and Storage of Waste Materials. Fifty years of production of defense-related nuclear materials has generated large volumes (hundreds of millions of gallons) of complex wastes that contain large amounts of radioactive materials as well as hazardous chemical wastes. The processing of these mixed wastes is one of the most difficult technical challenges faced by the DOE. Processing tank wastes will require retrieval of the wastes from the underground storage tanks; physical separation of liquids from solids and further processing of solids to remove liquids and soluble compounds; and development of chemical processes to separate specific radionuclides and chemicals from the waste streams as well as to destroy organic compounds. Separations of radionuclides is important to minimize the volume of highly radioactive wastes that will require costly handling and storage. It is also necessary to remove species that may inhibit the formation of a durable waste form or may generate toxic, difficult-to-handle off-gases (e.g., sulfates, halogens, NO_x, and volatile metals such as Cs, Pb, Hg, Rb, Bi, Cd, Ag, and As). Molecular-level studies will provide fundamental information about the factors that control the binding of ionic species (e.g., metal cations, metal-oxide anions, etc.) to sequestering agents. This fundamental information will provide the basis for the design of new agents and new processes for selective and efficient separations.

The long-term storage of much of the tank waste will require converting it to a durable solid form. The waste form must be able to dissolve substantial quantities of wastes without significant loss of durability; it must immobilize hazardous materials for hundreds to thousands of years and be resistant to leaching by water. Most disposal options for the tank wastes use glass as the final waste form. There are still unanswered questions about the best formulation of the glass to meet these requirements. The high variability of the composition of the tank wastes provides a major challenge, since one formulation may not work for all waste streams, although that is the current baseline assumption. Fundamental understanding of the mechanisms of network forming in amorphous materials and of glass dissolution will provide the basis for design of new glass formulations with desired properties. Molecular-level knowledge of the binding of contaminant species in glass, and the polymerization and depolymerization reactions important in glass melts and in the dissolution mechanism will provide insight into the chemistry of these systems that will improve our understanding of the microscopic mechanisms responsible for phenomena such as phase separation, enhanced dissolution with ionic aqueous solutions, etc.

Cellular Effects of Chemical and Radiological Insult. Development of science-based human and environmental health guidelines requires a comprehensive understanding of the response of human cells to insults from radioactive and toxic chemi-

cals. There is thus a critical need for fundamental data on health effects as an integral component of managing waste cleanup activities. In the past, animal and tissue studies furnished the primary basis for understanding the adverse health effects of toxic materials and for establishing regulatory guidelines. A new generation of risk assessment will require a fundamental understanding of crucial cellular mechanisms and processes at the molecular level to provide a more accurate evaluation of risk and the establishment of genuinely protective statutes and standards. This mechanistic extension is required for both accurate extrapolations at high dose levels in animal studies and the low exposure/dose levels needed to set regulatory guidelines for humans. The EMSL focus in this effort is to provide the structural basis at the molecular and cellular level for the mechanisms. To address these problems we have initiated research in cellular processes involved in genomic protection, cellular response to chemical insults, and mechanistic investigations for the basis of bioremediation. The specific research areas include: The Structural Basis for DNA Damage Recognition; Functional Micro-Spectroscopy of Live Single Mammalian Cells; and Structural and Mechanistic Investigations of Proteins Involved in Bioremediation.

The critical research tools, many of which are unique to the EMSL, are high-field liquid and solid state NMR, EPR, high field Fourier-transform ion cyclotron resonance mass spectrometry, laser spectroscopy, novel microscopies, and advanced computational capabilities.

Atmospheric Chemistry. Understanding tropospheric chemistry is key to DOE's response to national concerns about global change and the effects of energy production and use on air quality. Major public concerns include tropospheric ozone levels, decreased visibility due to haze, health effects due to inhalation of particulate matter and oxidants, and climate change (global warming) due to modification of the radiative properties of the atmosphere. The development of emissions standards and rational control strategies requires a detailed knowledge of the physical and chemical processes at work in the atmosphere. The earth's atmosphere is complex, consisting of a multiphase mixture of gases, liquid cloud and precipitation droplets, solid ice crystals, and liquid and solid aerosols. Even though gas-phase processes in the atmosphere have been extensively studied, a number of significant unanswered questions remain. For example, the mechanisms of oxidant formation in the troposphere remain uncertain and the tropospheric chemistry of naturally occurring (e.g. terpenes) and anthropogenic organics are poorly understood. The role of heterogeneous atmospheric processes are even more poorly understood; for example, heterogeneous processes are now known to play an important role in acid rain formation and Antarctic ozone depletion, but they are not understood quantitatively, and the role of heterogeneous processes on oxidant and aerosol formation in the troposphere is even less well understood. The lack of a fundamental molecular-level understanding of important atmospheric processes greatly limits our ability to model the impacts of emissions on atmospheric chemistry, air pollution, and global change and to design effective control strategies that have minimal impact on human activities.

The EMSL program in atmospheric sciences focuses on the molecular chemistry of tropospheric oxidants and aerosols, research areas with significant impact on all of the major atmospheric quality factors. The research approach has strong, integrated efforts in both experimental and computational chemistry. Important research areas include condensed-phase chemistry, gas-phase–aerosol interactions, and gas-phase chemistry.

Although the primary focus of the research program is on understanding the role of emissions on tropospheric chemistry, the fundamental knowledge gained from this research will have an impact on problems such as ozone depletion in the stratosphere, halohydrocarbon effects on tropospheric and stratospheric chemistry, and on other atmospheric issues related to economic and human health.

Problem Selection for Impact on Environmental Needs

Care must be taken in the selection of the systems to be studied and the types of information that need to be obtained in designing a fundamental science program which is expected to impact specific applications. It is generally not sufficient just

to do the correct *type* of fundamental science research (e.g., surface chemistry, interfacial chemistry, development of sensitive spectroscopies, etc.), but the data and understanding themselves must be responsive to specific environmental needs. Thus, we use a combination of several approaches to making these selections.

Multidisciplinary Collaborations: Establishing collaborations with those working more directly on environmental problems is one of the most direct ways to select the most impactful research projects. An example is Thom Orlando's research aimed at providing the DOE with information needed to move old fuel rods from a water storage basin to dry storage. There is a concern about the radiolytic generation of gases (hydrogen and oxygen) from residual water. This collaboration helped focus our DOE work on radiochemistry mechanisms and yields for water on oxidized surfaces. There are numerous similar examples.

Materials Chemistry Selection: Often it can be established that particular chemical process in or on particular materials are of broad importance. Most environmental materials are found in an oxidized form. Hence, the emphasis on the structure and chemistry of oxide materials, particularly when in contact with water. Furthermore, the emphasis must be on naturally occurring oxides (minerals or models of minerals such as silicon, aluminum, and iron oxides) or materials important to energy-related environmental problems (e.g., ZrO cladding of fuel rods). This understanding leads to the design of the solid/liquid and gas/solid interfacial chemistry components of our Program.

Chemical Processes Selection: In some cases, the types of chemical processes that are important to addressing environmental needs have not been addressed in the past with sufficient accuracy and detail, or for the correct systems. For example, the design of separations agents for removal of radioactive elements from complex solutions demands a simultaneous understanding of the kinetics and energetics of solvation, complexation, and transport between different fluids for specific elements with specific ligands in specific fluids. The treatment of similar processes with idealized species in simple (atomic) fluids is generally inadequate. This analysis led to the selection of the chemical processes and systems for study in our work on molecular process in liquids and on liquid interfacial chemistry and dynamics.

Capabilities Development: One reason for the current lack of important information is that the demands derived from environmental needs often exceed the present state-of-the-art. The level of theoretical precision for treating complex systems must be advanced. The theoretical approach for treating new materials must be evaluated, requiring benchmarking calculations and experimental data. The existing tools for physical and chemical characterization of materials have been developed around the study of conducting, not insulating oxide, materials. Examples such as these have led to our work on model systems (e.g., clusters) and on methods development which provides the underpinning for the remainder of the DOE program. As an important added advantage, the methods development work enables the broader scientific community to join with the EMSL scientists in addressing DOE's environmental problems by using or building upon these new methods and capabilities.

Principal Research Areas

Molecular Processes in Clusters and Liquids. Research in this area is aimed at providing a molecular-level understanding of solvation and reactions in simple and complex fluids as they relate to remediation of complex wastes and contaminated soils and ground water. A common element in these environmental problem areas is the need to understand molecular processes in aqueous solutions. Model systems, such as molecular clusters and solid amorphous water, provide an opportunity for detailed studies of solvation and the effects of solvation on chemical reactivity, and can provide information about intermolecular interactions that lay the foundation for accurate modeling of solution processes. Studies in this area provide detailed information about the factors controlling the rates of reactions in solution that are important for the fate of contaminants in aqueous environments, and information about the factors influencing the selectivity of ligands for specific ions that is important in developing separations agents for use in waste processing.

Liquid Interfacial Chemistry and Dynamics. Another common element in the environmental problem

areas is the need to understand molecular processes at the interface between aqueous solutions and different organic solutions. Some separation processes for tank waste materials use organic liquids to extract species from the aqueous waste solutions. The efficiency of separation process in binary liquids can be significantly influenced by molecular processes occurring at the liquid–liquid interface, such as the interface activity of the separation agent. Molecular processes occurring at liquid–liquid interfaces can also play important roles in the transport of contaminants from organic solvents (such as chlorinated hydrocarbons) into groundwater. This is a newer element of our program and is driven by the need to develop fundamental molecular information that will improve waste separations processes and provide knowledge about the partitioning of waste species in different organic and aqueous phases in soils contaminated with organic liquids.

Solid/Liquid and Gas/Solid Interfacial Processes. It is also crucial to understand molecular processes at the interface between aqueous solutions and environmentally important materials, such as aerosols, minerals, and glasses, as these are central to addressing fundamental science needs related to contaminant fate and transport and waste immobilization. The adsorption of contaminants on and incorporation in minerals in the soil can affect the transport of contaminants in the subsurface environment. Mineral interfaces can also enhance reactivity (e.g., environmental catalysis), leading to the degradation or transformation of contaminants. A knowledge of molecular processes at solid/liquid interfaces is also important for understanding the stability of glasses proposed for encapsulating high-level radioactive wastes. Over the long half-lives of the radionuclides, nuclear waste glasses that come into contact with water can dissolve, resulting in release of radioactive material into the environment.

Energetic Processes in Condensed Phases. This research area focuses on obtaining a mechanistic understanding of chemical transformations of molecules and materials, be they driven by thermal, radioactive, or optical sources. Energetic processes are important in the degradation of nuclear waste glasses from radiolytic decay, and can drive chemistry occurring in solid and liquid phases of tank wasters. The use of laser techniques for the characterization of waste materials relies on an understanding of molecular processes driven by optical sources.

Aerosol Photochemistry. Understanding the processes that control the loading, geographical distribution, and chemical and physical properties of anthropogenic atmospheric aerosols is a basic problem of atmospheric chemistry and is central to key environmental issues affecting the nation's energy economy. There is an emphasis in EMSL on molecular processes in the gas phase and at gas/liquid and gas/solid interfaces (droplets and aerosols). Our instrumentation and computational capability have also been developed to support investigations of gas-phase and interfacial processes, which are known to provide unique computational and experimental challenges. Examples of techniques that have been developed for these purposes include interfacial second harmonic generation, an analytical method in which the entire signal arises from interfacial molecules, providing information on the thermodynamic driving forces that determine the rates of transport of gas phase atmospheric species into aqueous solutions representing rain drops or heavily hydrated aerosols; and development of a novel free-jet reactor, which can quantitatively measure gaseous products resulting from aerosol surface reactions over a wide range of temperatures and pressures. Apparatus is also being developed to obtain IR absorption spectra and mass spectra of gaseous species resulting from the reactions of atmospheric gases with selected solids and solutions, which will allow measurements of the rates and products of interfacial reactions of atmospheric gases as a function of the composition and phase of the substrate material. A temperature-controlled aerosol chamber will also be installed in which these same reactions can be studied on aerosol particles themselves. The advantage of this combined approach is that the composition and phase of the model solids and solutions can be controlled with greater precision than can the properties of aerosol particles, providing a sound basis for the interpretation of the direct aerosol reaction studies.

Molecular-Level Studies of Biological Systems. Recent advances in fluorescence microscopy, including those made at PNNL, have made it possible not only to detect single molecules at room temperature, but also to conduct spectroscopic measurement and monitor dynamical processes on single

molecules. Recently we have also demonstrated fluorescence imaging of single molecules by two-photon excitation with a femtosecond Ti:sapphire laser, which has the advantages that the excitation volume is small, the penetration is deep, and photodamage can be reduced for biological samples. This offers the opportunity of viewing chemical reactions in a living cell in real time. Recently, the crystal structures of many membrane proteins, such as light-harvesting proteins and reaction-center proteins, have been solved. In contrast, our knowledge of how these proteins are assembled in the membrane is extremely limited. The formation of the photosynthetic membrane during cell growth has never been directly monitored on a single-cell basis, and the mechanism for formation of other membrane proteins is also unknown. The advantage of photosynthetic proteins is that they have naturally fluorescent chromophores with distinct spectroscopic identities that can be followed by optical measurements. Previous spectroscopic measurements of photosynthetic bacterial growth have been done on large ensembles of cells. These averaged results often preclude detailed information due to cell heterogeneity. Single-cell measurements are likely to produce new information otherwise hidden, and will open up many exciting possibilities for probing cellular processes.

Capabilities Development. This area of research is an enabling activity required to keep the experimental programs working effectively at the state of the science.

1997

This was a significant year for CS&D: beginning in early spring our laboratories were moved into the newly-completed Wiley Laboratory. In June the offices moved, and by the end of the fiscal year (September), the construction and equipment acquisition phase of the EMSL project was complete. In the remainder of calendar 1997 all laboratories were brought up to full functionality. The Wiley Laboratory provides CS&D with 11,900 square feet of modern laboratory space, 2400 square feet of service and storage, and 4600 square feet of offices.

CS&D activities in calendar 1997 are summarized in this report. That the move was accomplished with minimal impact on the research programs, and that the individual laboratories were able to continue their high level of productivity in supporting DOE research, constitutes a testimony to the staff of CS&D and EMSL management.

Web Addresses

Pacific Northwest National Laboratory:
http://www.pnl.gov
William R. Wiley Environmental Molecular Sciences Laboratory:
http://www.emsl.pnl.gov

2. Reaction Mechanisms at Interfaces

Molecular Beam–Surface Scattering and Kinetics Instrumentation

G. A. Kimmel, M. A. Covert, S. E. Barlow, R. S. Smith, and B. D. Kay

Supported by DOE Office of Basic Energy Sciences and the EMSL project.

Molecular beam scattering from surfaces is a powerful experimental tool for studying the dynamics and kinetics of the interaction of molecules with surfaces. The coupling of surface science, molecular beam, and laser technologies makes possible the measurement of total energy disposal and redistribution in gas–surface scattering. Previously these experimental methods have been employed to acquire detailed surface kinetics and state-to-state scattering measurements of molecules interacting with metallic substrates. Such experiments have resulted in a fairly detailed understanding of surface chemistry on metals. Unfortunately, we currently do not have a similar understanding of the elementary dynamical and kinetic processes occurring on ice and oxide surfaces. Such interactions are clearly important from an environmental viewpoint, since they form the molecular-level basis for the complex physiochemical processes that take place on the surface of atmospheric aerosols, at the aqueous–mineral geochemical interface, and at the vapor–liquid interface. Our goal is to apply and extend molecular beam surface scattering techniques to these systems in an effort to elucidate the relevant interactions. Toward this goal we have designed three new state-of-the-art molecular beam-surface scattering and kinetics instruments. This unique set of instrumentation will allow us to investigate the dynamics and kinetics of surface interactions in unprecedented detail. Two of these instruments are currently operational and the third is expected to become operational summer of 1998.

EMSL Molecular Beam Surface Scattering Facility

As part of the EMSL project, we have constructed two molecular beam scattering machines (ICS-1 Instruments I and II) and a low-energy ion beam line. A plan view of the EMSL Molecular Beam Surface Scattering Facility is displayed in Fig. 2.1. These ultra-high vacuum (UHV) machines will have a base pressure of 1×10^{-10} torr in the scattering chambers. Both Instruments I and II are equipped with three coplanar molecular beam lines which intersect at the sample target location within the scattering chamber. The two outer beams are at an angle of ±15° with respect to the central beam. Each beam can be independently controlled and can be run as a continuous or pulsed effusive or supersonic beam. The three beams can be synchronously modulated via computer-controlled high-speed chopper wheels with microsecond time resolution. The primary difference between Instruments I and II is the distance the beam sources reside from the scattering target. Instrument I has an increased source-to-target distance that allows direct backscattering geometries to be examined. The source-to-target distance on Instrument II is much shorter, allowing more intense beams to be generated.

In each instrument the surface scattering target is mounted on a 4-axis manipulator and placed at the intersection point of the three molecular beams. The sample is cooled with a closed-cycle helium refrigerator, and will attain a base temperature of 20 K. The sample stage is designed to allow rapid thermal cycling between 25 K and 1200 K. The sample's temperature is maintained by a programmable temperature controller.

Both the incident and scattered molecular beams can be detected via a differentially-pumped neutral atom/molecule detector. This detector is mounted on a large rotary flange assembly whose axis of rotation is perpendicular to the plane defined by the molecular beams, and passes through the intersection point of the beams. The detector consists of an electron impact ionizer, an electrostatic quadrupole bender, and a quadrupole mass spectrometer. The detector is mounted inside a doubly-differentially-pumped manifold to significantly increase the signal-to-background ratio for the desorbed/scattered flux of atoms or molecules. With this detector we will be able to measure velocity and angular distributions of the scattered/desorbed flux. In addition, the detector is designed to allow the incident beam to pass through it so that it can measure the directly backscattered flux in Instrument I.

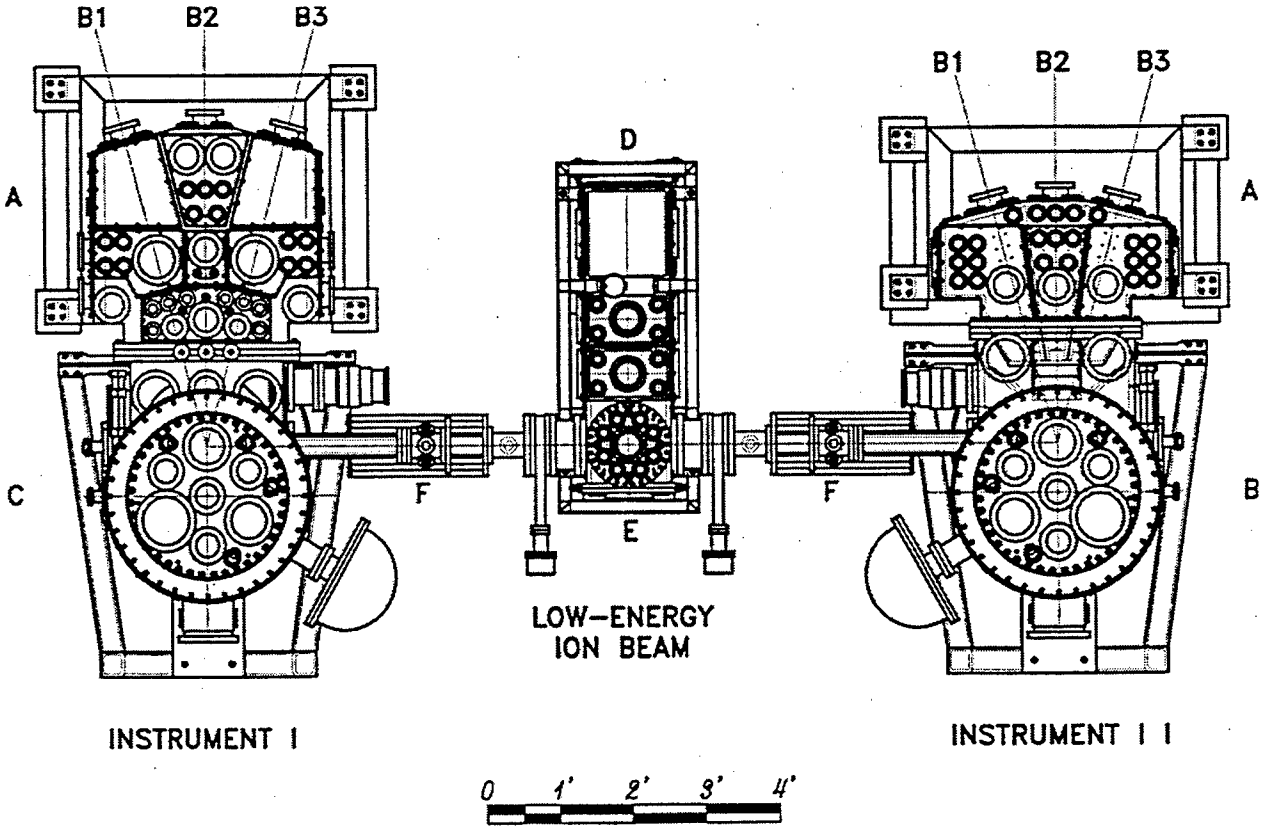

Figure 2.1. Plan view of EMSL Molecular Beam Surface Scattering Facility, comprised of ICS Instrument I, Instrument II, and the Low-Energy Ion Beam. (A) Triply-differentially-pumped beam source vacuum chamber; (B1–3) molecular beam lines; (C) doubly-differentially-pumped UHV surface scattering chamber; (D) differentially-pumped ion beam source and mass filter; (E) electrostatic quadrupole ion beam bender; (F) retractable ion beam focusing and deceleration lens assembly.

The target sample manipulator is also mounted on a large rotary flange assembly, allowing the sample to be positioned either at the intersection point of the molecular beams or in front of a number of surface preparation and characterization instruments. Both instruments are equipped with a sputter ion gun for sample cleaning, an Auger electron spectrometer (AES) and a low-energy electron diffraction (LEED) spectrometer for monitoring surface composition and order, respectively. The UHV chamber can also house a number of effusive beam evaporators. These evaporators will be employed to synthesize compositionally-tailored nanoscale oxide and ice surfaces.

In addition to the dedicated surface analytical instrumentation described above, Instruments I and II share a suite of specialized instrumentation comprised of an X-ray photoelectron spectrometer (XPS), a Fourier-transform infrared (FTIR) spectrometer, a Kelvin probe, a six-axis sample manipulator, and a low-energy ion beam line.

The ion beam line can produce mass-selected, monoenergetic ion beams with energies ranging from 10 eV to 3000 eV. The ion beam line can be operated in two different modes, depending on the final energy of the ions. For high-energy beams ($E_i \geq 400$ eV), the ions are transported through the beam line at their final energy. However, due to space-charge spreading of the ion beam, this approach does not work for low-energy beams. Therefore, for $E_i < 400$ eV, the ions are transported through the beam line at 400 eV and decelerated to their final energy just prior to striking the sample. An electrostatic quadrupole bender can be used to direct the ion beam into either Instrument I or II. The ion beam is focused onto the target using a retractable deceleration lens assembly. This assembly can also be employed to deposit very low energy (<5 eV) ions

onto the target. The scattered ion flux can be detected with a rotatable electrostatic energy analyzer and/or quadrupole mass spectrometer.

Beam Surface Kinetics Instrument

Supported by DOE Office of Basic Energy Sciences.

We have designed and are currently assembling a state-of-the-art molecular beam surface-scattering instrument for examining surface kinetics. The design of this instrument enables the simultaneous detection of both gaseous and surface species while the target is exposed to a flux of two reagents. The instrument has a modular design to facilitate interchangeability and adaptability for collaborative research. A plan view of the Beam Surface Kinetics instrument (BSK) is displayed in Fig. 2.2. In this instrument two molecular beams intersect at 90° on a target surface residing within a UHV scattering chamber. Each beam can be independently controlled and can be run as a continuous or pulsed effusive or supersonic beam. Both beams can be synchronously modulated via computer-controlled high-speed chopper wheels with microsecond time resolution. Each beam line is independently triply-differentially-pumped while maintaining a source-to-target distance sufficiently short to enable intense beams having fluxes in excess of 100 monolayers/sec to be employed. A differentially-pumped stationary neutral atom/molecule detector resides between the two incident beams and can detect particles scattering or desorbing along the surface normal. Other geometries can be examined by rotating the target surface. The detector is an electron impact quadrupole mass spectrometer whose axis lies within the principal scattering plane. This detector can also be used to detect ions issuing from the surface or generated via laser photoionization.

The surface scattering target is mounted on a 4-axis manipulator and placed at the intersection point of the two molecular beams. The sample is cooled with a closed-cycle helium refrigerator, and will attain a base temperature of 20 K. The sample stage is designed to allow rapid thermal cycling between 25 K and 1200 K. The sample's temperature is maintained by a programmable temperature controller. The target sample manipulator is also mounted on a large rotary flange assembly which allows the sample to be positioned either at the intersection point of the molecular beams or in front of a number of surface preparation and characterization instruments. The instrument is equipped with a sputter ion gun for sample cleaning, and an Auger electron spectrometer (AES) and a low-energy electron diffraction (LEED) spectrometer for monitoring surface composition and order, respectively. The UHV chamber can also house a number of effusive beam evaporators. These evaporators will be employed to synthesize compositionally-tailored nanoscale oxide and ice surfaces. In addition to the dedicated surface analytical instrumentation described above, the instrument has a Fourier-transform infrared (FTIR) spectrometer and a secondary ion mass spectrometer (SIMS) that can be employed while the sample target is being exposed to reagent fluxes from the two molecular beams. This novel feature enables both the gaseous and surface species to be simultaneously monitored under actual reaction conditions.

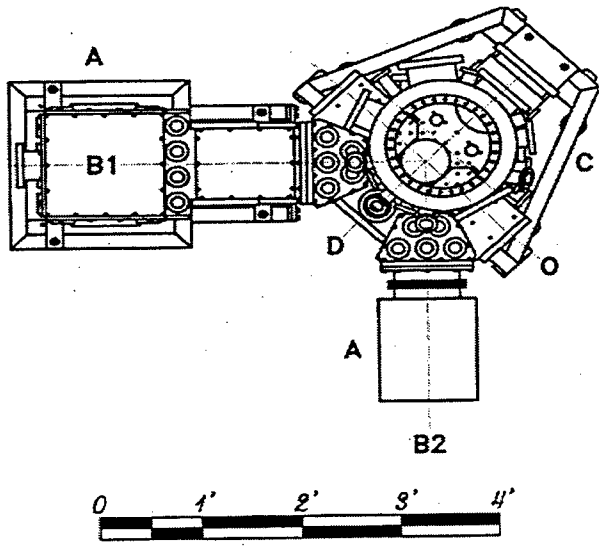

Figure 2.2. Plan view of the Beam Surface Kinetics instrument. The instrument is comprised of (A) triply-differentially-pumped beam source vacuum chamber; (B1) and (B2) molecular beam lines; (C) UHV surface scattering and analysis chamber; (D) fixed-angle differentially-pumped detector; and (O) optical access for FTIR and REMPI studies.

Structure and Reactivity of Ice Surfaces and Interfaces

K. P. Stevenson, Z. Dohnalek,**
G. A. Kimmel, R. S. Smith, and B. D. Kay

Supported by DOE Office of Basic Energy Sciences.

*Postdoctoral Research Associate.

Amorphous materials are important in a wide variety of scientific disciplines including chemistry, physics, materials science, and biology. Amorphous solid water (ASW) is of special importance for many reasons, including the open question of its applicability as a model for liquid water, and fundamental interest in the properties of glassy materials. In addition to the properties of ASW itself, understanding the microscopic intermolecular interactions between ASW and an adsorbate is important in such diverse areas as solvation in aqueous solutions, cryobiology, and desorption phenomena in cometary and interstellar ices.

1. Diffusivity of Amorphous Water Ice

One approach to unraveling the mysteries of normal liquid water has been to study the behavior of supercooled liquid water. In a classic paper, Speedy and Angell observed that supercooled liquid water also showed anomalous behavior.[1] Several thermodynamic and transport properties showed an unusual power-law temperature dependence of the form $(T/T_s - 1)^{-x}$, where T is temperature and T_s and x are fit parameters. On cooling, various physical properties diverge as a common value of T_s = 228 K is approached. This surprising divergence at T_s and the apparent impossibility of supercooling water below T_s has led to the proposal that T_s may represent a new thermodynamic or physical point in the water phase diagram. Several theoretical explanations for this singularity have been proposed, but no consensus has emerged.[2]

On the other hand, it is known that an amorphous form of water can be formed by several methods at temperatures below 140 K. The above-mentioned singularity, and thermodynamic continuity arguments based on entropic restrictions, have led to the question of whether amorphous water is a thermodynamic metastable extension of normal supercooled liquid or a distinct liquid phase. Knowledge of the diffusivity as a function of temperature is requisite to determining if ASW is a metastable extension of supercooled liquid water or a distinct thermodynamic phase. We employ molecular beams with high spatial resolution and temperature programmed desorption (TPD) to examine the nature of the molecular diffusivity in amorphous solid water. Compositionally-tailored ultrathin films (<5000 Å) of solid amorphous $H_2{}^{16}O$ and $H_2{}^{18}O$ are created by sequential dosing of the water isotopes. The desorption spectra reveal the details of the extent of mixing between the $H_2{}^{16}O$ and $H_2{}^{18}O$ layered interfaces.

Our initial experiments showed that long-range molecular translational diffusion occurs at a rate estimated to be $10^{6\pm1}$ greater than an Arrhenius extrapolation for diffusion in crystalline ice.[3] This finding suggested that the amorphous material exhibits liquid-like translational diffusion prior to crystallization at temperatures near 155 K. A mathematical model that couples our previous mean-field description of the desorption/crystallization kinetics[4] to a one-dimensional representation of the diffusive motion between layers was used to extract the temperature-dependent diffusion coefficient for the amorphous phase from our experimental isotope mixing data.

Figure 2.3 shows the temperature dependence of the ASW diffusivity (open symbols) in the temperature range 150–158 K. Also displayed are tabulated data for the diffusivity of liquid water, supercooled liquid water, and crystalline ice (solid symbols), and the dashed lines are Arrhenius extrapolations of these diffusivities. Our amorphous diffusivity results are clearly inconsistent with both Arrhenius extrapolations, exhibiting a much stronger temperature dependence with an apparent activation energy of ~40 kcal/mole over the 10-K temperature range of our experiment. It is known that glass-forming liquids exhibit markedly non-Arrhenius behavior as they are supercooled below their freezing point. As the temperature is further lowered toward the glass temperature, the diffusivity effectively vanishes due to the diverging viscosity of the supercooled liquid as it approaches the glassy state upon cooling. The temperature dependence of this phenomenon is well represented by the viscosity-scaled version of the Vogel-Fulcher-Tammann (VFT) equation, $D = D_o T e^{-(E/(T-To))}$, where T is temperature and D_o, E, and T_o are fit parameters. The solid line labeled "VFT" in Fig 2.3 is the VFT calculation with a T_o of

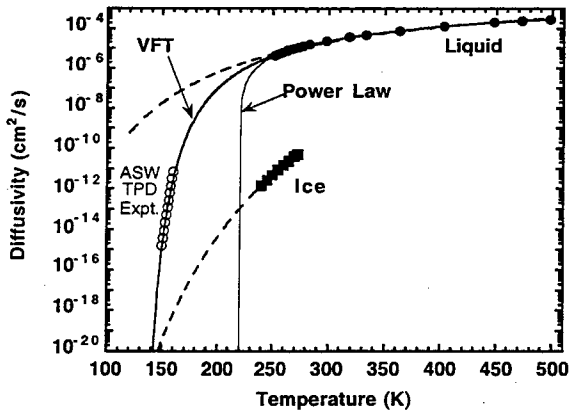

Figure 2.3. Temperature dependence of the ASW diffusivity (open symbols) in the temperature range 150–160 K. Also displayed are tabulated data for the diffusivity of liquid and supercooled liquid water (solid circles) and crystalline ice (solid squares). The dashed lines are Arrhenius extrapolations of these diffusivities. The solid line labeled "VFT" is a fit of the liquid/supercooled liquid data and ASW diffusivity data to the viscosity-scaled version of the Vogel-Fulcher-Tammann equation. The solid line labeled "Power Law" is from a published fit of the liquid/supercooled liquid data to the power law equation.

125 K. These VFT parameters predict a glass transition temperature of 142 K (defined as the temperature where the diffusivity is ~10^{-20} cm^2/s), which is in good agreement with the experimentally-determined value of 136 K for ASW.

The solid line labeled "Power Law" in Fig. 2.3 is from a published fit of the liquid/supercooled liquid data to the power-law equation, $D = D_o T^{1/2}(T/T_s - 1)^{\gamma}$, where T is temperature and D_o, γ, and T_s are fit parameters.[5] It is clear that the power-law equation with a temperature singularity of 220 K can not simultaneously fit the liquid, supercooled liquid, and ASW diffusivity data.

The quality of the fit to the liquid and supercooled liquid data has been used as evidence in support of the power-law equation and the temperature singularity. Figure 2.4 shows an Arrhenius-type plot of the power law and the VFT fits to these data. Over this temperature range (252–500 K) a comparison of the fits does not provide unambiguous evidence in support of either equation. Only at the low end of the temperature range do these two equations begin to show a difference. This difference occurs for temperatures below which the data for supercooled water exist.

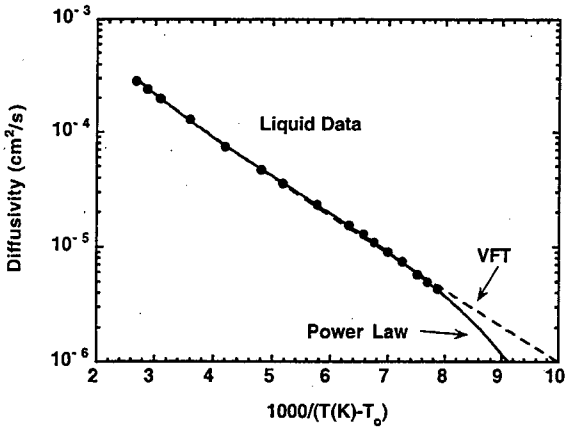

Figure 2.4. An Arrhenius-type plot of the diffusivity of liquid and supercooled liquid data (solid circles) and ASW (solid squares). The lines are the calculations of the power law (solid line) and VFT (dashed line) equations.

In Fig. 2.5 the diffusivity data for liquid, supercooled liquid, and ASW are plotted along with the power-law and VFT calculations. Over this temperature range 150–500 K there are clear differences between the two equations. It is evident that the power law does not fit the ASW data, whereas the VFT equation fits all the data.

The diffusivity data are only one part of the data needed to completely resolve the continuity question. In either case, our data show that the apparent diffusivity in ASW obtained from the experimental data is a factor of $10^{6\pm1}$ greater than an Arrhenius extrapolation for diffusion in crystalline

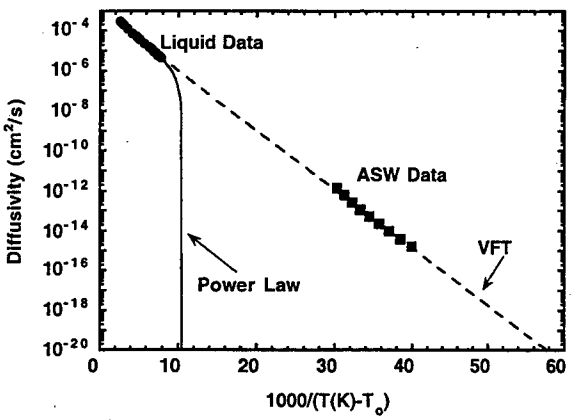

Figure 2.5. An Arrhenius-type plot of the diffusivity of liquid and supercooled liquid data (solid circles) and ASW (solid squares). The lines are the calculations of the power law (solid line) and VFT (dashed line) equations.

ice. This suggests that the amorphous material exhibits liquid-like translational diffusion prior to crystallization at temperatures near 155 K. Thus the observed diffusive behavior may be more consistent with that of a liquid (albeit a very viscous liquid) than a solid. A diffusivity of $10^{-12\pm1}$ cm^2/s for ASW near 155 K would imply a viscosity $10^{7\pm1}$ times greater than liquid water at 300 K. Near 160 K the diffusivity of ASW reaches ~10^{-12} cm^2/sec, roughly 10^{-7} times the diffusivity of normal liquid water at room temperature. Such a diffusivity would be nearly impossible to observe with a macroscopic sample—a 1-cm-thick film would require ~10^5 years to mix!

Furthermore, the diffusion data are consistent with a viscosity-scaled extrapolation (VFT equation) of the liquid and supercooled liquid data, and suggest that there is a continuity in the diffusive behavior between normal supercooled liquid water and the highly viscous melt of ASW. This important finding demonstrates that studies of nanoscale thin films of ASW at 140–160 K are germane to physical and chemical processes in normal liquid water.

2. Structural Thresholds During the Amorphous to Crystalline Water Ice Phase Transition

The interactions between water and an absorbate have important applications in atmospheric and astrophysical science. The desorption kinetics of a species interacting with a water ice layer can be used to probe the dynamics of this interaction. We use molecular beams with high spatial resolution to create ultra-thin (<1000 Å) films and temperature-programmed desorption (TPD) to study the desorption kinetics of the layered interfaces.

Water and CCl_4 are immiscible, and as such are an ideal model system for studying hydrophobic interactions. The TPD spectra show that CCl_4 desorption is impeded by the amorphous water overlayer until the temperature range for amorphous water crystallization. At this higher temperature, the abrupt CCl_4 desorption occurs completely over a narrow temperature range prior to the desorption of the majority of the water film. The CCl_4 desorption peak shifts with the temperature of the phase transition "bump" for both H_2O and D_2O. This correspondence suggests that the CCl_4 desorption through the water overlayer is directly correlated with the amorphous-to-crystalline phase transition. These experiments demonstrate that the CCl_4 is trapped beneath the ice until the phase transition occurs, and that desorption occurs in a dramatic fashion in concert with the crystallization of amorphous ice. We have termed the abrupt desorption the "Molecular Volcano."[6]

Figure 2.6 displays the structural changes that may accompany the crystallization kinetics and that ultimately are responsible for the episodic release of CCl_4 as the "Molecular Volcano." The abrupt desorption occurs through connected pathways that are formed during the nucleation and growth of crystalline ice. The onset of the abrupt desorption corresponds to the threshold for dynamic percolation. This threshold physically corresponds to the point at which the grain boundaries between the growing crystallites impinge upon each other and form a connected escape path that traverses the water overlayer.

The development of the ICS-1 instruments as part of the EMSL project has allowed us to extend the temperature range down to 20 K for these experiments. This capability allows us to probe structural dynamics occurring in the amorphous material in the low-temperature regime and allows us to study additional probe molecules.

Initial results using a variety of underlayer species

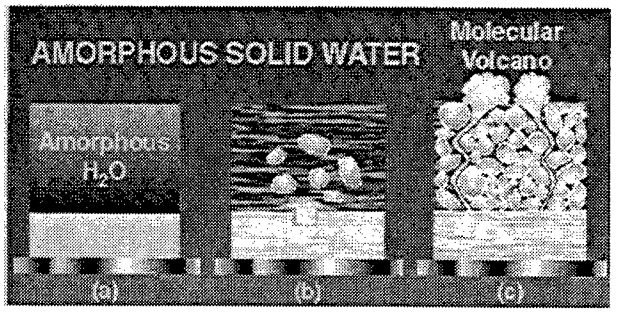

Figure 2.6. (a) Amorphous solid water is a noncrystalline form of water that can be made in the lab at very cold temperatures. (b) Above a temperature of 140 K, the disorderly frozen molecules begin to form tiny crystalline grains of ice. (c) When enough ice grains have formed, carbon tetrachloride (CCl_4) molecules, trapped under the amorphous water layer, can now escape by percolating up between the ice grains and emerge as a "molecular volcano." Figure from *Physics News Graphics*, July 17, 1997 (http://www.aip.org/physnews/Graphics).

are displayed in Fig. 2.7. These experiments show that the "molecular volcano" desorption mechanism is a general phenomenon, and accounts for a large fraction of the total desorption. At lower temperatures (25 to 100 K) the onset of additional desorption mechanisms are observed. Although these desorptions appear to be minor pathways, they may reflect the structural changes in the amorphous ice. We are now analyzing the data to understand these low-temperature desorption features.

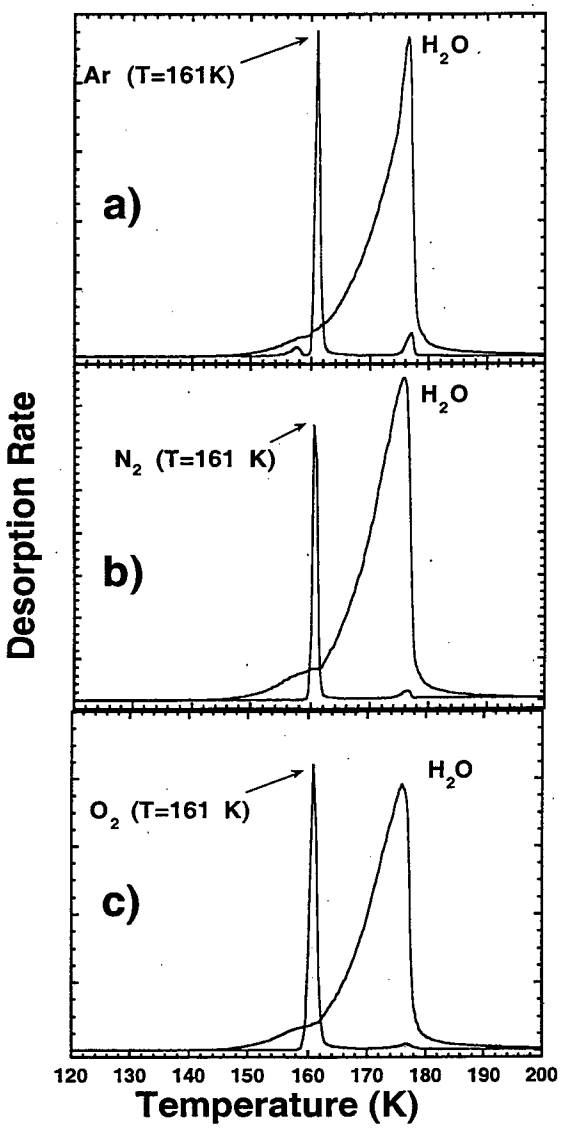

Figure 2.7. TPD spectra for nanoscale films of 120 ML of H_2O ASW grown on top of 5 ML of (a) Ar, (b) N_2, and (c) O_2. The "bump" in the water desorption spectra at ~156 K for H_2O arises from the irreversible phase transformation of ASW into crystalline ice. The spectra in (a), (b), and (c) show that the underlayer species is trapped beneath the ASW deposit and then desorbs abruptly in concert with the ASW crystallization.

References

1. R. J. Speedy and C. A. Angell, *J. Chem. Phys.* **65**, 851 (1976).
2. P. G. Debenedetti, *Metastable Liquids: Concepts and Principles* (Princeton University Press, 1996).
3. R. S. Smith, C. Huang, and B. D. Kay, *J. Phys. Chem. B* **101**, 6123 (1997).
4. R. S. Smith, C. Huang, E. K. L. Wong, and B. D. Kay, *Surf. Sci. Lett.* **367**, L13–18 (1996).
5. F. X. Prielmeier, E. W. Lang, R. J. Speedy, and H.-D. Ludemann, *Phys. Rev. Lett.* **59**, 1128 (1987).
6. R. S. Smith, C. Huang, E. K. L. Wong, and B. D. Kay, *Phys. Rev. Lett.* **79**, 909 (1997).

The Structure of Metal Oxide Surfaces

S. A. Joyce, J. P. Cowin, and B. J. Roop*

Supported by DOE Office of Basic Energy Sciences, Material Sciences Division; the EMSL Project; Laboratory Directed Research and Development (LDRD); and the DOE Environmental Management Science Program (EMSP).

*AWU Visiting Scientist.

Heterogeneous reactions on metal oxide surfaces are central to a better understanding of numerous environmental problems, ranging from the transport of pollutants through soils and groundwaters to the catalytic destruction of toxic chemicals and the long-term stability of high-level wastes in glass or ceramics storage forms. The scanning tunneling microscope (STM) is capable of imaging solid surfaces and molecular adsorbates with atomic-scale resolution. As a real space probe, the STM can directly determine the role of surface structure, especially at defects such as steps, vacancies, etc., in the adsorption and heterogeneous chemistry of molecules on surfaces. Many surfaces of relevance to environmental chemistry are, however, unsuitable for detailed studies due to the insulating nature of many materials, the lack of large, single-phase crystals, and/or difficulties associated with surface preparation. Our approach has been to use bulk single crystals, either natural or man-made, when available, and

to use thin-film epitaxy for those systems where bulk materials are not suitable.

Much of our effort in 1997 was devoted to bringing a new variable-temperature STM system on line for the EMSL project. The STM itself is from Omicron Associates, and was coupled to an in-house designed sample preparation/analysis system with sample transfer capabilities. The sample preparation system has capabilities for sample cleaning as well as Auger electron spectroscopy and low-energy electron diffraction for sample characterization. Sample temperatures in the STM can be varied from 25 K up to 1500 K (the high temperature limit is sample dependent). The ability to image at low temperatures is critical for directly imaging adsorbates and their interactions with defects. Single-site residence times for all but the most strongly-bound adsorbates are too short at room temperature to allow for imaging. Lowering the temperature exponentially increases the residence time, so that for a 25-K substrate essentially any molecular adsorbate could be imaged. All components of the new system were assembled, tested, and integrated, and were found to perform within design specifications.

The remainder of our work in 1997 involved the continuation of earlier projects as well as the investigation of several new systems. In collaboration with J. R. Rustad (EDS) and M. A. Henderson (IPS), the surface structure of two different natural α-Fe_2O_3 (001) surfaces were examined using LEED and scanning tunneling microscopy. The surfaces were cleaned in vacuum by ion sputtering and oxidation at elevated temperatures. After repeated cleaning cycles, the surfaces were found to be clean by Auger electron spectroscopy. Hematite is a semiconductor with a ~2-eV band-gap, and is intrinsically an insulator at room temperature. Often, however, either bulk oxygen vacancies or trace impurities act as electronic dopants, yielding samples with sufficient conductivity to allow the use of electron-based surface analytical tools. For the first sample examined, the resistivity was found to sufficiently low for Auger and LEED studies, but too high for the STM. This sample was annealed repeatedly in vacuum in an attempt to decrease the resistivity. Diffraction studies after this treatment revealed a complex surface reconstruction. Similar to the 2×1 reconstruction on the (012) surface, this is presumably due to oxygen loss and reduction of the iron leading to Fe^{2+} sites at the surface.

The second sample had a low enough resistivity even for the STM, assumed to be due to trace bulk impurities. To date, only the ideal bulk terminated 1×1 surface has been studied on this sample. A typical STM image is shown in Fig. 2.8. Large flat terraces, some extending for thousands of Å, are observed, and well-ordered, highly oriented steps are seen. By comparison with the diffraction measurements, we index the steps in the high-symmetry ⟨100⟩ and ⟨010⟩ directions. The step densities are on the order of only a few percent of the surface, which compares quite favorably the step densities of high-quality synthetic samples of metals and semiconductors. Several other extended defect structures are also present. Emergent screw dislocations were commonly seen (screws appear as steps emerging from an otherwise flat terraces). A low-angle grain boundary was detected with LEED. Grain boundary and screw defects are common in natural samples, but due to their low densities, especially with respect to the steps, they are expected to play only a very small role in the surface chemistry.

In collaboration with S. A. Chambers (IPS), we have examined the structure of MBE (molecular beam epitaxy)-grown magnetite (Fe_3O_4) films. The presence of reduced iron in Fe_3O_4 allows this mate-

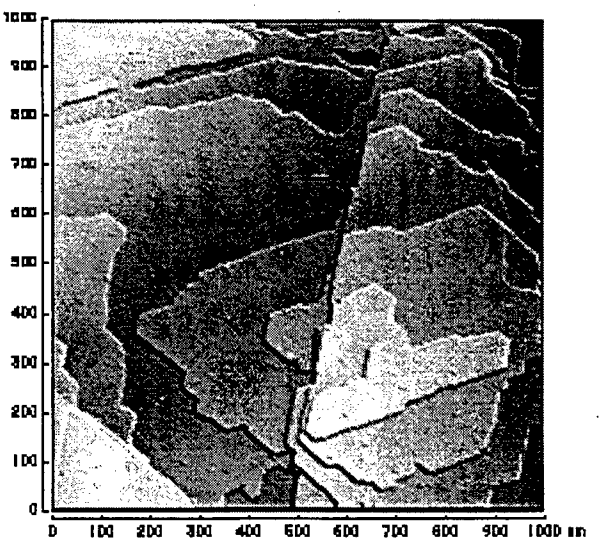

Figure 2.8. STM image of a natural α-Fe_2O_3 (001) surface. Scan range 1000 nm × 1000 nm. Note the large, flat terraces separated by atomic-height steps running along the ⟨010⟩ and ⟨100⟩ directions. A screw dislocation is evident in the lower right hand region.

rial to convert toxic pollutants such as hexavalent chromium and halogenated hydrocarbons into less harmful species. Fe_3O_4 (001) samples grown on MgO (001) substrates were studied. MgO, an insulator, was chosen as the substrate due to a near-perfect lattice matching (less than 0.3% difference) with Fe_3O_4. Fe_3O_4 is a metallic conductor above the Verwey transition (120 K), and films as thin as 500 Å have been imaged without conductivity problems. A representative image of a 2500-Å thick film is shown in Fig. 2.9. The film is clearly highly crystalline, with a dominant step direction in the ⟨110⟩ direction. The step density is ~10–15%. The hillock formations are believed to result from limited transport during growth, due to the relatively low substrate temperatures employed. Lower temperatures during growth were used to avoid the formation of magnesioferrite ($MgFe_2O_4$), which is known to form during high-temperature growth. The defect densities and their crystallographic orientations will be used in conjunction with planned spectroscopic probes of adsorbate interactions on similar surfaces (C. Peden, IPS) to determine the role of the defects in heterogeneous chemistry.

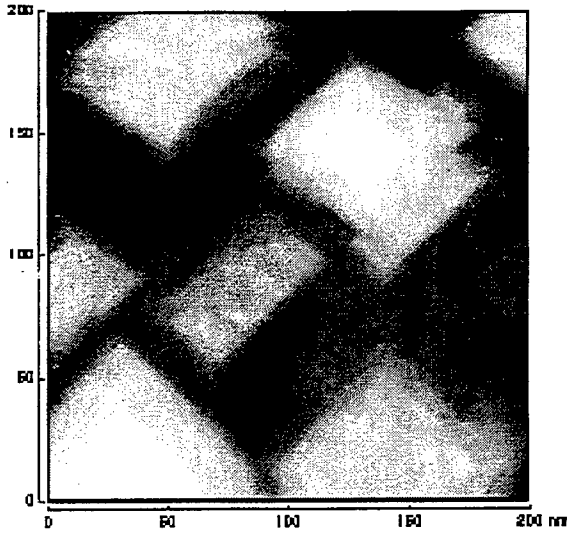

Figure 2.9. STM image of MBE-grown Fe_3O_4. Scan range 200 nm × 200 nm.

Intrinsic Affinity of Metal Ion Complexants for Alkali Metal Cations

D. Ray, M. B. More, and P. B. Armentrout**

Supported by DOE Office of Basic Energy Sciences and the National Science Foundation.

*Department of Chemistry, University of Utah.

Non-covalent interactions between ions and neutral molecules are of fundamental importance in molecular recognition phenomena occurring in complex chemical and biochemical systems. The study of a series of cation–ether complexes composed of different metal cations and a selection of ligands ranging from simple, monodentate ethers to cyclic polyethers provides an opportunity to examine the non-covalent interactions operative in "simple" ion–molecule complexes. Cation–ether complexes are also interesting from a practical point of view. Crown ethers have been proposed for use in new chemical separations technologies and in the development of advanced analytical methods. Computational models capable of reliably predicting ligand selectivity in a variety of condensed-phase environments would be valuable tools for the advancement of separations technologies. Such methods are currently under development; however, the development is hindered by a lack of suitable experimental data. One goal of this project is to provide accurate experimental data to address this deficiency.

In the present work, cross sections for the collision-induced dissociation by xenon of selected cation–ether complexes were measured with a guided-ion-beam mass spectrometer, an instrument specifically designed for measurements of the kinetic energy dependence of collision-induced phenomena. The cross section thresholds are interpreted to yield 0- and 298-K bond dissociation energies (BDEs) after accounting for the effects of multiple ion–molecule collisions, internal energy of the complexes, and unimolecular decay rates. Measurements have been made on complexes of dimethyl ether, 1,2-dimethoxyethane, 12-crown-4, triglyme, 15-crown-5, and 18-crown-6 with Li^+, Na^+, K^+, Rb^+, and Cs^+. These experiments provide the first benchmark data for *ab initio* electronic structure calculations of the selectivity and affinity of macrocyclic ligands for ions.

The experimentally determined bond dissociation energies for the complexes are generally in good agreement with conventional ideas of electrostatic ligation of gas-phase ions and with recent *ab initio* calculations by Feller and coworkers.[1,2] In fact, the agreement of the experimental results with the *ab initio* results is sufficiently good to conclude that the BDEs determined experimentally for Rb^+(12-crown-4) and Cs^+(12-crown-4) were not for the lowest-energy C_4 structure, but rather for a metastable state of the ion–molecule complex in which the crown ether has S_4 symmetry. Correlations between the measured bond dissociation energies and the equilibrium structures calculated by Feller and coworkers validate the prediction of Hay *et al.*[3,4] that the orientation of the C–O–C moieties relative to the metal cation can be more important than the M^+–O bond length in determining the stability of the complexes.

References

1. S. E. Hill, E. D. Glendening, and D. Feller, *J. Phys. Chem.*, submitted.
2. E. D. Glendening, S. E. Hill, and D. Feller, *J. Phys. Chem.*, submitted.
3. B. P. Hay and J. R. Rustad, *J. Am. Chem. Soc.* **116**, 6316 (1994).
4. B. P. Hay, J. R. Rustad, and C. J. Hostetler, *J. Am. Chem. Soc.* **115**, 11158 (1993).

Spectroscopy of Molecules at Liquid Interfaces

D. S. Karpovich and D. Ray*

Supported by DOE Office of Basic Energy Sciences.

*Postdoctoral Research Associate.

Processes at liquid interfaces can play a significant role in important natural and artificial multiphase chemical systems (e. g., the Earth's atmosphere, chemical separations processes, etc.). A detailed understanding of these processes, or at least accurate values of the critical parameters, is essential to the development of models of multiphase chemical systems with predictive capabilities. A goal of this work is the direct spectroscopic measurement of the structure and thermochemistry of molecules at liquid interfaces and the kinetics of mass transfer across liquid/liquid and liquid/vapor interfaces. The data we obtain, along with results of molecular-scale simulations performed by staff in the Molecular Theory and Modeling Group, allow us to begin to construct accurate molecular-level descriptions of the elementary processes occurring at, or near, liquid interfaces.

The basic experimental approach is to measure the orientation, the adsorption isotherm, and the solvation kinetics of selected adsorbates at liquid interfaces by surface second harmonic generation (SHG) using a high-repetition-rate femtosecond laser and a photon-counting detection system. Current work is focused on the adsorption thermochemistry of metal ion complexants (e. g., benzo-18-crown-6), and on ascertaining whether interphasial transport of small molecules (e. g., dimethyl sulfoxide) is diffusion-controlled or an activated process.

Measurements of the adsorption isotherm of benzo-18-crown-6, a typical species-selective metal ion complexant, at the liquid/vapor interface of water, arguably the simplest hydrophilic/hydrophobic interface, measured using surface SHG is given by the open squares in Fig. 2.10. A fit of the data to the Langmuir model of interfacial adsorption, given by the dashed line in Fig. 2.10, yields a value for the Gibbs free energy of adsorption of 25 kJ/mol. The open circles in Fig. 2.10 correspond to the adsorption isotherm of Na^+(benzo-18-crown-6) at the liquid/vapor interface of 1-M NaCl. A fit of the data to a Langmuir model modified to account for the electrical double layer with the Gouy-Chapman model, given by the solid line in Fig. 2.10, yields a value for the Gibbs free energy of adsorption of 50 kJ/mol. Since the complex is more soluble in aqueous solution, the data indicate that there is an increased driving force to bring the cation–crown ether complex to the interface. This suggests that a structural change accompanies the transport of uncomplexed benzo-18-crown-6 from the bulk aqueous phase to the liquid/vapor interface.

Surface SHG was used to measure the adsorption isotherm of dimethyl sulfoxide (DMSO) at the liquid/vapor interface of water. The Langmuir model of interfacial adsorption was used to model the data allowing determination of -11.8 ($\sigma = 1.2$) kJ/mol for the Gibbs free energy of adsorption of DMSO to the liquid/vapor interface of water at 293 K. This value of the adsorption energy is combined with data obtained from the literature to yield a complete thermodynamic characterization

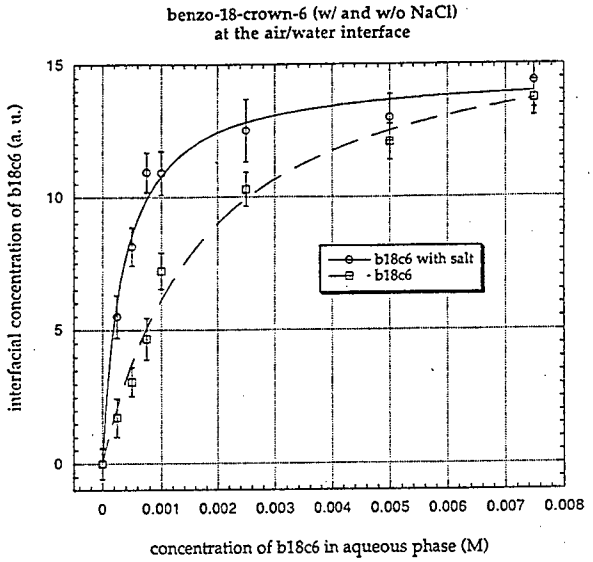

Figure 2.10. Adsorption isotherm of benzo-18-crown-6 at the liquid/vapor interface of water measured using surface SHG (open squares) and a fit of the data to the Langmuir model of interfacial adsorption (dashed line). Adsorption isotherm of Na^+(benzo-18-crown-6) at the liquid/vapor interface of 1 M NaCl (open circles) and a fit of the data to a Langmuir model modified to account for the electrical double layer with the Gouy-Chapman model (solid line).

of a model potential energy surface for the transport of DMSO across the liquid/vapor interface of water (given by the solid line in Fig. 2.11).

The potential energy surface (PES) given by the solid line in Fig. 2.11 is not consistent with recent molecular dynamics (MD) simulations of the transport of methanol or ethanol (which are roughly the same size as DMSO and have similar amphiphilic character) across the liquid/vapor interface of water. A PES which is monotonically increasing from the interface, as indicated by the dashed line in Fig. 2.11, or one with a barrier much smaller than ΔG_{evap}, is consistent with the MD simulations. Regardless of which PES best describes the transport process, the free energy minimum at the surface will trap molecules undergoing inelastic collisions with the interface. Measurements of the kinetics of the elementary reactions involved in interfacial transport would distinguish between these potential energy surfaces; such measurements are in progress.

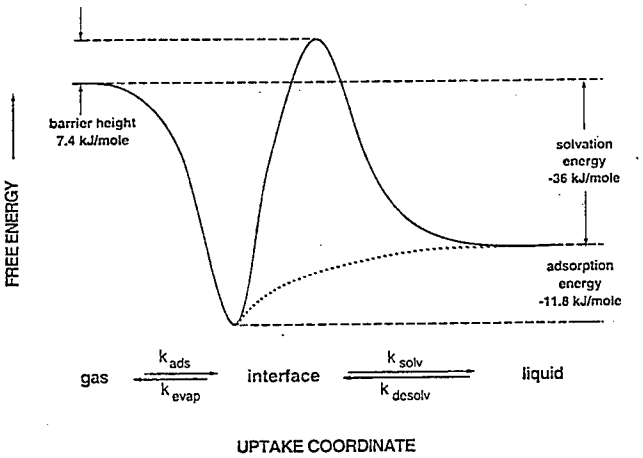

Figure 2.11. Model potential energy surfaces for the transport of DMSO across the liquid/vapor interface of water. The adsorption energy is determined from surface SHG data. The solid line is consistent with measurements of droplet uptake kinetics by Worsnop, Davidovits and coworkers.[1] The dashed line is consistent with recent molecular dynamics simulations of the transport of methanol and ethanol across the interface by Wilson and Pohorille[2] and Taylor, Ray and Garrett.[3]

References

1. D. R. Worsnop, M. S. Zahniser, C. E. Kolb, J. A. Gardner, L. R. Watson, J. M. Van Doren, J. T. Jayne, and P. Davidovits, *J. Phys. Chem.* **93**, 1159 (1989).
2. M. A. Wilson and A. Pohorille, *J. Phys. Chem. B* **101**, 3130 (1997).
3. R. S. Taylor, D. Ray, and B. C. Garrett, *J. Phys. Chem. B* **101**, 5473 (1997).

A Liquid-Beam Source–Ultrahigh Vacuum System for Liquid Interface Studies

N. G. Petrik, R. G. Tonkyn, W. C. Simpson,† S. E. Barlow, and T. M. Orlando*

Supported by DOE Office of Basic Energy Sciences and the EMSL project.

*Visiting Scientist.

†Postdoctoral Research Associate.

A liquid-beam/droplet source (LDS), designed to produce micron-sized beams of homogeneous liquids and heterogeneous solutions in a high vacuum environment, has been developed. The system will be utilized to study electron- and photon-induced processes occurring at vacuum/liquid and tailored ice/solid interfaces. The stability and flow of the beam allows experiments to be carried out on liquid surfaces that are continuously replenished and therefore pristine.

The machine consists of two sections. The first, shown in Fig. 2.12, is a high-vacuum, liquid-beam source equipped with a doubly-differentially pumped quadrupole mass spectrometer, as well as a time-of-flight (TOF) mass spectrometer (not shown). The TOF is magnetically shielded for photoelectron energy measurements. The second section is shown in Fig. 2.13. It consists of an ultrahigh-vacuum chamber equipped with a cryogenically-cooled sample manipulator, a pulsed low-energy electron-gun, a quadrupole mass spectrometer, and a second TOF mass spectrometer. The UHV section can be operated independently or coupled to the liquid beam source. When the chambers are coupled, the sample can be positioned directly under the liquid jet for dosing. The sample can then be withdrawn through a gate valve back into the UHV chamber for further study.

The liquid jet (Fig. 2.14) is formed by forcing solvent through a small (10–20 μm) aperture at high pressure. In order to maintain the background pressure as low as possible, a cryogenically cooled

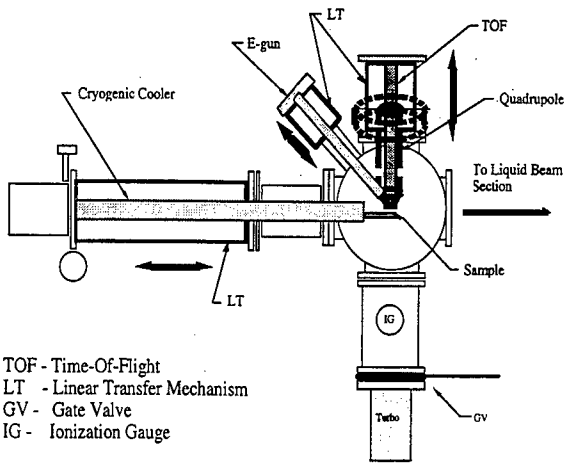

Figure 2.13. UHV chamber with long manipulator for transfer between chambers.

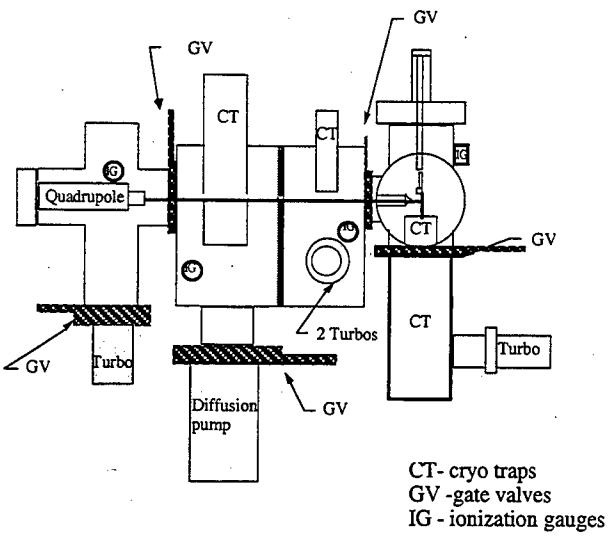

Figure 2.12. Liquid-beam source chamber.

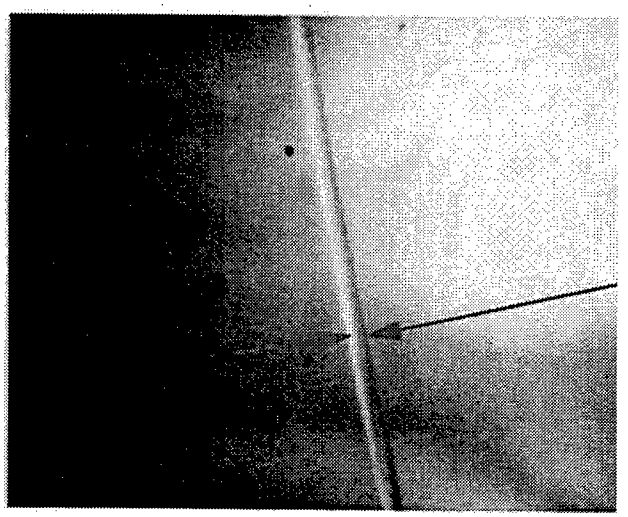

Figure 2.14. Liquid beam at 2–3 mm from the nozzle. The measured diameter of the beam is 7 μm. The nozzle had a 10-μm aperture.

surface catches the beam just a few centimeters beneath the aperture. Typical background pressures in the main chamber are in the mid-10^{-4} torr range. The liquid jet is rapidly supercooled by evaporation, reaching temperatures well below freezing. As the beam evaporates, the diameter drops as well. In principle one can study the liquid as a function of temperature simply by moving the jet up and down. Rather than move the detector, the nozzle itself is mounted on a very fine XYZ stage.

A skimmer located 1–2 mm from the jet is used to sample the liquid vapor into a quadrupole mass spectrometer. Due to the small diameter and low background pressure of the beam, this vapor suffers few, if any, gas-phase collisions, allowing a direct measurement of molecules at the liquid interface. Photodesorption/photoionization experiments are carried out by striking the beam with laser light and detecting the resulting ions with the time-of-flight spectrometer. Preliminary data are shown in Fig. 2.15. We tentatively assign mass 1, 2 and 3 to the 3 peaks shown. At longer times there are unresolved peaks corresponding to water ions and water cluster ions.

Future plans include upgrading the TOF to a reflectron–TOF in order to improve the mass resolution.

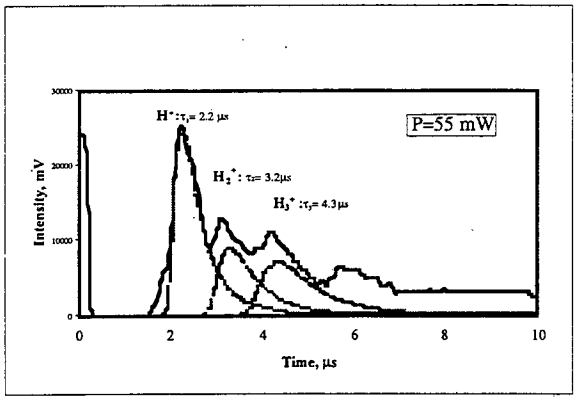

Figure 2.15. TOF spectrum of H_2O liquid beam photolysis products. Laser wavelength of 266 nm.

Spectroscopy and Dynamics of Single Proteins

*H. P. Lu, L. Ying,**
L. Xun,† and X. S. Xie

Supported by DOE Office of Basic Energy Sciences, and in part by Laboratory Directed Research and Development (LDRD).

*Graduate Student, Peking University.
†Washington State University Department of Microbiology.

One exciting application of the single-molecule methodology is the study of conformational and chemical dynamics of proteins. Flavoproteins are ubiquitous in nature because of their capabilities to undergo redox reactions in a thermodynamically and kinetically fully reversible manner. Their enzymatic reactions not only facilitate various electron transfers in our bodies, but also involved in biodegradation. In Fig. 2.16, (A) shows a fluorescence image of single molecules of a flavoenzyme embedded in agarose gel of 99% water. We spin-coat a cover glass with a thin film of gel containing dilute enzyme, and detect the natural fluorescence with a He-Cd laser (442 nm) and an inverted fluorescence microscope. The emission is from the enzyme's single active site, flavin adenine dinucleotide (FAD) (B). The emission spectrum (C) fluctuates with time on the subsecond time scale (D), reflecting spontaneous conformational changes of the active site, a phenomenon that is otherwise hidden in ensemble-averaged measurements. The single-enzyme experiment permits detailed investigation of conformational dynamics and energy landscapes for a specific active site. Interestingly, the spectral fluctuations observed occur at the time scale of enzymatic turnovers, indicating the influence of the conformational changes on the enzymatic reactions. We have recently developed a methodology to study the room temperature spectral diffusion.[1]

To investigate chemical kinetics, we monitor enzymatic turnovers of single enzyme molecules in real time. While the enzyme molecules are immobilized by the gel, the substrate molecules are essentially free to diffuse within the gel. The flavoenzyme being studied is cholesterol oxidase, a 53-kD enzyme that catalyzes oxidation of cholesterol by oxygen (Fig. 2.17A). The active site, FAD, is fluorescent in its oxidized form but not in its reduced form. Upon addition of the substrate,

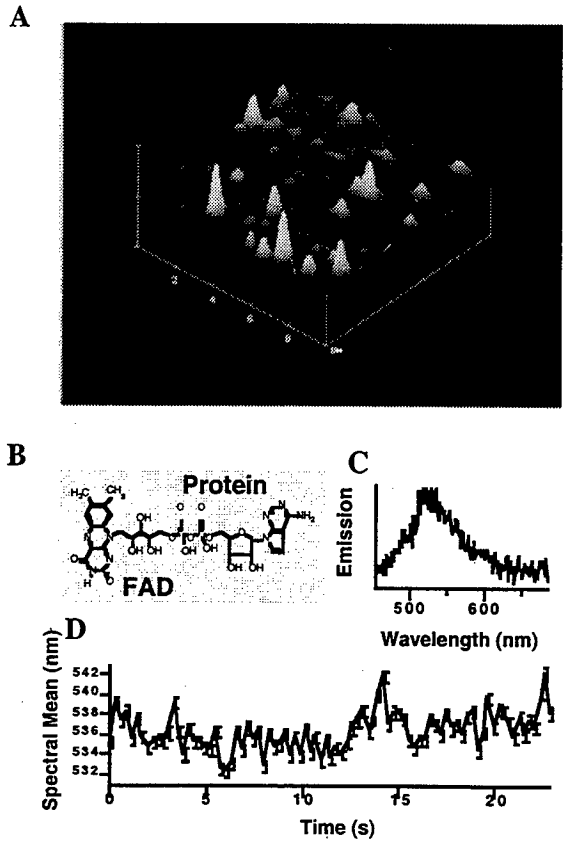

Figure 2.16. (A) Fluorescence image (10 μm × 10 μm) of single flavoenzyme molecules (pentachlorophenol monooxygenase) immobilized in a thin film of agarose gel of 99% water. Each diffraction-limited peak is due to an individual enzyme molecule with a single fluorescent active site, flavin adenine dinucleotide (FAD, shown in B). The image was taken at room temperature with 442-nm excitation. (C) Emission spectrum of a single enzyme molecule taken in 270 ms. (D) Change of spectral mean position with time for the single enzyme molecule in C.

the emission exhibits on-off behavior (B), each on-off cycle reflecting an enzymatic turnover. Statistical analyses of the turnover trajectories allow us to examine chemical kinetics at the single-molecule level and to obtain new insights into the enzymatic reaction. Combined spectral and turnover trajectories provide new clues on how conformational fluctuations influence enzymatic reactions. The single-molecule approach will be particularly useful for enzymology in general.

Allophycocyanin (APC) is a light-harvesting protein complex in photosynthetic cyanobacteria. The crystal structure of APC has been solved recently,

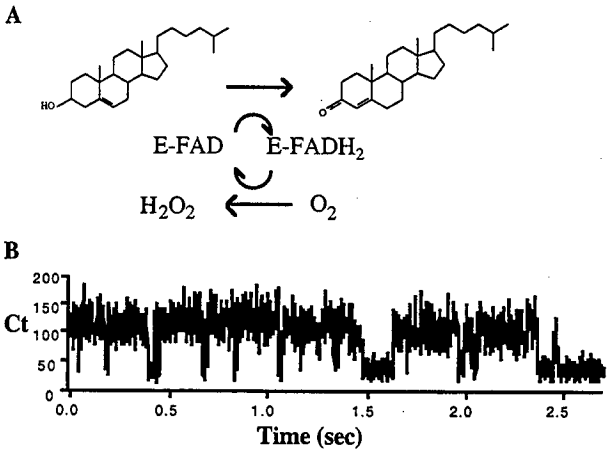

Figure 2.17. (A) Enzymatic cycle of cholesterol oxidase. (B) Real-time observation of the enzymatic turnovers of a single cholesterol oxidase molecule. The oxidized FAD is fluorescent, while the reduced FAD is not. Each on-off cycle of the emission corresponds to an enzymatic turnover.

showing a trimeric structure, Fig. 2.18. Each monomer unit of the trimer structure contains two open chain, tetra-pyrrole chromophores (α84 and β84) covalently bound to the protein structure. The three interacting pairs of α84 and β84 chromophores give rise to a strong excitonic band with absorption and emission peaked at approximately 650 nm and 660 nm, respectively.

Figure 2.18 also shows the emission spectrum of a

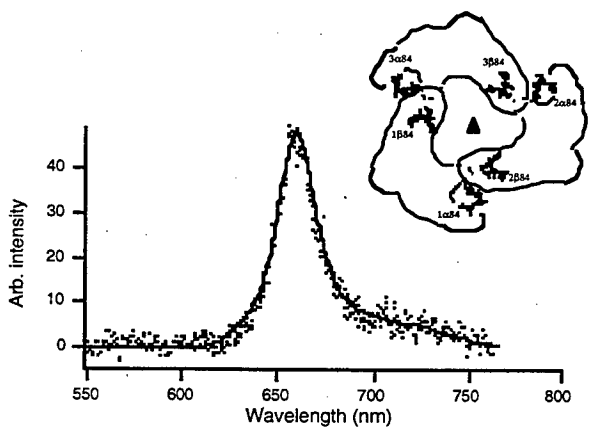

Figure 2.18. Structure of APC trimer containing six tetra-pyrrole chromophores forming three interacting pairs; and emission spectrum of a single APC trimer (dotted line) and ensemble-averaged spectrum (solid line).

single APC trimer (dotted line), which is identical to the ensemble-averaged spectrum (solid line), indicating a homogeneously broadened spectrum. Figure 2.19 shows the fluorescence decay of a single APC trimer, which is a single exponential decay. In contrast to the emission spectra, there is a distribution of fluorescence lifetimes of the individual APC trimers (inset). The distribution of the lifetimes arises from the exciton traps in the APC trimer. The photophysics of this system is being investigated.

Reference

1. H. P. Lu and X. S. Xie, *Nature* **385**, 143 (1997).

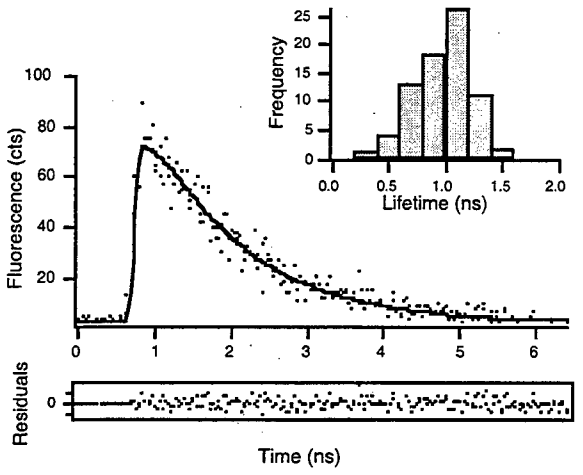

Figure 2.19. Fluorescence decay of an APC trimer fitted with a single exponential decay (1.2-ns lifetime). Inset: Distribution of fluorescence lifetimes of single APC trimers.

A Soft-Landing Ion Beam for Re-Creating Ionic Interfaces

*J. P. Cowin, M. J. Iedema, and G. B. Ellison**

Supported by DOE Office of Basic Energy Sciences.

*University of Colorado.

Ionic processes take many forms, and ion-beam methods have long been used to conduct and understand these processes. Yet a class of very common ionic systems, solutions containing ions, has seldom found direct use for ion beams. Ion-beam sources should in principle be excellent for re-creating condensed systems, which then could be used for study by a wide variety of bulk and surface analytical methods. But this requires ion beams that are well mass-selected and very clean (low neutral flux), intense (1–1000 nA), include important solution-phase ions (H_3O^+, NH_4^+, OH^-, NO_3^-, alkali ions, etc.), and have very low energy (0.5–5 eV) to prevent impact-induced chemistry. To meet these needs we have built a unique ion source in collaboration with Professor Barney Ellison at the University of Colorado, Boulder.[1]

The substrates for the ion deposition are crystalline or amorphous ice films, whose low vapor pressures allow us to employ vacuum-based surface analytical methods and the vacuum-based ion beam. Many solvents, including water, can be grown epitaxially in glassy states, which closely resemble true liquids. But we have the advantage that the ion/substrate can be put into a well-determined initial state, with distances controlled (normal to the surface), and solvent composition controlled including abrupt phase boundaries.

Reference

1. J. P. Biesecker, G. B. Ellison, H. Wang, M. J. Iedema, A. A. Tsekouras, and J. P. Cowin, *Rev. Sci. Instr.* **69**, 485 (1998).

Soft-Landed Ions: Hydronium and Cs^+ In Organic Films

*J. P. Cowin, M. J. Iedema, and A. A. Tsekouras**

Supported by DOE Office of Basic Energy Sciences.

*Visiting Scientist.

Organic liquids are routinely used to separate ionic species from aqueous solutions, such as radioactive cesium from DOE waste streams. Just how ions move in organic solvents, and move across the interface from aqueous phases, have been difficult to study. The use of the soft-landing ion beam, built to re-create ionic interfaces, can probe these interfaces in a most direct way. Other organic system applications may be charge-transport mechanisms in organic conductors, proton transfer in biological films, and ion transfer across sensor membranes or fuel cells.

Figure 2.20 (top) shows a cartoon of a 3-methyl pentane film experiment. A 37-monolayer amorphous film is grown at 30 K on a Pt(111) substrate. Cs^+ ions are deposited on top at 30 K, to charge the film, with the voltage being proportional to the average ion height above the Pt(111) surface (even when the ions diffuse into the film). Then the temperature is ramped at 0.17 K/s while the film voltage is measured via a non-contact UHV work-function probe. In the bottom of Fig. 2.20 the ions are seen to move through the film near 85 K, seen as a voltage fall. The viscosity of 3-methyl pentane is known down to near 70 K, and can be used to estimate the ion motion via the Stokes-Einstein ion mobility expression. This agrees fairly well, as shown by the dashed curve in Fig. 2.20.

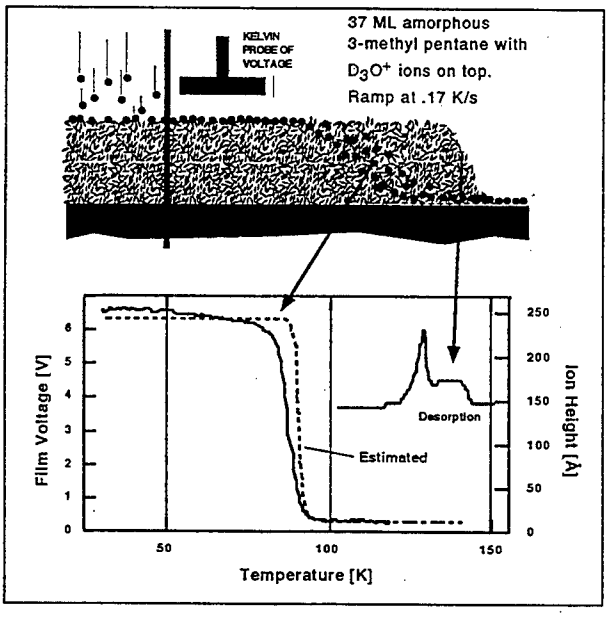

Figure 2.20. Ion diffusion in 3-methyl pentane studied by soft-landed ions. Ions soft landed (top right of cartoon) on top of amorphous solvent ice at 30 K, subsequently migrate through film as temperature is ramped upward. (Bottom) mean ion position measured by work function probe.

We have similarly studied Cs^+ and D_3O^+ ions diffusing through a hexane film. This case is more complicated, as the hexane crystallizes during the ion diffusion. The ion motion through the liquid-like hexane shows simple ion motion, in proportion to the field strength. When the ions percolate through the crystallizing hexane, the field dependence disappears.[1]

Reference

1. A. A. Tsekouras, M. J. Iedema, and J. P. Cowin, *Int. J. Mass. Spectrom. Ionic Processes* (1998), in press.

Soft-Landed Ion Study of Hydronium, Cs^+, and H-Bonding Defect Diffusion in Organic Films

*J. P. Cowin, M. J. Iedema, and A. A. Tsekouras**

Supported by DOE Office of Basic Energy Sciences.

*Visiting Scientist.

Applications of the soft-landed ion source to aqueous system ionic processes requires a good understanding of the basic ion diffusion process in water ices, and the ice's temperature-dependent dielectric properties. To do this, the transport of Cs^+ and hydronium ions (D_3O^+) and L- and D-type hydrogen bond defects were explored in deuterated crystalline ice films grown on a Pt(111) surface. Hydronium ions have by many been claimed

to tunnel through water ice, and we expected hydronium and Cs^+ ions to likely differ greatly, the former perhaps not being possible to keep on top of ice films.

The results were surprising in many respects, and challenge several long-standing though ill-proved notions about water/ice.[1-3] In brief, the hydronium (or Cs^+) did not diffuse in crystalline water films up to at least 190 K, nor in amorphous ice up to the crystallization temperature near 165 K. D-defects diffuse in crystalline ice at 124 K at zero field, but this shifts rapidly with field strength, extrapolated to 0 K at 1.6×10^8 V/m. Ice grown at 160 K and then hydronium-dosed at 160 K shows an active dielectric constant down to 30 K, strongly suggesting that L-defects have zero activation barrier for their migration (i.e., they tunnel). The slight ferroelectric nature of amorphous and crystalline ice films was also studied.[3]

Figure 2.21 shows that neither hydronium or Cs^+ ions move in amorphous (not pre-annealed) ice. Had they, the thick-film results would have superimposed on the thin-film data shown. Enough ions were deposited (to 30 to 70 V) so that after the dielectric constant transiently turns on,[2] the residual voltage is still clear. Near 165 K the amorphous ice crystallizes, causing a spike in the film voltage. Between the glass temperature of 135 and 165 K, we would have expected the ions to move, if it were a true liquid. Either it is not (as some feel), or the ions nucleate the crystallization around the ion at an earlier temperature. In crystalline ice, we saw that neither ion moved up to about 200 K. No evidence for tunneling motion is seen, contrary to many prior assertions.[2]

Figure 2.22 shows results for a crystalline ice film (grown at 140 K) dosed with D_3O^+ ions at 30 K, then *T*-ramped. The initial film voltages were from 10 to 30 volts and initial coverages were from 600 to 5060 monolayers thick. The voltages are normalized to the initial voltage. No ion diffusion was found. The voltage fall-offs had different shapes, but formed a continuous family versus electric field strength. The fall-off near 150 K is the expected onset of ice's dielectric constant due to formation of L/D defect pairs. The drop near 120 K we identify as due 1–1.5 D-defects per hydronium deposited becoming mobile and moving through the ice. Given their effective "charge" of 1/3 $|qe|$, the 1/3 to 1/2 voltage drop is immediately understood. Most literature sources would have assigned the L-defect as becoming mobile at this temperature, but they lack our direct approach. The temperature of the "120-K" drop is very field dependent.

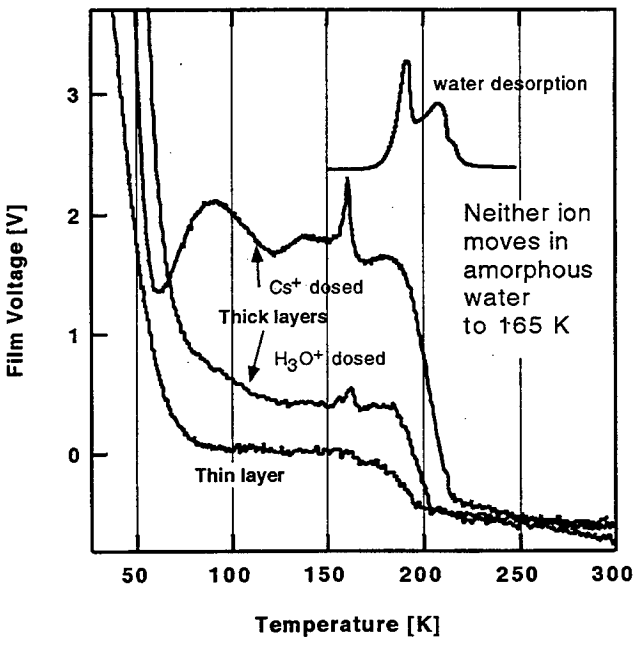

Figure 2.21. Hydronium ions and Cs^+ ion placed on amorphous water film at 30 K show dielectric response of water at about 50 K as temperature is increased, shown by work function change. If ions diffused, the thick film curves should match the thin film curve. Conclusion: neither ion diffuses, even above water glass-temperature of 135 K.

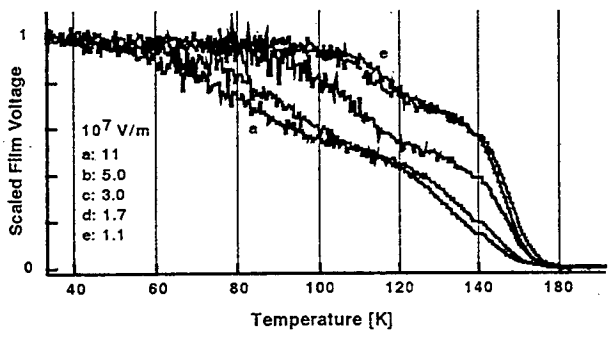

Figure 2.22. Hydronium ions on top of crystalline water films of various thicknesses create different electric field strengths, which probe dielectric (solvation) response. H-bond defect (D-type) moves at 120 to 80 K and is very field-sensitive. H-bond defect pairs are created near 150 K.

References

1. A. A. Tsekouras, M. J. Iedema, and J. P. Cowin, *Int. J. Mass. Spectrom. Ionic Processes* (1998), in press.
2. A. A. Tsekouras, M. J. Iedema, and J. P. Cowin, *Phys. Rev. Lett.*, submitted.
3. M. J. Iedema, A. A. Tsekouras, M. Dresser, J. B. Rowland, D. Doering, and J. P. Cowin, in preparation.

3. High-Energy Processes at Environmental Interfaces

IR-MALDI of Low-Molecular-Weight Compounds Using a Free Electron Laser

W. P. Hess, H. K. Park, O. Yavas,* and R. F. Haglund Jr.**

Supported by DOE Office of Basic Energy Sciences.

*Department of Physics and Astronomy, Vanderbilt University.

Ethylenediaminetetraaceticacid (EDTA) is a tetradentate carboxylic acid used to chelate metal ions. Thousands of tons of EDTA have been added to mixed-waste holding tanks in an effort to sequester metal radionuclides and reduce the liquid volume of the waste. Unfortunately, chelation of these metal ions also enhances migration of radioisotopes through the subsurface.[1] Therefore, knowledge of the transport and ultimate fate of complexed and uncomplexed EDTA is crucial to determining the spread of hazardous waste contamination from leaking storage tanks.

Chemical analysis of EDTA has proven difficult without extensive processing and wet chemical analysis; moreover, purification of the samples is not generally feasible because it would create undesirable secondary waste streams. The high (femtomolar to picomolar) sensitivity of matrix-assisted laser desorption/ionization (MALDI) is a potentially important advantage for analyzing this material.[2] MALDI using an infrared laser would confer an additional advantage by virtue of being able to use a wider array of matrix materials, given that UV MALDI works best with aromatic matrices.

In this report we describe IR MALDI studies of EDTA in succinic acid, a matrix that has been extensively studied using free-electron, Er:YAG, and CO_2 lasers.[3] We find that the IR MALDI irradiance threshold is a strong function of sample morphology. Moreover, the wavelength dependence of the MALDI threshold does not simply track the absorption of either the succinic acid matrix or the EDTA analyte.

The principal laser used in these experiments was the Vanderbilt mid-infrared free-electron laser (FEL). The FEL was tuned over the range 2.8–6.5 μm with energies from 20 to 60 mJ. The nominal 4-μs macropulse can be delivered at a pulse repetition frequency of up to 30 Hz; each macropulse comprises about 10^4 micropulses, each 1 ps in duration, separated by intervals of 350 ps. The IR optical train incorporates a fast electro-optic switch (Pockels cell) to slice a short micropulse train ($t \geq 80$ ns) out of the FEL macropulse.[4] We used a linear time-of-flight mass spectrometer equipped with a microchannel plate detector; it consists of a one-meter TOF tube and a turbo-molecular-pumped vacuum chamber. An airlock for fast sample insertion allows vacuum to be restored within a few minutes after changing the sample.

The samples were prepared in accordance with the standard "dried-droplet" protocol. The succinic acid matrix was dissolved in water to a concentration of 30 mg/ml to produce a nearly saturated solution. Analyte molecules Na_2EDTA and EDTA-free acid were dissolved in water to concentrations of 5 mg/ml and 0.5 mg/ml, respectively. The matrix and analyte solutions were combined in matrix:analyte ratios ranging from 10:1 to 300:1 on the stainless steel substrate. A 10-μl sample drop was applied to the substrate and dried for 10 minutes in a stream of unheated air. Sample crystal structure was observed using an optical microscope prior to introduction of the dried sample into the vacuum chamber.

Figure 3.1 displays the TOF mass spectra for 2.94-μm MALDI of EDTA following excitation from an Er:YAG laser and the Vanderbilt FEL. The MALDI response from a succinic acid matrix is quite similar for the long pulse (200 ns) of the Er:YAG and the 100 ns pulse train of the FEL. Although the 100-ns portion of the macro pulse provides a similar irradiance as the YAG pulse, the fluence of each micro pulse is 1000 times greater. That the MALDI threshold depends upon irradiance rather than fluence is contrary to UV MALDI results,[5] as noted in recent FEL MALDI work.[3] We observe no ions without added matrix molecules, as the EDTA laser desorption ionization threshold is higher than the MALDI threshold.

The MALDI response obtained in the 5- to 6-μm region displays a distinct wavelength threshold near 5.9 μm. At wavelength of 5.9 μm and greater,

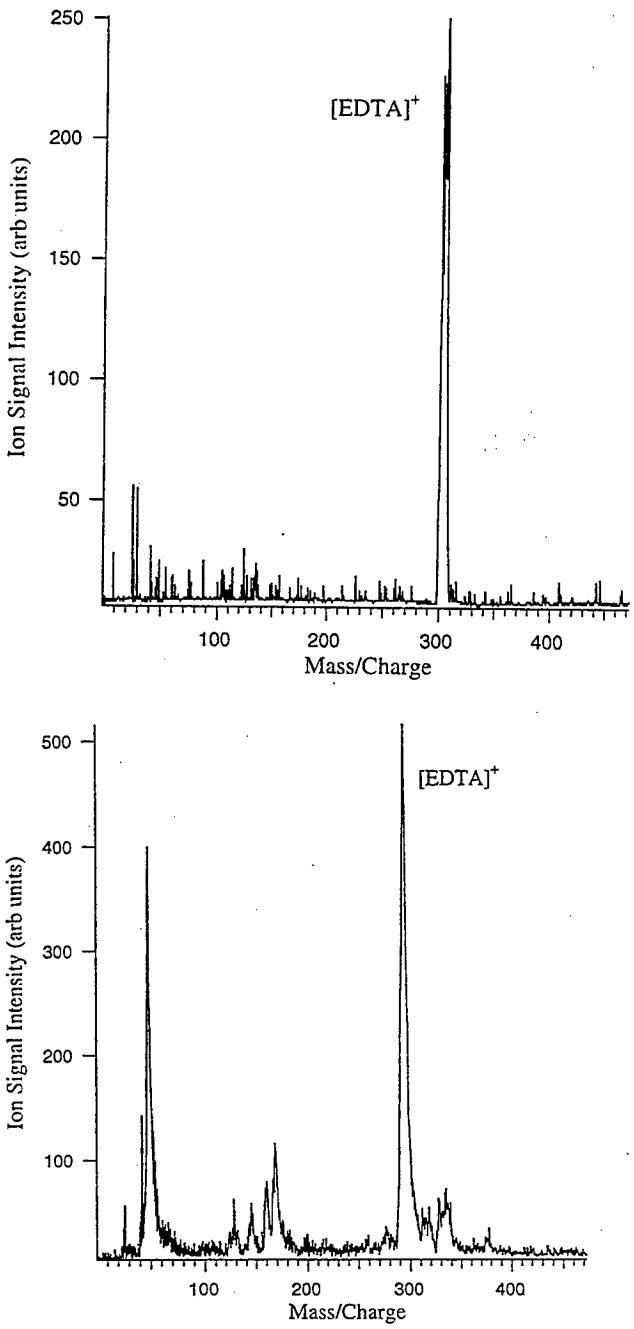

Figure 3.1. Comparison of (above) FEL and (below) Er:YAG spectra of EDTA at 2.94 μm. The FEL IR MALDI spectra display a strong parent mass peak and little matrix ionization. Considerable variability is observed on a shot-to-shot basis, however, and we conclude that FEL and Er:YAG MALDI at 2.94 μm produce largely similar mass spectra. The mass shift observed between the two spectra is an artifact of the linear TOF mass spectrometer and is likely due to different initial velocities of the analyte ions.

few analyte ions are observed, but they are readily observed for wavelengths between 5.4 and 5.8 μm. Oddly, the wavelength threshold does not correlate directly with IR absorption bands of either the succinic acid matrix or the Na_2EDTA analyte. One might expect the desorption threshold to decrease linearly or superlinearly with sample absorption as a function of wavelength. The IR absorption spectrum of the matrix displays a strong C=O stretch band centered at 5.9 μm. The short wavelength tail begins near 5.6 μm and extends to 5.0 μm. It is therefore surprising that the MALDI threshold is obtained only for wavelengths less than the 5.9-μm absorption maximum. A similar threshold wavelength behavior has been observed previously in the IR MALDI of small proteins in the 3-μm (O–H stretch band) and 6-μm (C=O stretch band) regions.[3] In both the current and previous studies, the MALDI threshold is higher for wavelengths near the band center than for wavelengths well into the "blue edge" of the absorption band. A plausible explanation for this behavior assumes that surface species, whose absorption maxima are shifted to higher frequencies, yield analyte ions much more easily than bulk species. The question remains as to whether the absorption bands are shifted enough to mirror the threshold wavelength dependence.

The relative threshold irradiance for an analytically useful MALDI response has been qualitatively determined in two wavelength regions. The O–H and C=O stretching bands of succinic acid centered at 3.3 and 5.9 μm, respectively, provide strong IR absorption and are excellent targets for FEL MALDI. Figure 3.2 displays the succinic acid absorption spectrum and relative MALDI threshold in the 2.5 to 6.5 μm region. The usual model for UV and IR MALDI assumes that a strong matrix absorption feature must have considerable overlap with the emission wavelength of the excitation source. Therefore, one might expect that the MALDI threshold, as a function of wavelength, will mirror the target absorption feature. We find that, contrary to these expectations, the lowest MALDI threshold, for excitation of the O–H stretch band, is at 2.87 μm and for the C=O stretch band, near 5.7 μm. Both threshold minima are well off the peak of the IR absorption features.

We add a cautionary note when discussing MALDI threshold determinations: the erratic nature of both UV and IR MALDI signals has been noted in the literature. While the cause of the large fluc-

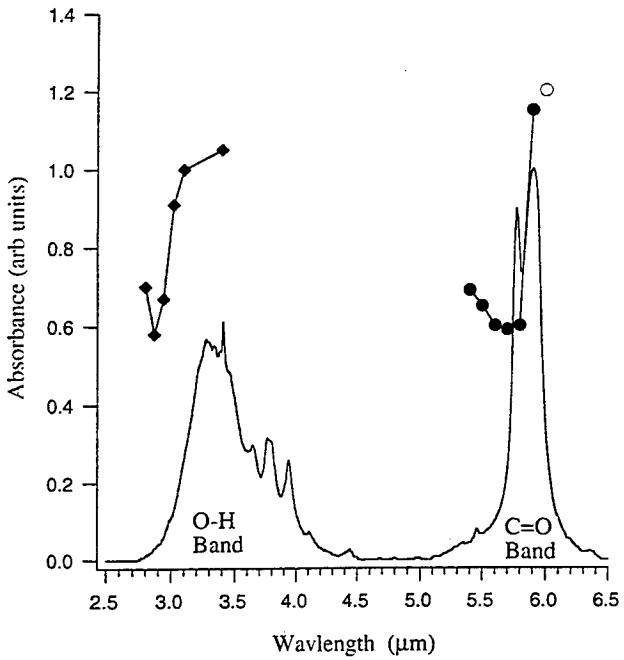

Figure 3.2. Relative threshold for IR MALDI of EDTA in succinic acid in the 6-μm (solid circles) and 3-μm (solid diamonds) regions. The minima in MALDI threshold is shifted to the high-energy side of the C=O and O–H stretch band maxima. The open circle indicates that no MALDI response is observed at 6 μm and greater wavelengths.

tuations in MALDI ion production is due to several factors (including the highly nonlinear power dependence), inconsistent sample preparation is a strongly suspected source of signal fluctuation. Since sample preparation involves rapid crystallization (usually) and crystallization is quite sensitive to sample concentrations and environmental conditions, multiple crystal structures can be observed for even similar preparation procedures. We have noted at least two different regimes of crystal growth: the dominant growth regime produced large rock-like crystals, while the minor growth regime produced much finer dendritic crystals. These different crystal structures, in turn, yielded quite different irradiance thresholds for the MALDI response.

References

1. A. P. Toste and R. B. Myers, *RWM-6 Radioactive Waste Management Committee, OECD Nuclear Energy Agency, Paris, France* (1986), 57.
2. S. C. Goheen, K. L. Wahl, J. C. Campbell, and W. P. Hess, *J. Mass Spectrom.* **32**, 820 (1997).
3. R. Cramer, R. F. Haglund Jr., and F. Hillenkamp, *Int. J. Ion Proc.* (to be published, 1997).
4. K. Becker, J. B. Johnson, and G. Edwards, *Rev. Sci. Instrum.* **65**, 1496 (1994).
5. K. Dreisewerd, M. Schurenberg, M. Karas, and F. Hillenkamp, *Intl. J. Mass Spectrom. Ion Processes* **154**, 171 (1996).

Time-Resolved Interferometric Measurements of Carrier Dynamics in Wide-Band-Gap Materials

R. M. Williams and W. P. Hess*

Supported by DOE Office of Basic Energy Sciences.

*Postdoctoral Research Associate.

Environmental samples are often difficult to analyze for possible contamination, and require sophisticated analytical techniques. Some of these techniques rely upon laser ablation as a primary means of vaporization and/or ionization. They include matrix-assisted laser desorption/ionization (MALDI) and laser ablation mass spectrometry (LAMS). Nanosecond lasers have usually been used as the irradiation source for laser ablation, but many of the key processes (i.e. electron/hole–pair recombination, trapping, electron/phonon interactions, etc.) involved in laser/solid interactions occur on a sub-nanosecond time scale. An important first step in optimizing methods based on laser ablation lies in the understanding of these fundamental processes. The goal of this research effort is to study these important aspects involved in energetic laser/solid interactions, where the solid material is usually an environmentally relevant wide-band gap material, such as magnesium oxide, calcium carbonate, or sodium nitrate.

Femtosecond transient absorption spectroscopy is one of the most widely used techniques in the study of ultrafast dynamics in transparent materials. In a typical transient absorption experiment, a subpicosecond pump pulse excites carriers (electrons and holes) in a material, and the absorption of a second subpicosecond probe pulse is measured as a function of delay between the pulses. The wavelength of the probe pulse is selected to be absorbed by the transient carriers, so the temporal evolution of the transient absorption can be related directly to the carrier dynamics (e.g.

recombination or trapping, etc.). Transient absorption spectroscopy measures the change in the *imaginary* part of the index of refraction resulting from pump-pulse excitation.

Recently, the addition of a frequency-domain interferometric detection technique to a traditional pump/probe transient absorption apparatus[1-3] has allowed determination of the transient phase shift of the probe pulse, as well as any transient absorption. The transient phase shift of the probe pulse is a measure of the change in the *real* part of the material's index of refraction upon pump-pulse excitation. Information about both parts of the index of refraction forms a complete picture of the material's dielectric response (i.e. charge-carrier dynamics) to the excitation pulse.

Obtaining the transient phase shift is accomplished by measuring the shift of the spectral interference pattern between a reference pulse and the probe pulse, which arrive at the sample before and after the pump pulse, respectively. Figure 3.3 is a schematic representation of our experimental optical arrangement for transient phase measurements; the inset depicts the relative timing of the reference, pump, and probe pulses. The reference and probe pulses are identical and are generated in a simple Mach-Zehnder interferometer in which a temporal delay between the pulses can be set. A periodic intensity modulation (with a spacing $\Delta\omega$) is observed in the spectral profile of the reference/probe pulse-pair, and is related to the temporal separation (ΔT) of the reference and probe pulses:

$$\Delta\omega = \frac{2\pi}{\Delta T}.$$

Examples of such interference spectra with different values of ΔT are shown in Fig. 3.4 (in the absence of any pump pulse).

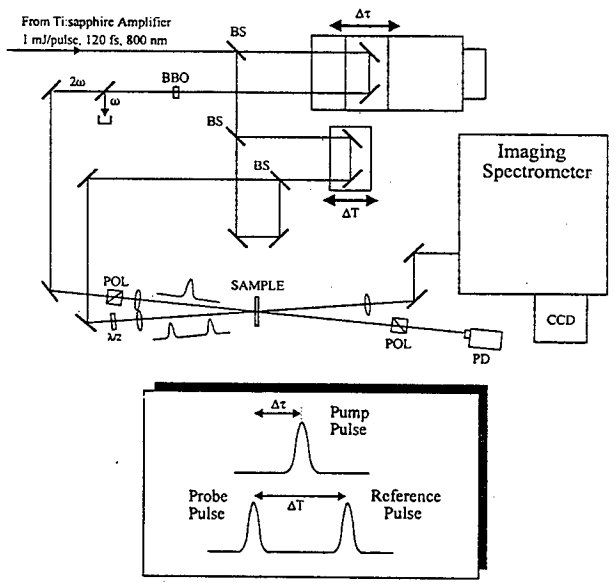

Figure 3.3. Experimental optical layout for transient phase measurements. The crossed polarizers and the half-wave plate in the pump and reference/probe beams, respectively, allow for a third-order cross-correlation Kerr signal to be detected in the pump beam, simplifying spatial and temporal overlap of the beams in the sample. The inset shows the relevant timing between the reference and probe (ΔT) and pump and probe beams ($\Delta\tau$).

The probe pulse will "experience" a different index of refraction from the reference pulse if the pump pulse has excited a sufficient number of charge-carriers in the material, thereby causing an induced phase shift in the measured spectral profile of the pulse pair. A decrease in the spectral modulation depth is observed if there is an accompanying transient absorption of the probe pulse. By measuring the magnitude of the phase shift and any absorption as a function of temporal delay between the pump and probe pulses, the real and imaginary parts of the index of refraction can be inferred and used to describe the dielectric response of the material as a result of the pump pulse excitation.

In the experimental apparatus under development, an amplified titanium-sapphire (Ti:sapphire) based laser system is incorporated. A mode-locked Ti:sapphire oscillator, producing <100 fs pulsewidths at a repetition rate of 82 MHz, is used to seed a Ti:sapphire regenerative amplifier (pumped at 20 Hz by the frequency-doubled output of a Q-switched Nd:YAG laser), which increases the energy of the femtosecond pulses into the 1–10 mJ/pulse range while maintaining pulsewidths ~120 fs. The system is capable of producing energy densities $>10^{15}$ W/cm^2. The fundamental wavelength of the system can be tuned ~750–850 nm, while frequency doubling and tripling in nonlinear crystals can be used to extend the wavelength coverage into the visible and UV. Plans are underway to extend the wavelength into the VUV and soft X-ray region using

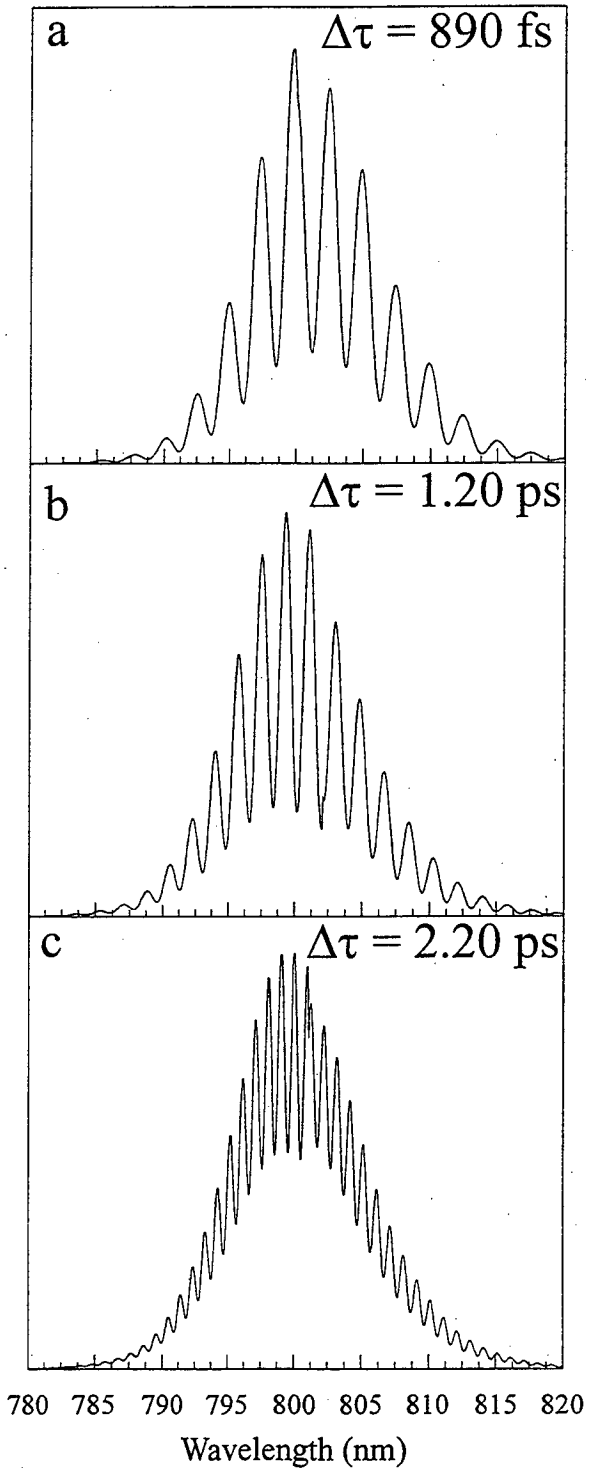

Figure 3.4. Frequency interference spectra of the reference/probe pulse pairs shown with various amounts of temporal delay ($\Delta\tau$). The decrease in fringe contrast with increasing delay is attributed to the finite spectral resolution of the spectrometer.

high-harmonic generation in rare gases. Pulse diagnostics include second-harmonic autocorrelation to measure the temporal characteristics of the pulses; spectral information is obtained using conventional spectrometers. Also under development is a diagnostic technique known as FROG[4] (frequency-resolved optical gating), in which the temporal and spectral characteristics (including spectral phase) of the femtosecond pulse can be measured simultaneously. Samples can be mounted in ultra-high vacuum chambers capable of heating and cooling over a broad range (10–500 K), or they can be studied under ambient conditions.

Using the techniques described above, we hope to gain additional insight into some of the key energetic processes that accompany laser/solid interactions. Of particular interest in these materials is the role which defects may play in effecting the deposition of laser energy.

References

1. P. Martin, S. Guizard, Ph. Daguzan, G. Petite, P. D'Oliveria, P. Meynadier, and M. Perdix, *Phys. Rev. B* **55**, 5799 (1997).
2. E. Tokunaga, A. Terasaki, and T. Kobayashi, *J. Opt. Soc. Am. B* **12**, 753 (1995).
3. E. Tokunaga, A. Terasaki, and T. Kobayashi, *Opt. Lett.* **17**, 1131 (1992).
4. R. Trebino, K. W. DeLong, D. N. Fittinghoff, J. N. Sweetser, M. A. Krumbugel, B. A. Richman, and D. J. Kane, *Rev. Sci. Inst.* **68**, 3277 (1997).

Photoreaction Quantum Yields of Condensed-Phase Acid Chlorides

J. B. Rowland, W. P. Hess, P. R. Winter,†§ and G. B. Ellison§*

Supported by DOE Office of Basic Energy Sciences.

*Postdoctoral Research Associate.
†Graduate Student.
§University of Colorado.

The study of condensed-phase energetic processes is vital to understanding reactions that occur on heterogeneous surfaces and in condensed media, and is relevant to environmental concerns. Unfortunately, the standard extrapolation of gas-phase results can produce poor models of condensed-phase processes and yield inaccurate results. Recently, we have shown that reaction mechanisms differ between the gas- and condensed-phase photolysis of acetyl chloride (CH_3COCl).[1,2] Here we report preliminary results of the condensed-phase reaction quantum yields for a series of acid chlorides. The results elucidate various aspects of inter- and intra-molecular effects on the condensed-phase photochemistry.

Ultraviolet photoexcitation of acetyl chloride promotes an electron from the electronic ground-state singlet (S_0) to an excited-state singlet (S_1). The ensuing condensed-phase reaction then occurs through a direct elimination mechanism that produces an $HCl \cdot H_2C{=}C{=}O$ complex arranged in a T shape. After the initial 266-nm excitation, the electronic energy (~107 kcal/mol) interconverts to S_0, producing hot acetyl chloride molecules. These hot molecules have enough energy to overcome the modest barrier (~48 kcal/mole)[3] for direct elimination of HCl.

Reaction is not the only pathway available for the photoexcited acid chloride. The absorbed energy may migrate (exciton migration), emit (fluorescence), intersystem cross, or interconvert to S_0. Although we have shown that reaction proceeds following interconversion, not all "hot" ground-state molecules necessarily undergo elimination. Vibrational relaxation may be expected to reduce the photoreaction efficiency. This "intramolecular" relaxation will depend on the matrix composition. Therefore, molecular structure, intramolecular relaxation, and intermolecular relaxation are expected to have a direct effect on the photoreaction quantum yield.

We study the photoreactions of acetyl, propionyl (CH_3CH_2COCl) and valeryl ($CH_3(CH_2)_3COCl$) chloride by measuring their elimination quantum yield using FTIR spectroscopy. Quantum yields are calculated from the IR absorption data, and are used to determine the reaction efficiency of absorbed energy in various solid samples. For example, we determine photoproduct quantum yields of acetyl, propionyl, and valeryl chlorides in neat films and in argon, krypton, and xenon matrices. The quantum yields are compared to expose intermolecular and intramolecular factors affecting photoreaction efficiency.

Matrix-isolated and neat thin films are deposited to a thickness of 1–6 μm. Samples of matrix-isolated (300:1) and neat acid chloride films are vapor-deposited onto a KBr substrate cooled to ~20 K by a closed-cycle helium cryostat. Film thickness is determined using optical interference measurements with a 633-nm helium-neon laser.[1] For photolysis with 248-nm light, an excimer laser was used to irradiate films for 1 to 5 minutes with an average pulse energy of 7 mJ at a 10-Hz repetition rate. For the 266-nm experiment, the fourth harmonic of a Nd:YAG laser was used to irradiate films for 5 to 10 minutes with an average pulse energy of 2 mJ at a 20-Hz repetition rate. Infrared spectra are taken before and after irradiation using a Fourier-transform infrared (FTIR) spectrometer at a resolution of 2 cm^{-1}. The precursor molecules and photoproducts are readily identified in the IR spectra.

The infrared spectra of matrix-isolated acetyl, propionyl, and valeryl chlorides are shown in Fig. 3.5. The CO stretch of the acid chlorides are easily identified at 1811 cm^{-1} (acetyl chloride), 1798–1848 cm^{-1} (propionyl chloride), and 1810 cm^{-1} (valeryl chloride). Spectra taken after 248-nm irradiation clearly show the consumption of the precursor acid chlorides and the emergence of photoproducts. The IR spectra of the photoproducts (HCl•ketene, HCl•methyl ketene, and HCl•propyl ketene) are identified by the CO stretching frequencies of ketene (2141 cm^{-1}), methyl ketene (2127 cm^{-1}) and propyl ketene (2122–2143 cm^{-1}), and by the HCl bands at 2686 cm^{-1} and between 2596 and 2622 cm^{-1}. All photoproducts observed are consistent with a direct elimination mechanism.

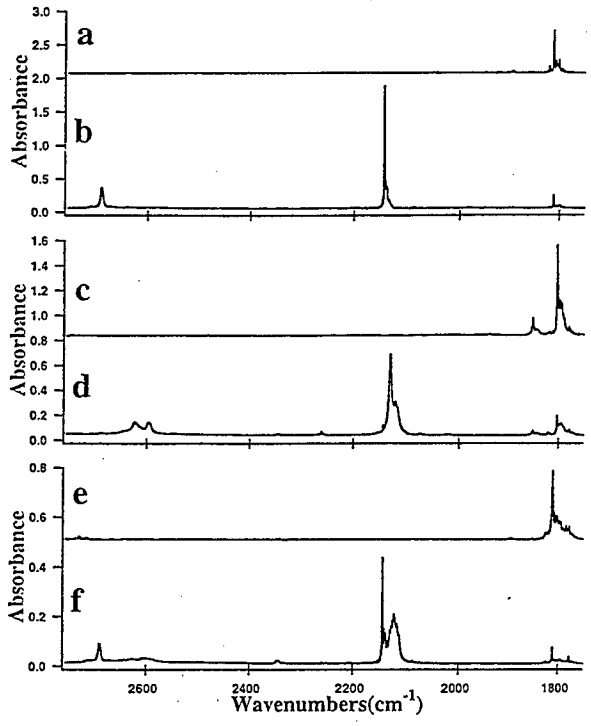

Figure 3.5. Infrared spectra of precursor (a) acetyl chloride, (c) propionyl chloride, and (e) valeryl chloride matrix-isolated in argon (300:1) at ~20 K. Photoproduct spectra of HCl, ketene (b), methyl ketene (d), and propyl ketene (f) are observed after 248-nm irradiation of each precursor.

Concentrations of precursor and photoproducts are determined from the IR spectra and the known absorption cross sections. The known precursor concentrations and absorption cross section, film thickness, and measured product concentrations are used to calculate quantum yields for photoproduct formation (Table I). Quantum yields for 248- and 266-nm irradiation are quite similar for all samples. However, the measured quantum yields are a factor of ~2 lower in neat acid chloride films than in matrix-isolated films. The results also show that the quantum yields for the photolysis of acetyl chloride are ~2 times greater than the quantum yields for the larger propionyl and valeryl chloride molecules.

The decrease in quantum yields from acetyl chloride to other acid chlorides is attributed primarily to the geometric factors and to the fact that the number of available α-hydrogen atoms is reduced from 3 to 2. It is also possible that greater vibrational state density of the longer-chain acid chlorides further reduces the quantum yield. Geometric hindrance results from a reduction in the access to the intramolecular transition state. Simply put, the α-hydrogen atoms are not initially in the right position for abstraction. We note that the quantum yields are most lowered by neat matrices, which may result from rapid relaxation of the hot ground state following S_1 to S_0 interconversion. The vibrational modes of the surrounding matrix molecules match those of the hot acid chloride providing "resonant" relaxation paths. Rare gas matrices lack the resonant vibrational modes necessary for efficient intermolecular relaxation such that greater quantum yields are observed in matrix-isolated samples.

Table I. Preliminary quantum yields for 266-nm and 248-nm photolysis of neat and argon matrix-isolated acid chlorides.

	248 nm		266 nm	
	neat	Ar matrix	neat	Ar matrix
acetyl chloride	0.21	0.43	0.20	0.44
propionyl chloride	—	0.20	0.12	0.20
valeryl chloride	0.13	0.15	0.10	0.18

Systematic error is estimated at ± 25%.

References

1. B. Rowland and W. P. Hess, *J. Phys. Chem. A* **101**, 8049 (1997).
2. S. Deshmukh, J. D. Myers, S. S. Xantheas, and W. P. Hess, *J. Phys. Chem.* **98**, 12535 (1994).
3. R. Sumathi and A. K. Chandra, *J. Chem. Phys.* **99**, 6531 (1993).

Quantum-State Resolved Products via 157-nm Photostimulated Desorption From Geologic Calcite

K. M. Beck and W. P. Hess

Supported by DOE Office of Basic Energy Sciences and the Strategic Environmental Research Development Program.

Geologic calcite is an environmentally important crystal form of calcium carbonate ($CaCO_3$). Naturally, it contains small and varying amounts of ionic impurities (e.g. Cs^{3+}, Mn^{2+}, Pb^{2+}, Mg^{2+}) which tend to replace Ca^{2+}, or lie in vacant interstitial positions within the crystal lattice. The dynamics of crystal growth are not well understood, but it is believed that the calcite crystalline plane may be stabilized by impurity ions. This may well be a reason that calcium carbonate acts to form a protective layer (caliche) which "traps" heavy metal leakage below the mixed waste storage tanks on the Hanford Reservation.

The melting point of calcite is 1339°C, reflecting its high thermodynamic stability and resistivity to chemical assault. In contrast to the stable crystalline structure, the carbonate anion (CO_3^{2-}) itself is unstable outside strongly ionic environments. These characteristics are demonstrated by the interaction of water with calcite. Stability is seen in the minute absolute solubility of calcite, 0.000014 gm/cm^3 at 0°C to 0.000018 gm/cm^3 at 100°C. Atomic force microscopy studies also suggest that within an aqueous environment the calcite surface does not play host to hydrated species, but retains the same top-lying oxygen structure of the cleaved crystal, with dissolution occurring through creation of rhombic pits.[1] The unstable nature of the carbonate anion is apparent in that most dissolved carbonate takes the forms HCO_3^- and H_2CO_3, with only ~9% of the total dissolved carbonate taking the form CO_3^{2-} in neutral water.

We pose the question, "What effect does radiation energy and crystal absorptivity have on the destructive photostimulated dissolution and desorption processes in calcite?" We begin to answer this by monitoring the desorption activity of photostimulated CO products from the calcite surface following ultraviolet and vacuum ultraviolet radiative excitation. In this study, we use low-fluence (<300 μJ/cm^2) 157-nm excimer laser radiation. This wavelength coincides with an intense absorption peak (absorption coefficient = 4.39×10^5 cm^{-1}), such that most excitation occurs near or at the crystal surface. We continue experimental studies involving PSD processes by examining laser/solid interactions following excitation of single-crystal calcium carbonate by measuring the velocity distribution and quantum-state resolved internal energy distributions of desorbed CO. Comparison is then made with the PSD results of analogous studies on calcite following 193-nm and 213-nm excitation.[2]

The experimental apparatus consists of a liquid-nitrogen-trapped diffusion-pumped ultrahigh vacuum chamber (base pressure 3×10^{-10} torr) equipped with laser access ports, and quadrupole (QMS) and time-of-flight (TOF) mass spectrometers. Prior to irradiation, the calcite sample is heated *in vacuo* to 450°C for 12 hours to reduce surface contamination and, in these experiments, allowed to cool to 295°K. CO itself does not easily adsorb to insulators and insulating oxides *in vacuo* at temperature above 180 K.

The $CaCO_3$ crystals are irradiated with 3-ns pulses of 157-nm excimer laser emission (200–300 μJ/cm^2) incident on the sample at 40° normal to the crystal face. For the detection of CO we have chosen (2+1) resonance-enhanced multiphoton ionization (REMPI). The (2+1) process involves two-photon excitation of the $B^1\Sigma \leftarrow X^1\Sigma$ transition, followed by one-photon ionization of the B state.[3]

Other work[4,5] has been conducted on complex ionic crystals like calcite, which are interesting because their wide band-gaps readily allow optical interrogation of the electronic transitions between the highest valence levels and the lowest unoccupied conduction band(s). Many exhibit what has been interpreted as strong and separated "molecular" and "charge transfer" UV absorptions associated with these transitions (e.g. $NaNO_3$). In Fig. 3.6 we see, in contrast, that calcium carbonate shows a continual rise in optical absorption up to ~8 eV with no identifiably separate "molecular" band. While no definitive measurements have been done, reflection electron energy-loss spectroscopy (REELS) measurements on calcite have estimated the onset of the band gap at $E_g = 6.0 \pm 0.35$ eV, and associates a small loss feature just above 5 eV with a surface state.[1]

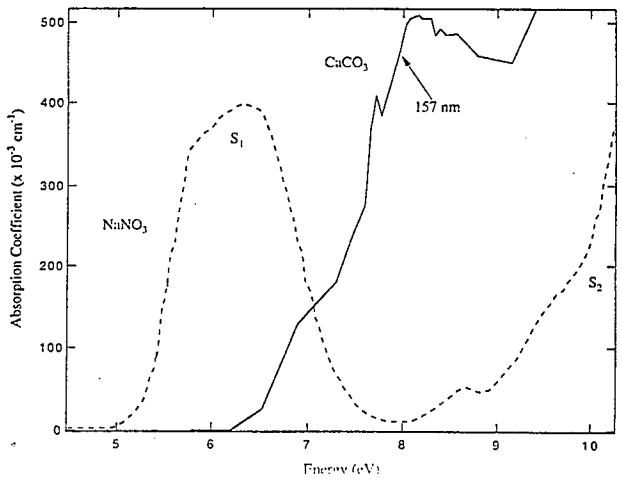

Figure 3.6. Graphic representation of numerically tabulated optical absorption spectra of calcium carbonate (—) and sodium nitrate (----) single crystals in the energy range between 4.5 eV and 10.2 eV (adapted from Ref. 6). The broad sodium nitrate feature, S_1, near 6.25 eV has been identified as the "molecular" ($\pi^* \leftarrow \pi$) transition of the nitrate anion.[6] The "charge transfer" band in sodium nitrate, S_2, is partially visible at about 10 eV. In contrast, there is no separate optical absorption assigned to the ($\pi^* \leftarrow \pi$) transition in calcium carbonate.

The emission of CO products appears with initial irradiation at 157 nm, but the intensity decreases slowly and asymptotically to ~75% of the initial value after considerable exposure (~one week). No dramatic growth in CO desorption products occurs after repeated irradiation, unlike non-resonant excitation of sodium nitrate at 248 nm and 266 nm, which displays an increase in desorption yield following an incubation period, often interpreted as indicating that photostimulated desorption depends on the buildup of additional surface defect sites. The absence of such a process in calcite might be taken to imply that defect-driven desorption mechanisms from photoproduced defect sites do not play a dominant role.

An approximate material removal rate can be estimated through comparison of the TOF signal intensities obtained from CO desorbed from calcite and those obtained from the gas sample with a known number density (3.0×10^{-8} torr). The calcite surface density is ~6×10^{14} molecules/cm^2 ($\rho_{calcite}$ = 2.71 gm/cm^3), and we assume a plume volume of 0.014 cm^3 at the moment the plume is probed. From these values we estimate that less than 0.01% of a monolayer is removed per laser pulse.

Figure 3.7 represents the velocity distribution for desorbed CO ($v = 0, J = 5$) at a substrate temperature of 295 K. The TOF spectra are fit to a half-range Maxwell-Boltzmann velocity distribution function.[6] The TOF spectra can be fit with a translational temperature, T_{trans} = 105 ± 15 K. Previously published work showed that the fitted Doppler widths of the recorded CO rotational spectra could be used to calculate a translational distribution for desorbed CO normal to the surface if the angular distribution of CO was known. We conducted a cursory study which showed a narrow angular distribution of desorbed CO ± 20° to normal.

Figure 3.8 displays the resolved Q-branch [CO (0,0) $B^1\Sigma \leftarrow X^1\Sigma$] of product CO obtained following PSD from room temperature $CaCO_3$. The appearance of Q-band structure is not unexpected, since the difference between the X and B state rotational constants causes a splitting of Q-branch transitions that increases with J. This splitting is greater than the combined Doppler and laser bandwidths for $Q(J) > 7$ and approaches 1.0 cm^{-1} for $Q(J) = 20$. Superimposed upon Fig. 3.8 is a spectrum simulating a thermal distribution at 295 K for CO rotational states up to the $Q(J) = 23$. The rotational spectra of CO products, in contrast to the translational energy, appears similar to a thermal

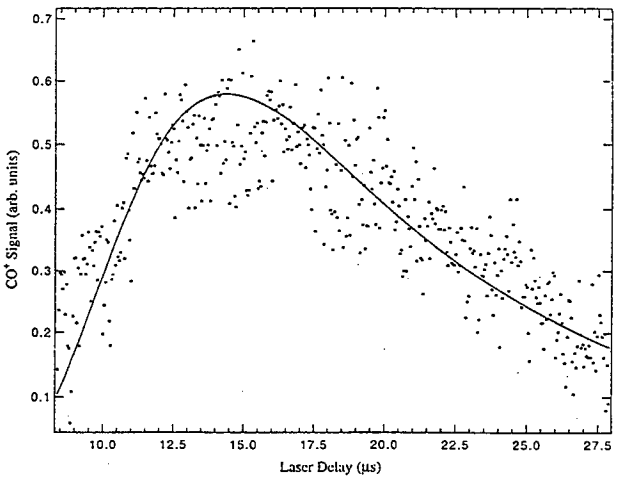

Figure 3.7. Velocity dependence of CO desorbed from $CaCO_3$. The solid curve represents the best fit to a translational temperature, T_{trans} = 105 ± 20 K, using a half-range Maxwell-Boltzmann velocity distribution function.

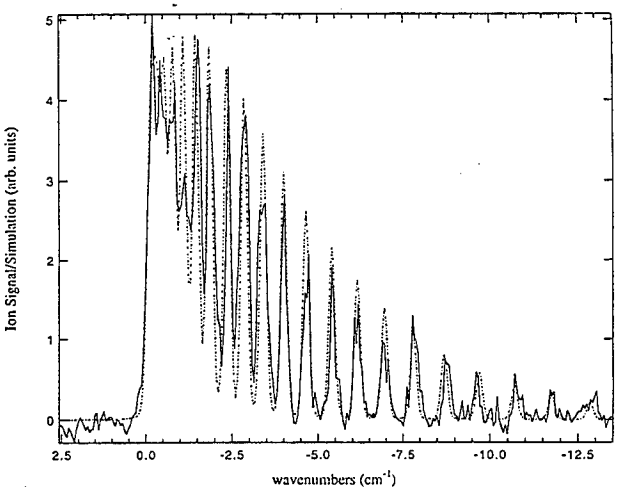

Figure 3.8. Rotationally-resolved Q-branch spectra of desorbed CO. The (2+1) REMPI scheme contains the entire Q-band within a narrow frequency range of <20 cm^{-1}. The solid and dashed lines represent the recorded spectra and the 295 K simulated fit, respectively.

simulation done at the substrate temperature of 295 K. The parameters used to simulate the spectra of Fig. 3.8 are a temperature of T = 295 K, a two-photon bandwidth of 0.084 cm^{-1}, and a Doppler width of 0.087 cm^{-1}.

The similar velocity and energy state distributions of CO desorbed from calcite at 157 nm, 193 nm, and 213 nm leads us to conclude that the products result from the decomposition of unique surface species or states. Furthermore, it is likely that the details of the excited-state electronic structure near or within the bandgap (i.e. direct "excitonic excitation") and the excited state electronic structure enmeshed in the "charge-transfer" band determine the details of the respective diatomic product state distributions.

For example, periodic Hartree-Fock density-of-states calculations for bulk and clean slab surfaces of a $NaNO_3$ suggest that because the upper states are generated solely from nitrogen and oxygen orbital contributions, there is no overlap between sodium and nitrogen or oxygen orbitals. Excitation of this band might be characterized by nitrate anion "molecular" transitions as assigned in the optical absorption spectrum.[6]

In contrast, recently calculated projected-density-of-states spectra of the lowest unoccupied band in $CaCO_3$ show a much broader band than those seen in $NaNO_3$, with a low-energy tail region that contains significant contributions from carbon orbitals and weaker contributions from oxygen and calcium orbitals.[7] This tail region is connected to an upper, broader band which is dominated by calcium 4*s* orbitals. This indicates that the lowest-energy transition in $CaCO_3$ is likely to show more "charge-transfer" character. The lowest-energy transition in $CaCO_3$ has not been assigned experimentally.

This suggests that the differences in the PSD of calcite and "molecular ionic" crystals, such as sodium nitrate, could arise from the different nature of their respective excited states. Furthermore, the decay of a calcite surface species or states, possibly arising as a result of the high degree of orbital mixing, produce CO desorption products with similar energy distributions over a range of excitation wavelengths and absorption depths. The variations in orbital mixing between the lowest tail region and the broader upper band region in calcite absorption may give rise to the subtle differences in the observed state distributions. The photostimulated desorption of CO from calcite has prompted several projects. We are extending the present experimental study to different substrate temperatures, and other desorption products.

References

1. Y. Liang, A. S. Lea, D. R. Baer, and M. H. Engelhard, *Surf. Sci.* **351**, 172 (1996); Y. Liang, D. R. Baer, J. M. McCoy, J. E. Amonette, and J. P. LaFemina, *Geochim. Cosmochim. Acta* **60**, 4883 (1996).
2. K. M. Beck, D. P. Taylor, and W. P. Hess, *Phys. Rev. B* **55**, 13253 (1997).
3. P. J. H. Tjossem and K. C. Smyth, *J. Chem. Phys.* **91**, 2041 (1989).
4. R. A. Bradley, E. Lanzendorf, M. I. McCarthy, T. M. Orlando, and W. P. Hess, *J. Phys. Chem.* **99**, 11715 (1995).
5. D. R. Ermer, J.-J. Shin, S. C. Langford, K. W. Hipps, and J. T. Dickinson, *J. Appl. Phys.* **80**, 6452 (1996).
6. H. Yamashita, *J. Phys. Soc. Jpn.* **33**, 1407 (1972); H. Yamashita and R. Kato, *J. Phys. Soc. Jpn.* **29**, 1557 (1970).
7. K. M. Beck, M. I. McCarthy, and W. P. Hess, *J. Electron. Materials* **26**, 1335 (1997).

Low-Energy Electron-Stimulated Processes in Nanoscale Ice Films

M. T. Sieger, W. C. Simpson,**
R. G. Tonkyn, and T. M. Orlando

Supported by DOE Office of Basic Energy Sciences.

*Postdoctoral Research Associate.

We have a mutli-task program directed toward understanding nonthermal interfacial processes. In particular, we study low-energy (5–150 eV) electron and ultraviolet/vacuum ultraviolet (6–12 eV) photon-stimulated desorption, dissociation, and inelastic and reactive scattering on/in molecular thin-films of ice. We have carried out a series of low-energy electron-stimulated desorption (ESD) experiments on nanoscale amorphous and crystalline ice films. Our approach allows us to probe the details of radiation damage of wet interfaces, and the use of amorphous ice may allow us to extrapolate to radiation damage events that occur in the liquid state.

The bulk and surface properties of ice have been investigated with a wide variety of probes, including photoemission, infrared spectroscopy, electron diffraction, x-ray diffraction, thermal desorption, and electron energy-loss spectroscopy. ESD is a very sensitive and ultrafast local-probe of the surface terminal sites and local scattering potential. Therefore, we have carried out ESD studies on nanoscale ice films as a function of ice-film temperature, phase, and thickness. In FY97, we specifically studied the low-energy (5–100 eV) ESD of D^+ and D^- from thin (1–40 ML) D_2O films vapor-deposited on a Pt(111) substrate. We have also investigated the detailed mechanism of the stimulated production of molecular oxygen during electron irradiation of ice films. The latter is of considerable interest to the radiation chemistry, planetary, space, and astrophysics communities.

1. The Electron-Stimulated Desorption of D^+ from D_2O Ice: Surface Structure and Electronic Excitations[1]

We have completed a study of the electron-stimulated desorption of deuterium cations (D^+) from thin (1–40 monolayer) D_2O ice films vapor-deposited on a Pt(111) substrate. Measurements of the total yield and velocity distributions as a function of temperature (90–200 K) show that the D^+ yield changes with film thickness, surface temperature, and phase. We observe two energy thresholds for cation emission, near 25 and 40 eV, which are weakly dependent upon the ice temperature and phase. The cation time-of-flight (TOF) distribution is at least bimodal, indicating multiple desorption channels. A decomposition of the TOF distributions into "fast" and "slow" channels shows structure as a function of excitation energy, film thickness, and temperature. Figure 3.9 shows the temperature dependence of the D^+ yield from 40 ML of non-porous amorphous and polycrystalline ice on Pt(111). The D^+ yield generally increases with temperature, with an onset near 120 K on amorphous ice, and near 135 K on crystalline ice. The amorphous–crystalline phase transition at ~162 K causes a drop in total desorption yield.

The data collectively suggest that a thermally activated reduction of surface hydrogen bonding increases the lifetime of the excited states responsible for ion desorption, and that these lifetime effects are strongest for excited states involving a_1 bands. The process by which H bonds begin to break may be unique to the surface or may be related to transitions in the bulk

2. Effect of Surface Roughness on the Electron-Stimulated Desorption of D^+ from Microporous D_2O Ice[2]

The electron-stimulated desorption of D^+ from micro-porous D_2O films condensed on Pt(111) has

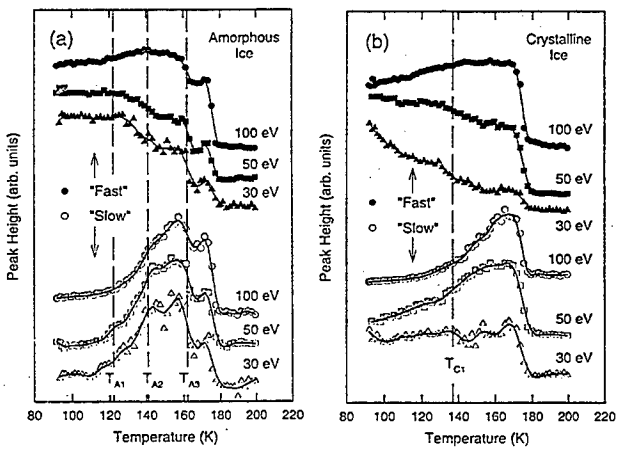

Figure 3.9. The temperature dependence of the D^+ yield from 40 ML of non-porous amorphous (grown at 110K) and polycrystalline (grown at 155K) ice on Pt(111).

been investigated. The total D^+ yield as a function of temperature from 90–180 K depends sensitively on the film roughness, surface temperature, and ice phase. In particular, we observe an irreversible increase in the cation yield as the micro-porous thin film is heated from 90 to 120 K, which we associate with a decrease in the surface roughness as the micropores collapse. We present evidence which suggests that the number of surface sites available for emission, the surface roughness, and the reneutralization or reactive scattering of the D^+ desorbate play major roles in determining the ion yield. A simple model which qualitatively addresses the role of surface roughening on ESD ion yields shows good agreement with the data, Fig. 3.10.

We use a model of the form $I = Ae^{-\gamma A}$, where A is the surface area and the exponential reflects the ion removal probability, which is proportional to the surface area. The surface area is assumed to depend on film thickness as $A(t) = 1 + \alpha(1 - e^{\beta t})$, where the smooth film is normalized to unit area, α is the additional surface area due to roughness and β governs how quickly the film reaches an equilibrium roughness with thickness. For the data in Fig. 3.10, the model gives the best-fit parameters α, β, and γ = 1.87, 0.08, and 0.64, respectively. These values are consistent with the known properties of vapor-deposited ice.

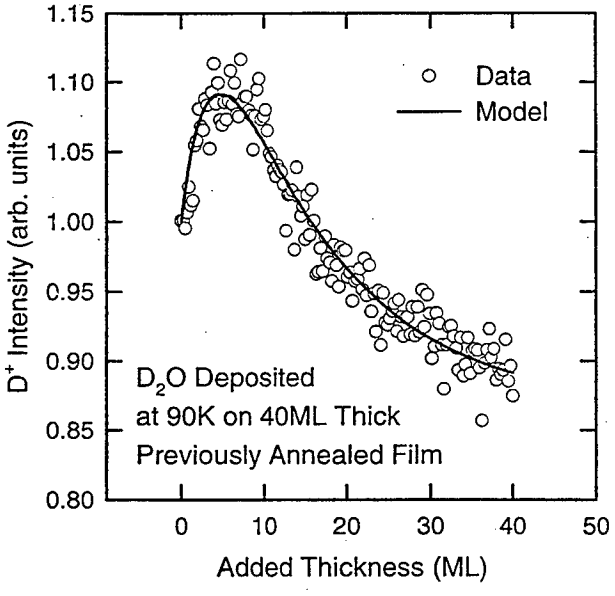

Figure 3.10. The circles represent the total D^+ yield as a function of added film thickness for D_2O deposited at 90 K on a 40-ML-thick ice film which had been previously annealed to 125 K. The data have been normalized to zero added thickness. The incident electron energy is 100 eV. The solid line is the best fit model of competing surface area–surface attenuation effects.

3. Electron-Stimulated Desorption of D^- (H^-) from Condensed D_2O (H_2O) Films[3]

The electron-stimulated desorption of D^- and H^- ions from condensed D_2O and H_2O films was investigated. Three low-energy peaks are observed in the ESD anion yield, which are identified as arising from excitation of $^2B_1$, $^2A_1$, and $^2B_2$ dissociative electron attachment (DEA) resonances. Additional structure is observed between 18 and 32 eV, which may be due to ion-pair formation or to DEA resonances involving the $2a_1$ orbital. The ion yield resulting from excitation of the $^2B_1$ resonance increases as the film is heated. We attribute the increase in the ion yield to thermally-induced hydrogen-bond breaking near the surface, which enhances the lifetimes of the excited states that lead to desorption. This is demonstrated in Fig. 3.11(a), which shows the H^- signal vs. temperature (filled circles) for an incident electron energy of 7.5 eV, collected from ~3 ML of amorphous ice grown at ~20K. Also plotted in Fig. 3.11(a) is a simulated temperature-programmed desorption (TPD) spectrum from this film (solid line), which was calculated (heating rate 0.007 K/s) using desorption rates and parameters measured by Smith et. al.[4] Figure 3.11(b) shows the D^- signal vs. temperature (filled circles) for an incident electron-energy of 7.2 eV, collected from a 60-ML polycrystalline D_2O film grown at 155 K. Also plotted is an experimentally obtained TPD spectrum, collected using the heating rate of 0.133 K/s.

4. Dissociative Electron Attachment in Nanoscale Ice Films: Temperature and Morphology Effects[5]

The electron-stimulated desorption of D^- ions from condensed D_2O films is investigated. Three low-energy peaks are observed in the D^- yield, which are identified as arising from excitation of $^2B_1$, $^2A_1$, and $^2B_2$ dissociative electron attachment resonances. The resonance energies and ion yields vary with the thickness, temperature and morphology of the D_2O film. Below 60 K, the work function of the ice films changes with temperature and the DEA resonances shift in energy. The D^- ESD yield generally increases with temperature,

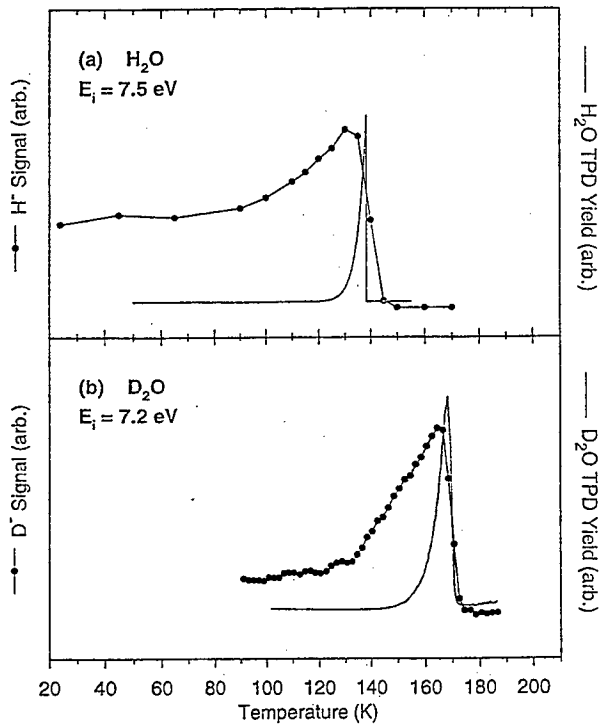

Figure. 3.11. (a) H^- signal vs. temperature (filled circles) for an incident electron energy of 7.5 eV, collected from ~3 ML of amorphous ice grown at ~20K. Also plotted is a simulated TPD spectrum from this film (solid line), which was calculated for the same heating rate (0.007 K/s) using desorption rates and parameters measured by Smith et al.[4] (b) D^- signal vs. temperature (filled circles) for an incident electron-energy of 7.2 eV, collected from a 60-ML polycrystalline D_2O film grown at 155 K, with an experimentally-obtained TPD spectrum collected using the heating rate of 0.133 K/s.

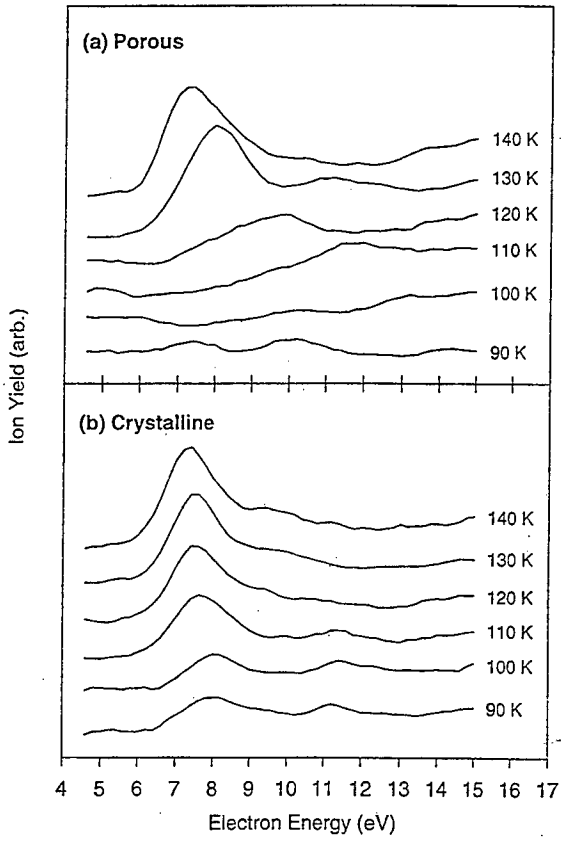

Figure 3.12. D^- ESD yield dependence on ice morphology and temperature. (A) D^- signal vs. incident electron energy, collected at various temperatures from 60-bilayer (ML) amorphous ice films grown at 90K. (B) D^- signal vs. electron energy, collected at various temperatures from 60-bilayer (ML) crystalline ice grown at 155 K. Individual scans are offset vertically for display and are labeled with the temperature at which they were collected.

but it deviates noticeably from this trend at temperatures corresponding to structural phase transitions in bulk ice. The ($^2B_1$) D^- temperature dependence is remarkably similar to that observed for D^+ ESD from D_2O ice, even though the two originate from different electronic excitations. These results are discussed in terms of changes in the hydrogen bonding network, which changes the lifetime of the predissociative states that lead to ESD, and which also allows for the reorientation of surface molecules. Figure 3.12 depicts the D^- ESD yield dependence on ice morphology and temperature. Figure 3.12(a) shows the D^- signal vs. incident electron energy, collected at various temperatures from 60-bilayer (ML) amorphous ice films grown at 90 K; figure 3.12(b) shows the D^- signal vs. electron energy, collected at various temperatures from 60-bilayer (ML) crystalline ice grown at 155 K.

5. Dissociative Electron Attachment in Nanoscale Ice Films: Thickness and Charge Trapping Effects[6]

The yield and kinetic energy (KE) distributions of D^- ions produced via dissociative electron attachment resonances in nanoscale D_2O ice films are collected as a function of film thickness. The $^2B_1$, $^2A_1$, and $^2B_2$ DEA resonances shift to higher energies and their D^- yields first increase and then decrease as the D_2O films thicken. The D^- kinetic energy distributions also shift to higher energy

with increasing film thickness. We interpret the changes in the DEA yield and the D^- KE distributions in terms of modifications in the electronic structure of the surface of the film as it thickens. A small amount of charge build-up occurs following prolonged electron-beam exposure at certain energies, which primarily affects the D^- KE distributions. Charge trapping measurements were also carried out in collaboration with Prof. Leon Sanche of the University of Sherbrooke. Briefly, charge trapping was measured using a refined low-energy electron transmission (LEET) technique, in which a magnetically-collimated electron beam of variable energy impinges on a D_2O film condensed either on a Kr film or a Pt substrate at 23 K. When electrons are trapped in the ice film, the LEET spectrum shifts to higher voltage by a potential barrier ΔV. The charge-trapping coefficient $A_s = d(\Delta V)/dt$ is obtained by collecting consecutive LEET spectra, from which an accurate measure of the trapping cross section can be made. The charge-trapping measurements indicate that an enhancement in the trapping cross section occurs at energies near zero and between 10 eV. This is related to DEA and is illustrated in Fig. 3.13, which shows the charge trapping coefficient for 5 bilayers of H_2O on a Pt substrate at 23 K, and for 0.3 bilayers of H_2O adsorbed on 15 monolayers of Kr at 23 K, as a function of incident electron energy.

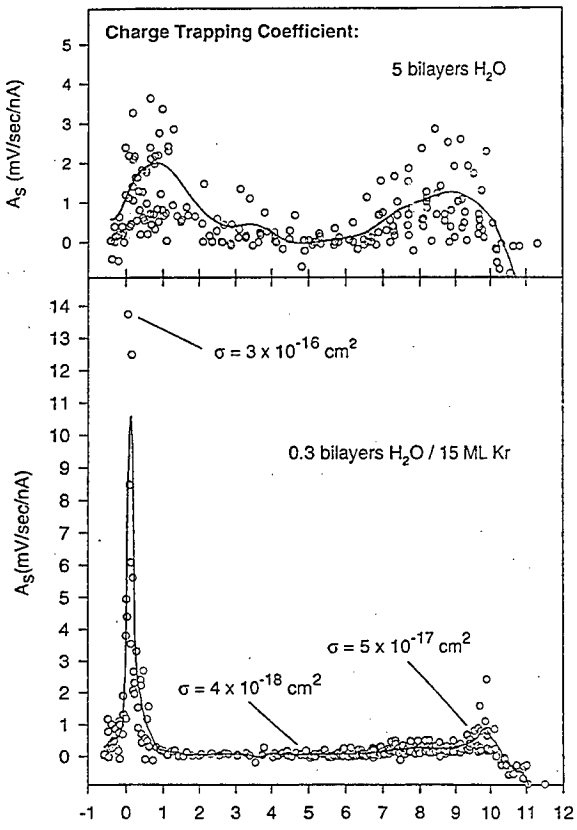

Figure 3.13. Charge-trapping coefficient for 5 bilayers of H_2O on a Pt substrate at 23 K, and for 0.3 bilayers of H_2O adsorbed on 15 monolayers of Kr at 23 K, as a function of incident electron energy. Since the data points are somewhat scattered, a smooth curve is added in each case to guide the eye.

6. The Role of Excitons and Substrate Temperature in Low-Energy (5–50 eV) Electron-Stimulated Dissociation of Amorphous D_2O Ice[7]

We have studied the interaction of low-energy (5–50 eV) electrons with nanoscale (~10 ML) ice films by probing the yields and quantum-state distributions of the neutral dissociation products using laser resonance-enhanced multiphoton ionization spectroscopy. In particular, we have observed the electron-stimulated desorption of D (^2S), O ($^3P_2$), and O ($^1D_2$) from amorphous D_2O films. These products are observed at threshold energies (relative to the vacuum level) of ~6.5–7 eV, and desorb with low kinetic energies (~60–80 meV), which are independent of the incident electron energy. We associate the ESD of atomic fragments from ice with dissociation of Frenkel-type excitons of $4a_1$ character which are near the bottom of the ice conduction band. These excitons can be created either directly or indirectly via electron–ion recombination. Changing the surface temperature from 88 to 145 K results in an increase in the thermal component. This is shown in Fig. 3.14. The distributions have both thermal and nonthermal components, and the dotted line represents the fit to the TOF data obtained at an ice temperature of 125 K. Note that the thermal distribution increases considerably with increasing temperature. We suggest that the change in neutral yield with substrate temperature results from a combination of (i) increased electron–ion recombination, (ii) exciton transport to the near-surface region, and (iii) dissociation followed by inelastic scattering and desorption.

7. Production of O_2 in Planetary Ices via Electronic Excitation[8]

The signature of condensed O_2 has been reported in recent optical reflectance measurements of the

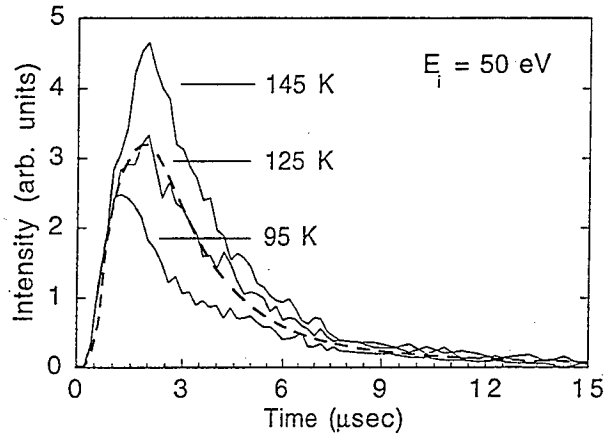

Figure 3.14. The D (^2S) time-of-flight distributions for several substrate temperatures. The distributions have both thermal and nonthermal components. The dotted line represents the fit to the TOF data obtained at an ice temperature of 125 K. Note that the thermal distribution increases considerably with increasing temperature.

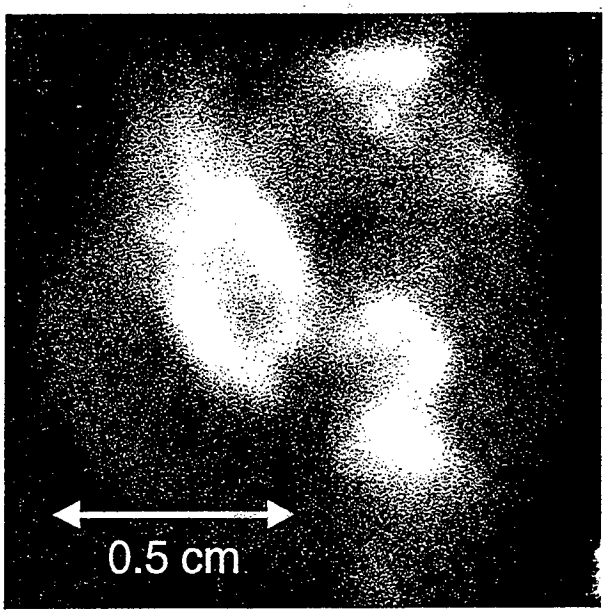

Figure 3.15. Image of the O_2 yield as a function of beam spot position on an ice/Pt(111) sample.

Jovian moon Ganymede, and a tenuous oxygen atmosphere has been observed surrounding Europa. Both moons, which are composed largely of water ice, are constantly bombarded by the energetic particles (ions, electrons, and ultraviolet photons) comprising Jupiter's magnetosphere. Thus, production of O_2 has been attributed, in part, to the electronic sputtering and radiolysis of the icy satellite surfaces. Yet the mechanisms behind O_2 formation remain unclear. We have demonstrated that O_2 is formed by electronic excitation of a stable precursor, probably HO_2, with an energy threshold of ~9 ± 2 eV. The O_2 production cross section increases over the temperature range typical of the Jovian system (90–150 K), and does not involve significant O-atom diffusion on or in the ice. We present a precursor dissociation model for O_2 formation and suggest a new interpretation of thermal effects in ice sputtering.

To demonstrate that a precursor is needed to form O_2, we exposed a region of a fresh ice sample (selected to spell out "O_2" using the e-beam steering optics) to a 10^{15} cm^{-2} dose of 50 eV electrons, representative of the dose received in less than a day at Ganymede due to incident ions and secondaries. After the initial exposure, the electron-beam was rastered quickly over the sample, and the O_2 yield was measured as a function of the beam spot position (Fig. 3.15). Bright and dark areas correspond to high and low O_2 yields respectively. The sample is 1 cm in diameter, and the electron beam has a spot size of about 0.4 mm^2. The image of the O_2 yield as a function of beam spot position on an ice/Pt(111) sample is shown in Fig. 3.15.

References

1. M. T. Sieger, W. C. Simpson, and T. M. Orlando, *Phys. Rev.* **B56**, 4925 (1997).
2. M. T. Sieger and T. M. Orlando, *Surf. Sci.* **390**, 92 (1997).
3. W. C. Simpson, L. Parenteau, R. S. Smith, L. Sanche, and T. M. Orlando, *Surf. Sci.* **390**, 86 (1997).
4. R. S. Smith *et al.*, *Surf. Sci. Lett.* **367**, L13 (1996).
5. W. C. Simpson, M. T. Sieger, T. M. Orlando, K. Nagesha, L. Parenteau, and L. Sanche, *J. Chem. Phys.* **107**, 8668 (1997).
6. W. C. Simpson, T. M. Orlando, K. Nagesha, L. Parenteau, and L. Sanche, *J. Chem. Phys.*, in press.
7. T. M. Orlando and G. A. Kimmel, *Surf. Sci.* **390**, 79 (1997).
8. M. T. Sieger, W. C. Simpson, and T. M. Orlando, submitted to *Nature*.

Nonthermal Surface/ Interface Processes

M. T. Sieger, W. C. Simpson,* R. G. Tonkyn, and T. M. Orlando*

Supported by DOE Office of Basic Energy Sciences.

*Postdoctoral Research Associate.

The creation of electron-hole pairs and the formation of excitons can lead to efficient desorption and degradation of materials and interfaces. We have carried out photon-stimulated desorption and low-energy electron-stimulated damage studies of wide-band-gap materials such as $NaNO_3$ and ZrO_2. We have also begun work which looks specifically at initial-state effects in electron-stimulated desorption with the intent of developing a site-specific probe of defect structure on oxide materials. Developing an understanding of such processes is critical if one hopes to unravel some of the complicated events that occur during the interaction of high-energy radiation (such as that produced by radioactive decay events) with solids and mixed-phase interfaces.

1. The Photon-Stimulated Desorption of Cations from Yttria-Stabilized ZrO_2 (100) Crystals[1]

The positive ion yield resulting from the interaction of a pulsed 266-nm laser with yttria-stabilized cubic zirconia crystals has been investigated. Although the photon energy (4.66 eV) is well below the nominal gap energy for ZrO_2 (5.0–5.5 eV), efficient photon-stimulated ion desorption (PSD) of trace impurities such as sodium and potassium occurs at laser fluences as low as 0.8 MW/cm^2. The PSD of Y^+, Zr^+, YO^+ and ZrO^+ begins at ~2.5 MW/cm^2, which we interpret as the onset of laser ablation. Above ~3 MW/cm^2, mass spectra of the desorbing cations resembles those obtained via secondary-ion mass spectrometry (SIMS). The similarity between the laser ablation and SIMS data demonstrates the importance of surface electronic structure effects in photon induced degradation of this material.

2. Photoemission, Photon-, and Electron-Stimulated Desorption of Yttria-Stabilized Cubic ZrO_2 (100) Surfaces[2]

It has been suggested that low-energy secondary electrons generated in Zr-based alloys and oxides by ionizing radiation lead to its degradation. However, the mechanisms are unknown. We have conducted a set of controlled experiments to investigate the role of low-energy electrons in the radiation damage of zirconia. Our approach is to take a well-characterized ZrO_2 surface and submit it to bombardment by a monochromatic beam of low-energy electrons or photons. Measurements of the O^+ desorption threshold and kinetic energy distributions, coupled with photoemission measurements of the electronic structure of the surface, enable the identification of the excitations that result in oxygen removal from the ZrO_2 surface. For both crystalline and amorphous ZrO_2, the O^+ photon- and electron-stimulated desorption thresholds are at 30 eV, corresponding to the removal of a Zr (4*p*) electron, and the ions have ~2 eV kinetic energy. These findings are consistent with the Knotek-Feibelman mechanism for stimulated ion desorption from metal oxides, in which the ionization of a shallow metal cation core level, followed by interatomic Auger decay, leads to the formation and rapid ejection of O^+ ions from the surface. The threshold energy for the electron-stimulated production and desorption of O^+ from amorphous and cubic zirconia is shown in Fig. 3.16 (top). The threshold energy for photon-stimulated production and desorption of O^+ form amorphous ZrO_2 thin films and cubic zirconia is shown in Fig. 3.16 (bottom).

3. The Role of Diffraction in Electron-Stimulated Desorption[3]

Electron-stimulated desorption is a popular experimental technique in which excitations in a solid, caused by an incident beam of electrons, leads to the ejection of atoms and molecules from a surface. ESD is a process of great interest for many diverse disciplines, from astrophysics to semiconductor device processing. Currently-popular models of ESD describe the desorption process with a two-step model. The vast majority of effort in experimental and theoretical ESD has focused on final state interactions on ESD yields. However, at the energies of interest for most ESD thresholds (10–100 eV), the elastic electron scattering amplitudes in the solid are large, and are comparable to the inelastic scattering cross-sections. The strength of the elastic scattering is the basis for such well-known experimental techniques as low-energy electron diffraction (LEED) and photoelectron diffraction (PED). The interference of the direct (or unscattered) electron wave

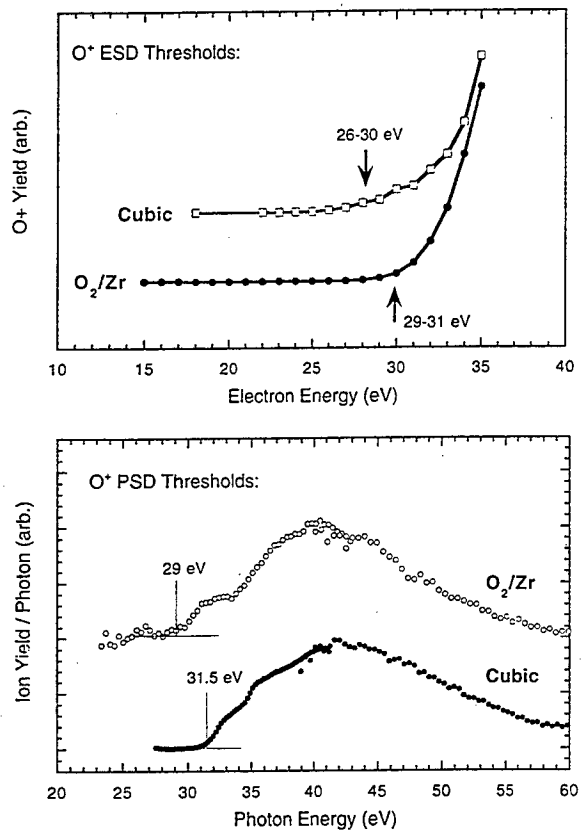

Figure 3.16. (Top) the threshold energy for the electron-stimulated production and desorption of O^+ from amorphous and cubic zirconia. (Bottom) the threshold energy for photon-stimulated production and desorption of O^+ form amorphous ZrO_2 thin films and cubic zirconia.

with the elastically scattered waves can be thought of as a standing wave at the surface, with spatially localized maxima and minima in the incident electron density. Since the probability of the inelastic scattering event which leads to desorption is proportional to the incident electron density at the absorber, *the ESD cross section depends upon the local atomic structure and the k-vector of the incident wave.* The total desorption yield, then, should carry information about the bonding geometry of the desorbate *before excitation*—this is an important distinction from ESD ion angular distributions (ESDIAD), which measures the desorption trajectories of the *excited* species, and may not necessarily reflect the true ground-state bonding geometry. We have developed a multiple-scattering theory, in collaboration with Prof. John Rehr, Department of Physics, University of Washington, of electron diffraction effects in ESD.

References

1. D. P. Taylor, K. Knutsen, W. C. Simpson, M. A. Henderson, and T. M. Orlando, *Appl. Surf. Sci.*, in press.
2. W. C. Simpson, W. Wang, J. A. Yarmoff, and T. M. Orlando, in preparation for *Phys. Rev. B.*
3. M. T. Sieger, G. K. Schenter, and T. M. Orlando, in preparation for *Phys. Rev. B*

Production of $O(^3P_j)$ and $NO(^2\Pi)$ from Low-Energy (5–100 eV) Electron Impact on Solution-Grown $NaNO_3$ Single Crystals

K. Knutsen, D. Camaioni,† and T. M. Orlando*

Supported by Environmental Management Science Program (EMSP).

*Postdoctoral Research Associate.
†EHS Analytical Chemistry Group.

Neutral products of the low-energy (5–100 eV) electron-stimulated degradation of solution-grown $NaNO_3$ single crystals are identified via quadrupole and laser resonance enhanced multiphoton ionization (REMPI) spectroscopy. The yields, threshold energies, velocity distributions, and internal state distributions are determined for the $O(^3P_j)$ and $NO(X^2\Pi)$ products, which result directly from electron impact. Other neutrals detected include O_2 and NO_2. These latter products are primarily produced indirectly from recombination of O atoms with O and NO. This work complements our earlier studies of the ionic and neutral products of electron-stimulated degradation[1] and photon-stimulated desorption (PSD)[2] of $NaNO_3$, and provides an important step in establishing the role of radiolysis of $NaNO_3$ in the production of N_2O in the Hanford mixed (radioactive/chemical) waste tanks.

The $NaNO_3$ crystal is heated to 423 K to maintain the surface stoichiometry and prevent charging during electron irradiation. A pulsed 6.4-eV photon or electron beam of well-defined energy strikes the $NaNO_3$ surface, releasing neutral products into the ultra-high vacuum chamber. A few millimeters from the surface, a UV laser pulse crosses the plume, selectively ionizing the neutrals via REMPI. The resulting ions are then detected with a time-of-flight mass spectrometer. Less

abundant products such as NO_2 and O_2 are detected via quadrupole mass spectrometry using phase-locked detection schemes.

The electron energy thresholds for O and NO production are both at ~(8 ± 2) eV. This energy corresponds, to within the experimental uncertainty, to either the charge-transfer band in $NaNO_3$ or direct excitation of the $\pi^* \leftarrow \pi$ band. The increase in the O and NO yields at ~15 eV likely corresponds to (i) inelastic scattering of secondary electrons, (ii) ionization of the $3a_1'$ level in NO_3^-, and (iii) the formation of two-hole states in the valence band. The time-of-flight (TOF) distributions of the $O(^3P_j)$ and $NO(X^2\Pi)$ fragments produced using either 6.4-eV photons or 100-eV electrons are shown in Fig. 3.17. Note that the TOF distributions are nearly identical, though the ESD is initiated with 100-eV electrons and the PSD with 6.4-eV photons. This implies that ESD and PSD are ostensibly the same for $NaNO_3$ and may involve the same final states.[3]

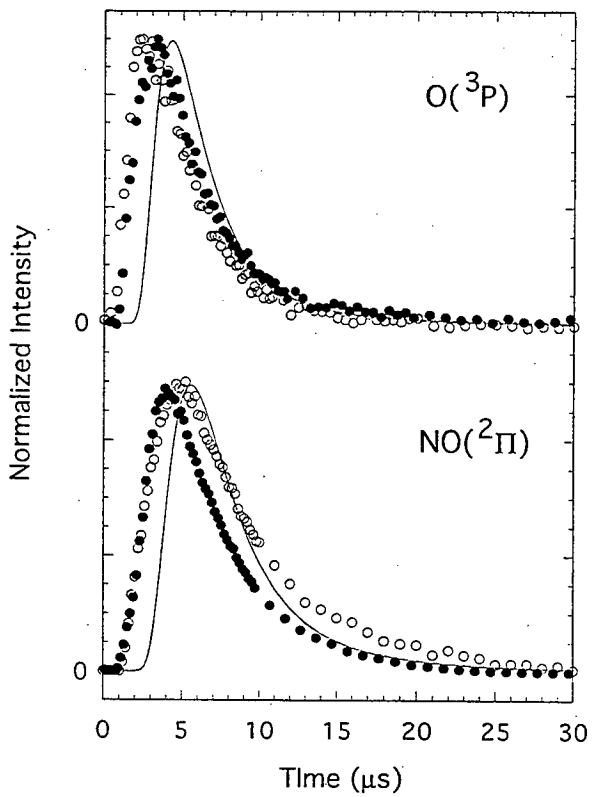

Figure 3.17. Time-of-flight distributions for $O(^3P_j)$ and $NO(X^2\Pi)$ from both 100-eV ESD (open circles) and 6.4-eV PSD (closed circles). The data were obtained using REMPI/TOF techniques and have been normalized for comparison. The solid lines are the 423-K Maxwell-Boltzmann distributions.

This experiment confirms that large amounts of O and NO are produced directly by low-energy electron impact on $NaNO_3$. Condensed-phase reactions of NO with H atoms and organic radicals are known to produce HNO. Although ion yields from ESD of $NaNO_3$ are two to three orders of magnitude smaller than neutral yields, NO^+ reacts at near the collision rate to produce HNO as well. In turn, HNO can react with HNO to produce N_2O. Thus, radiolysis of $NaNO_3$ produces reactive radicals and ions which can react with organics at the solid/liquid interface to produce a precursor to N_2O. Future experiments involving electron beam irradiation of $NaNO_3$/organic interfaces will determine the importance of this interfacial radiolysis to N_2O production in the waste tanks.

References

1. K. Knutsen and T. M. Orlando, *Surf. Sci.* **348**, 143 (1996).
2. K. Knutsen and T. M. Orlando, *Phys. Rev. B* **55**, 13246 (1997).
3. K. Knutsen and T. M. Orlando, *Appl. Surf. Sci.*, in press.

Laser-Stimulated Luminescence of Yttria-Stabilized Cubic Zirconia Crystals

N. G. Petrik, D. P. Taylor,† W. C. Simpson,† and T. M. Orlando*

Supported by Laboratory Directed Research and Development (LDRD) Funding and the Environmental Management Science Program (EMSP).

*Visiting Scientist.
†Postdoctoral Research Associate.

The laser-stimulated luminescence (LSL) of yttria-doped (9.5 mole %) cubic zirconia (yttria-stabilized zirconia, YSZ) has been investigated at three wavelengths. We observe luminescence from the decay of three excited states, at 2.70, 2.27, and 2.10 eV following 213-, 266-, and 355-nm laser excitation, respectively. These bands are shown in Fig. 3.18, and are in good agreement with previously published data[1,2] in which continuous and 0.01-ms pulsed xenon lamp excitation was utilized.

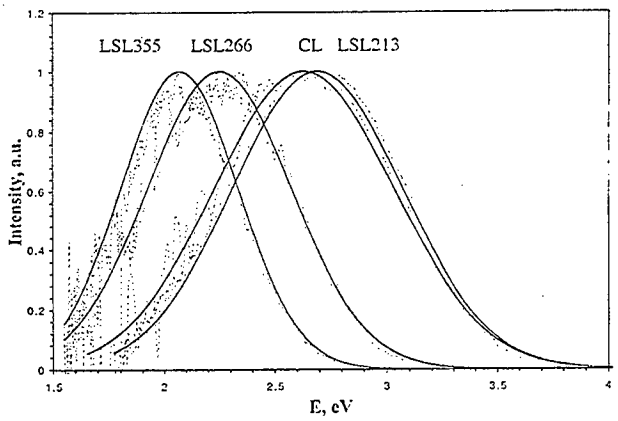

Figure 3.18. Laser-stimulated luminescence bands in yttria-stabilized cubic zirconia (100) crystals. The first band is due to excitation with 355-nm photons; the second band results from excitation using 266-nm photons. The last two bands result from above-gap excitation using 213-nm photons and 500-eV electrons, respectively.

We have also completed kinetic studies of each LSL band and have found that each exhibits a different excited-state lifetime. The emission kinetics for all of the luminescence bands are well modeled by the equation $I = I_0(1 + kt)^{-2}$, where I is the intensity and t is the decay time. This type of kinetics occurs when the luminescence is produced by the ionization followed by recombination. However, 266- and 355-nm photons have insufficient energy to produce an electron-hole pair in cubic YSZ, which has a nominal band gap of approximately 5.0–5.5 eV. Photoelectron spectra of identical ZrO_2•9.5%Y_2O_3 single crystals, which show a weak density of occupied states extending 2–3 eV above the valence band and into the middle of the band gap, reconcile this apparent discrepancy. These gap states, which can easily be ionized by 266- and 355-nm laser light to produce free carriers, are likely associated with oxygen vacancies. The temperature-dependence of the maximum luminescence intensities is well approximated by Mott's equation, $I = I_0[1 + A\exp(-Q/kT)]^{-1}$, where Q is an effective activation energy and T is temperature. The luminescence decay kinetics differ significantly from the dependencies of the maximum intensities, and can be approximated by the equation $t = t_0\exp(-T/T')$ where T' is a constant. We are continuing our investigations on the nature of the different mechanisms for generating the luminescence. Future work also involves examining how these defects and energy transport to the surface.

References

1. P. Camagni, P. Galinetto, and G. Samoggia, *Solid State Comm.* **83,** 943 (1992).
2. S. E. Paje and J. Llopis, *Appl. Phys. A* **57,** 225 (1993).

Vehicle Exhaust Treatment Using Electrical Discharge Methods

R. G. Tonkyn, S. E. Barlow, M. L. Balmer, T. M. Orlando, J. Hoard,† and M. Hemingway§*

Supported by a Cooperative Research and Development Agreement (CRADA) with the Low Emissions Technology Research and Development Partnership.

*Environmental and Health Sciences Division, Materials Group.
†Ford Motor Co.
§Delphi Energy and Engine Management Systems.

Operation of automobile engines at high air-to-fuel ratios (lean burn conditions) is an extremely desirable goal, since up to 6% of the vehicle fuel could be conserved. Unfortunately, the resulting exhaust stream is highly oxidative, and current "3-way" catalytic converters are ineffective for NO_x removal under these conditions. Although some catalysts have been shown to reduce NO_x under lean burn conditions, none exhibit the necessary activity and stability at the high temperatures and humidities found in typical engine exhaust.

The non-thermal, barrier-discharge approach to emissions treatment is an attractive alternative (or supplemental) technology with the potential to overcome some of the technical problems associated with more conventional catalysts. Although discharge chemistry has been shown to lower the concentrations of both hydrocarbons and NO in simulated exhaust, homogeneous gas-phase remediation by discharge technology alone will not have the necessary energy efficiency to be practical. However, techniques that combine discharges with surface chemistry may have this potential. Packed-bed barrier discharge reactors are well suited to take advantage of plasma–surface interactions due to the large number of contaminant-surface collisions in the bed. We present

data illustrating the importance of surface chemistry in determining the overall discharge-driven chemistry in synthetic lean-burn exhaust mixtures.

Both NO and NO_x were monitored with a chemiluminescent NO_x detector, with the difference attributed to NO_2 in the gas stream. The inlet gas contains only NO, so any difference in NO and NO_x signals indicates oxidation of NO to NO_2. Our data suggest that the NO removal rate is first order in the energy deposited per liter of gas flow. The loss of NO_x was also found to be exponential in the energy, but with a non-zero final value. By comparing the NO and NO_x signals, we can calculate the "fraction NO reduced." This is simply the total fraction of NO loss which is *not* a result of conversion to NO_2.

Molecular nitrogen product was not detected in the exhaust due to the excess of N_2 in the gas stream. However, we have investigated the possible production of other oxidative products. For example, if nitric acid were a major product, we would expect a reasonable fraction to be found in water condensed from the exhaust stream. However we typically find the water to be only slightly acidic. Using a mass spectrometer, we have found no evidence of organonitrate products. The production of N_2O is difficult to detect with a mass spectrometer due to the background (and product) CO_2 present. However, without CO_2 in the buffer gas, increases in the mass-44 signal appear to be correlated with the loss of propene signal (at mass 41) rather than with the NO or NO_x signal. This suggests that most of the product mass 44 arises from oxidation of propene to CO_2. Finally, the observed dependence of the NO reactivity on oxygen and propene is similar to those found in thermal lean NO_x reduction catalysts. It is also possible that surface adsorption could be mistaken for NO reduction, particularly on high-surface-area materials. Post-experiment thermal analysis of our most effective packing material indicates that less than 10% of the NO_x lost can be recovered as surface-bound material. The lack of observed alternative products suggests that reduction to N_2 is indeed occurring. Preliminary experiments using helium rather than nitrogen as the bath gas will soon be carried out to test for N_2 product.

We first considered as a packing material 3-mm spherical ZrO_2 beads, which have a relatively high dielectric constant (~10) and are non-porous. The fractional loss of NO_x was limited to approximately 20% in every case, but we did observe efficient oxidation of roughly 80% of the NO to NO_2. Our results using either soda glass beads or non-porous $BaTiO_3$ packings were quite similar to those for ZrO_2. We observed efficient oxidation of NO to NO_2, with only a small reductive channel. Although the energy requirements varied among these materials, the chemical similarity for these low-surface-area materials suggests that the results are indicative of the gas-phase discharge chemistry. Although a small reductive channel exists (presumably $N\bullet + NO \rightarrow N_2 + O\bullet$), the gas-phase discharge chemistry of NO under lean conditions is dominated by oxidation to NO_2. All non-porous, low surface area materials tried so far have yielded essentially the same results.

In contrast, certain zeolites have shown considerable promise for the treatment of lean-burn exhaust for NO_x emissions. In Table I we report on three different commercially available zeolites, labeled simply as materials A, B, and C to protect their exact identity for proprietary reasons. Figure 3.19 illustrates data taken with material B, the most efficient material found so far. As is evident, a significant "reductive" channel was observed.

Table I. Destruction of NO in lean exhaust with Materials A, B and C.

	T (°C)	$[NO_x]_0$	$\%[O_2]_0$	$[C_3H_6]_0$	b (J/l)	NO_x limit (fract.)
A	160	250	5.5	780	57	0.63
B	180	270	7.3	760	34	0.5
C	180	270	7.3	760	48	0.52

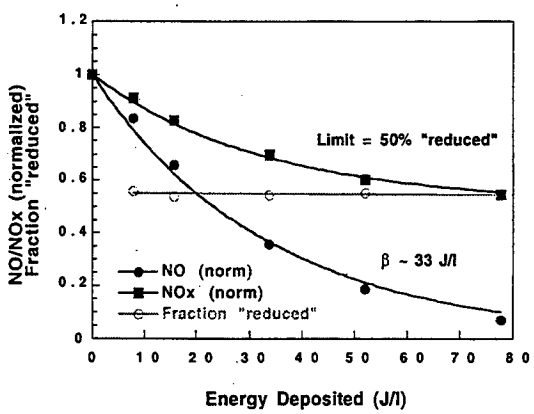

Figure 3.19. Plot of the normalized NO and NO_x concentrations vs. energy deposited for material B at 180°C.

Both the fraction reduced and the energy efficiency varied between the three zeolites, but their chemical behavior was similar. The maximum fraction of NO_x we were able to eliminate was approximately 50%. On one occasion we managed to increase the energy beyond that required to drop the NO concentration to our detection limit. No further change was observed in the NO_x concentration at higher energies.

We have studied the effect of varying either the oxygen or propene concentration in the gas stream at a constant input power. Interestingly, added oxygen improved the efficiency for both NO oxidation and reduction, but the *fraction* of the NO that was oxidized did not change. Similarly, increasing the propene concentration at constant power improved the energy efficiency with almost no effect on the fraction reduced. These results are similar to those observed in lean NO_x catalytic reduction studies, where the evidence suggests that the production of N_2 from NO under lean conditions proceeds first by oxidation of NO to NO_2, followed by reduction of the NO_2 by hydrocarbons. Increased oxygen enhances the conversion of NO to NO_2, while increased hydrocarbon concentration enhances the subsequent reduction step.

To investigate the effect of surface area, we sintered a sample of material B for 1 hour at 800°C, which reduced the BET surface area to near zero by collapsing the pores. The observed chemistry changed drastically, becoming identical to that found for non-porous ZrO_2 beads. The energy efficiency for NO loss did not change, but the NO_x destruction nearly disappeared. A similar test at 700°C only reduced the surface area by 7%, with little effect on the chemistry.

The evidence to this point suggests that the first step in our chemistry is oxidation of NO to NO_2. Certain packing materials can then catalyze the reduction of NO_2 to N_2 in the presence of propene. To confirm this sequence of reaction steps, we utilized a two-bed configuration in which the non-thermal plasma is confined to an area filled only with glass beads. We know from previous experiments with glass beads that most or all of the NO will be oxidized to NO_2, with very little loss in the total NO_x. We filled a separate region of our reactor with our most effective packing material to determine what, if any, part the discharge had on the subsequent surface chemistry. As can be seen in Fig. 3.20, the observed results are very similar: NO disappears, with approximately 50% showing up as NO_2. The other 50% is undetected, and is presumed to be reduced to nitrogen.

Not all zeolites tested worked as well in the plasma reactor as the ones illustrated here. Some zeolites were not at all effective at reducing NO_x, and in fact tended to promote coke formation in the reactor, suggesting that the discharge led to surface-bound graphite. Others acted very much like glass beads, with high oxidation of NO, but without significant NO_x loss. Finally, in the two-stage configuration we even found materials that apparently did nothing more than reduce the NO_2 almost completely back to NO.

Our data indicate that the identity of the packing material in our discharge reactor can strongly affect the chemistry observed in the treatment of lean NO_x exhaust streams. We have shown that certain zeolite materials increase what we have labeled the "reductive" channel from 20 to 50%. It is plausible, but by no means proven, that this channel is indeed reduction to N_2. The observed energy efficiency improves with increased oxygen and propene, but the branching ratio between oxidation and reduction is unchanged. We believe the mechanism involves the gas-phase oxidation of NO to NO_2 followed by surface reduction of the NO_2 by the available hydrocarbon. Experiments utilizing a two-stage reactor support this hypothesis.

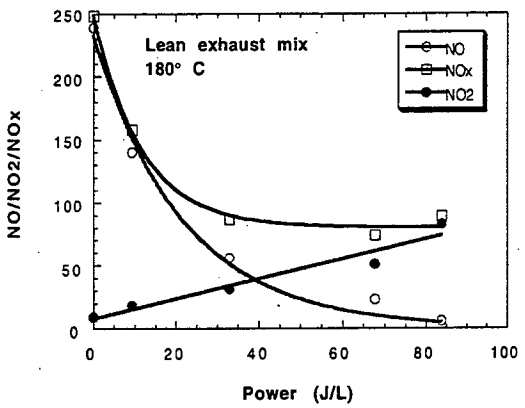

Figure 3.20. Data taken with material B in the second stage of a 2-stage reactor geometry. The discharge region contains only non-porous glass beads.

4. Cluster Models of the Condensed Phase

Cluster Model Studies of the Structure and Bonding of Environmentally-Important Materials

*L. S. Wang, J. B. Nicholas,**
S. D. Colson, H. Wu,†
X. B. Wang,†§ C. F. Ding,†§ and X. Li†

Supported by DOE Office of Basic Energy Sciences.

*EMSL Theory, Modeling, and Simulation.
†Washington State University.
§Postdoctoral Research Fellow.

Oxides of Si, Al, Mg, and Ti are major components of the earth and are important environmental materials. Their surface chemistries influence the storage and underground transport of waste materials. A major effort is being directed here to understand their surface and interface properties. We are engaged in a program to study the structure and bonding of these materials with cluster models, combining experimental and theoretical studies using anion photoelectron spectroscopy (PES) and quantum calculations. The smaller, controlled sizes of these cluster systems provide atomic-level models to enable us to better understand bulk surfaces and defect sites, and they are an excellent testing ground to benchmark theories intended for large and "real-world" systems.

A state-of-the-art magnetic-bottle time-of-flight PES spectrometer with a laser vaporization cluster source has been built for these studies. With high mass- and high electron-energy-resolution, this is a powerful apparatus for the study of clusters. In 1997, several studies were carried out on small clusters of silicon, aluminum, and titanium oxides. Preliminary studies on small alumino-silicate clusters have also been performed.

1. Si_3O_y (y = 1–6) Clusters: Models for Oxidation of Silicon Surfaces and Defect Sites in Bulk Oxide Materials[1]

The structure and bonding of a series of silicon oxide clusters, Si_3O_y (y = 1–6), have been studied using anion photoelectron spectroscopy and *ab initio* calculations. PES spectra of Si_3O_y were measured at 4.66-eV photon energy. The measured electron binding energies were compared to the calculated values, obtained by optimizing the structures of both the anions and neutral clusters (Fig. 4.1). For y = 1–3 the clusters represent the sequential oxidation of Si_3, and provide structural models for the oxidation of silicon surfaces (Fig. 4.2(a)). For y = 4–6, the clusters contain a central Si in a tetrahedral bonding environment, suggesting the onset of the bulk-like structure. Evidence is presented that suggests that the Si_3O_4 cluster (D_{2d}) may provide a structural model for oxygen-deficient defect sites in bulk SiO_2 materials (Fig. 4.2(b)).

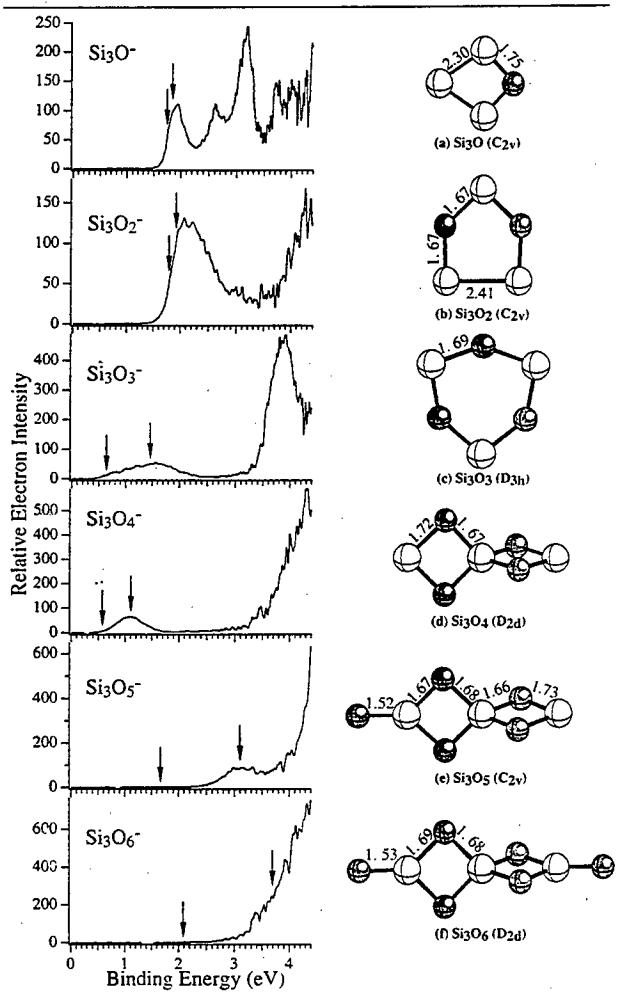

Figure 4.1. Photoelectron spectra of $Si_3O_y^-$ at 266 nm, the calculated adiabatic and vertical electron affinities (arrows), and the optimized structures for the neutral clusters. Calculations were done at the MP2/6-311+G* level. Bond lengths are in Å.

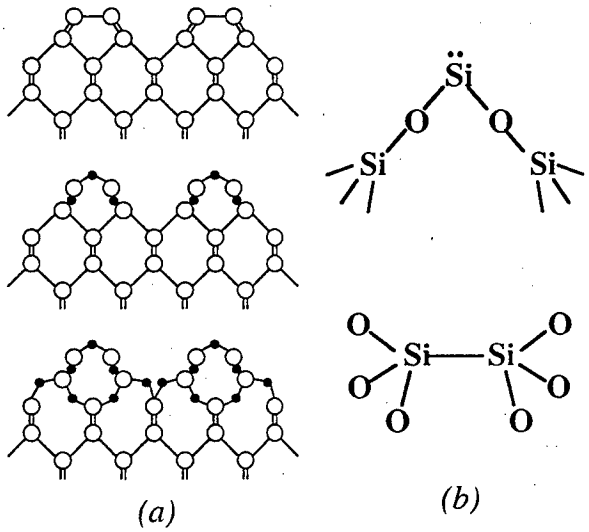

Figure 4.2. (a) Simplified structural models for oxidation of a clean Si(100)–(2×1) surface (top) by oxygen atoms with increasing coverage.[2] (b) Two atomic structure models proposed for the diamagnetic oxygen-deficient defects in bulk SiO_2. Note the similarity of the divalent Si in the top structure and that of Si_3O_4.

2. Electronic Structure of Titanium Oxide Clusters: TiO_y (y = 1–3) and $(TiO_2)_n$ (n = 1–4)[3]

The electronic structure of two series of small titanium oxide clusters, TiO_y (y = 1–3) and $(TiO_2)_n$ (n = 1–4), was studied. Vibrationally resolved spectra are obtained for TiO^- and TiO_2^-. Six low-lying electronic states for TiO are observed, with five of these excited states resulting from multielectron transitions in the photodetachment processes. TiO_2 is found to be closed-shell with a 2-eV HOMO–LUMO gap. The two lowest triplet and singlet excited states of TiO_2 are observed with excitation energies at 1.96 and 2.4 eV, respectively. TiO_3 is found to have a very high electron affinity (EA) of 4.2 eV, compared to 1.30 and 1.59 eV for TiO and TiO_2, respectively. The larger $(TiO_2)_n$ clusters are all closed-shell with HOMO–LUMO gaps similar to that of TiO_2 and with increasing EAs: 2.1 eV for n = 2, 2.9 eV for n = 3, and 3.3 eV for n = 4 (Fig. 4.3). The small HOMO–LUMO gaps for the clusters compared to that of bulk TiO_2 are attributed to the low coordination number of the clusters (4, see Fig. 4.3) compared to that of the bulk (6).

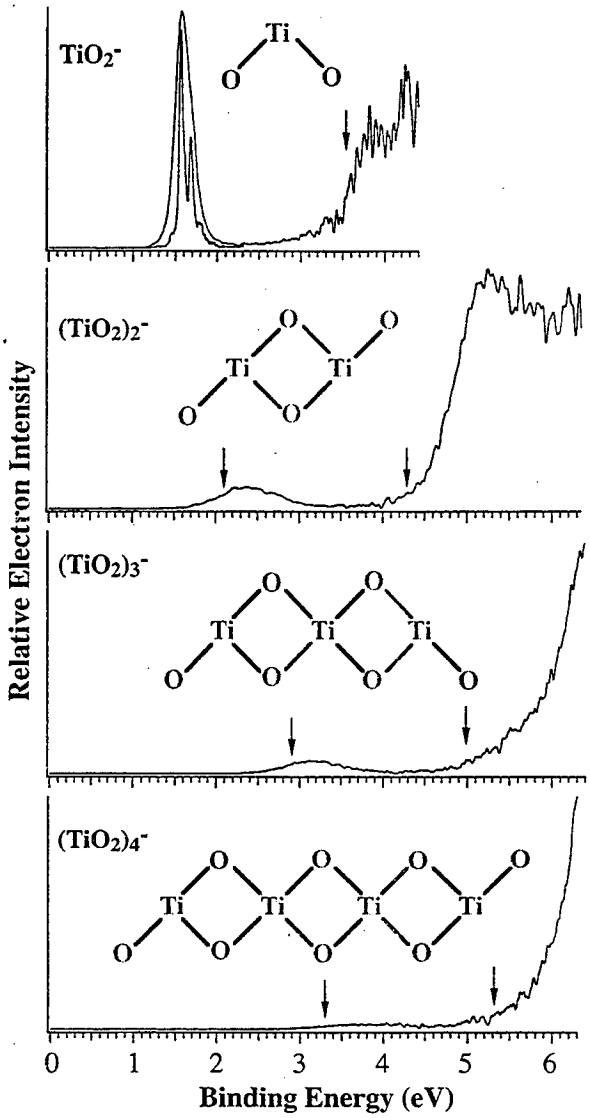

Figure 4.3. Photoelectron spectra of $(TiO_2)_y^-$ and the schematic structures of the neutral clusters. The vibrationally-resolved spectrum of TiO_2^- at 532 nm is also shown. The arrows indicate the HOMO–LUMO gap, which is similar in all the clusters.

3. A Study of the Structure and Bonding of Small Aluminum Oxide Clusters: $Al_xO_y^-$ (x = 1–2, y = 1–5)[4]

Anion photoelectron spectroscopy of aluminum oxide clusters, Al_xO_y (x = 1–2, y = 1–5), were studied and were compared with preliminary *ab initio* calculations. The spectra were obtained at four detachment photon energies: 2.33, 3.49, 4.66, and 6.42 eV. The 6.42-eV spectrum for AlO^- reveals the $X^2\Sigma^+$ ground state and two excited states of

AlO. The 6.42-eV spectrum for AlO_2^- also shows three states for AlO_2: the $X^2\Pi_g$ ground state and the $A^2\Pi_u$ and $B^2\Sigma_g^+$ excited states. The spectra for $Al_2O_y^-$ clusters show vibrationally-resolved ground states which come from Al *sp*-type orbitals and also high-binding-energy excited states, which are mainly of oxygen 2*p* character. Al_2O_2, which has a D_{2h} rhombus structure, has an electron affinity of 1.88 eV, and its singlet–triplet excitation energy is measured to be 0.49 eV. Much higher EAs are measured for the larger Al_2O_y clusters. The PES spectra of $Al_2O_3^-$, $Al_2O_4^-$, and $Al_2O_5^-$ show very similar electronic and vibrational structure. These observations lead us to suggest that these molecules all have a rhombus-like structure, similar to Al_2O_2, with the oxygen atoms sequentially attaching to the terminal aluminum atoms. The spectra are consistent with an ionic bonding view of these clusters, and the vibrational frequencies are in good agreement with the theoretical results.

4. Small Silicon Oxide Clusters: Chains and Rings[5]

We studied several silicon oxide cluster series with different Si:O stoichiometries: $(SiO)_n^-$ (n = 3–5), $(SiO_2)_n^-$ (n = 1–4), and $Si(SiO_2)_n^-$ (n = 2,3). The $(SiO)_n$ clusters are shown to be closed-shell molecules and the HOMO–LUMO gaps are observed from the PES spectra to decrease for larger n. These clusters are shown to have ring structures. Si_3O_4 is known to have a D_{2d} structure with two perpendicular Si_2O_2 rhombuses. The PES spectrum of $Si_4O_6^-$ is very similar to that of $Si_3O_4^-$. It is concluded that Si_4O_6 has a similar structure with a chain of three Si_2O_2 rhombuses. The $(SiO_2)_n$ clusters all exhibit high electron affinities, and only one band is observed at 4.66-eV photon energy. These clusters are shown to have similar chain structures containing Si_2O_2 rhombuses, but the two terminal Si atoms are bonded to an extra O atom each. The possibility of using these clusters to provide structural models for oxygen-deficient defects in bulk silicon oxides is evaluated.

References

1. L. S. Wang, J. B. Nicholas, M. Dupuis, H. Wu, and S. D. Colson, *Phys. Rev. Lett.* **78**, 4450 (1997).
2. T. Engel, *Surf. Sci. Rep.* **18**, 91 (1993).
3. H. Wu and L. S. Wang, *J. Chem. Phys.* **107**, 8221 (1997).
4. S. R. Desai, H. Wu, C. Rohlfing, and L. S. Wang, *J. Chem. Phys.* **106**, 1309 (1997).
5. L. S. Wang, S. R. Desai, H. Wu, and J. B. Nicholas, *Z. Phys. D: Atoms, Molecules and Clusters* **40**, 36 (1997).

Photoelectron Spectroscopy and Electronic Structure of Metal Clusters and Chemisorbed Metal-Cluster Complexes

L. S. Wang, H. Wu, X. B. Wang,*†*
C. F. Ding,† and X. Li**

Supported by the National Science Foundation.
*Washington State University.
†Postdoctoral Research Fellow.

One of the key issues in the study of metal clusters is to understand the electronic structures of these intermediate systems and their evolution toward bulk band structure as the cluster size increases. Transition-metal clusters are of particular interest in this regard because of their diverse physical and chemical properties. Primarily due to the presence of partially-filled *d*-orbitals, however, the transition-metal clusters have presented considerable challenges both experimentally and theoretically. Heretofore, very little has been known about the detailed structures of transition-metal clusters and their electronic properties. Our goals are to elucidate the evolution of the electronic structure of these clusters and to use the obtained electronic structure information to understand their chemical and physical properties.

The interactions between oxygen and metals are important in many areas of chemistry and materials sciences. Our laser vaporization cluster source and the high sensitivity of the magnetic-bottle PES apparatus provide a unique opportunity for us to investigate a broad range of metal oxide species that are otherwise impossible to study.

1. Photoelectron Spectroscopy of Small Chromium Clusters: Observation of Even-Odd Alternations and Theoretical Interpretation[1]

We performed an extensive photoelectron spectroscopy study of size selected Cr_n^- (n = 2–70) clusters. Even-odd alternations are observed for the small Cr_n clusters and in their electron affini-

ties. The spectra of clusters with an even number of atoms show less density of states near the threshold, while those of the odd clusters show more complex features (Fig. 4.4). A dimer growth path found in a previous theoretical study[2] is used to interpret the data and accounts well for the even-odd effects. This work provides a key contribution to the understanding of the complicated electronic structure of the Cr clusters.

2. A Study of Nickel Monoxide (NiO), Nickel Dioxide (ONiO), and Ni(O_2) Complex[3]

We carried out the first anion photoelectron spectroscopic study of nickel monoxide (NiO), nickel dioxide (ONiO), and nickel–O_2 complex, Ni(O_2). The adiabatic electron affinity (EA) of NiO is measured to be 1.46(2) eV. Five low-lying electronic excited states ($A^3\Pi$, $a^1\Delta$, $B^3\Phi$, $b^1\Sigma^+$, $c^1\Pi$) are observed for NiO at 0.43(4), 0.94(4), 1.24(3), 1.80(10), and 2.38(10) eV above the ground state, respectively. Two isomers are observed for NiO_2, i.e., the linear ONiO dioxide and the Ni(O_2) complex. The dioxide has a high EA of 3.05(1) eV, while the Ni(O_2) complex has a rather low EA of 0.82(3) eV. Two low-lying excited states are observed for ONiO at 0.40(2) and 0.77(3) eV above the ground state, respectively. The vibrational frequency of the ν_1 mode of the ground-state ONiO ($X^3\Sigma_g^-$) is measured to be 750(30) cm^{-1}. The excited states of the Ni(O_2) complex give broad photodetachment features starting at about 1.1 eV above the ground state. Information about the electronic structures of the nickel oxide species and chemical bonding between Ni and O and O_2 is obtained and will be valuable to compare with future *ab initio* calculations.

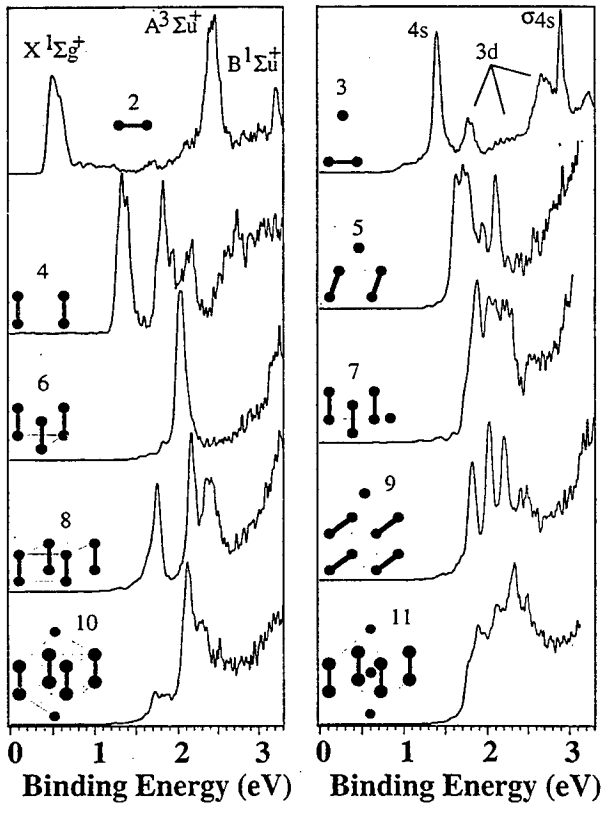

Figure 4.4. Photoelectron spectra of Cr_n^- for n = 2–11 at 3.49-eV photon energy. Note the difference between the even and odd clusters. The structure of each cluster from Ref. 2 is included schematically.

3. Chemical Bonding Between Cu and Oxygen–Copper Oxides vs. O_2 Complexes: A Study of CuO_x (x = 0–6) Species by Anion Photoelectron Spectroscopy[4]

An extensive photoelectron spectroscopic study on the CuO_x^- (x = 0–6) species is presented. The photoelectron spectra of these species are obtained at four detachment photon energies: 2.33, 3.49, 4.66, and 6.42 eV. The spectra of the copper atom are included to show the dependence of the detachment cross sections on the photon energies. An intense two-electron transition to the ^2P excited state of Cu is also observed in the 6.42-eV spectrum of Cu^-. For CuO^-, we observe an excited state of the anion, as well as photodetachment transitions to charge-transfer excited states of CuO ($Cu^{2+}O^{2-}$). Six transitions are observed for CuO_2^- at 6.42 eV, revealing all six valence molecular orbitals of the linear OCuO molecule. CuO_3^- is observed to undergo photodissociation at 3.49 eV to give an internally hot CuO^- plus O_2. It is shown to have an $OCuO_2$ type of structure, and its electronic structure can be viewed as that of CuO perturbed by an O_2. For CuO_4^-, two isomers are observed; one undergoes photodissociation at 3.49 eV and is shown to be a Cu/O_2 complex, $Cu(O_2)_2^-$. The second isomer yields spectra identical to that of the linear $OCuO^-$ with a slight energy shift, and is concluded to be an $OCuO^-$ solvated by a very weakly bonded O_2, $(OCuO^-)O_2$. CuO_6^- is shown to exhibit similar behaviors as CuO_4^- with a Cu/O_2 complex, $Cu(O_2)_3^-$, and an O_2-solvated CuO_2^-, $(OCuO^-)(O_2)_2$. The CuO_5^- spectrum is observed to be similar to that of CuO_3^-, and is shown to be due to a CuO_3^- solvated by an O_2, $(OCuO_2^-)O_2$.

4. Electronic Structure and Photoelectron Spectroscopy of AlSi Mixed Dimer[5]

The electronic structure of the hetero-dimer AlSi is experimentally studied using anion photoelectron spectroscopy. Four low-lying electronic excited states are observed for AlSi. The electron affinity of AlSi is measured to be 1.32(5) eV, which is lower than that of both Al_2 and Si_2. The electronic structure of AlSi is understood by comparing that of the known Al_2 and Al_2^- molecules. The ground state of AlSi is determined to be $X^4\Sigma^-$, with a vibrational frequency of 400(50) cm^{-1}. The four excited states are $A^2\Sigma^-$, $B^2\Delta$, $C^2\Pi$, and D^2S^+, with excitation energies of 0.23, 0.67, 0.82, and 1.13 eV, respectively. The photoelectron spectra of Al_2^- are also presented, and excited states of the Al_2^- anion are definitively observed. The electronic structure of AlSi is discussed and compared to that of the homonuclear dimers, Al_2 and Si_2.

References

1. L. S. Wang, H. Wu, and H. Cheng, *Phys. Rev. B* **55**, 12884 (1997).
2. H. S. Cheng and L. S. Wang, *Phys. Rev. Lett.* **77**, 51 (1996).
3. H. Wu and L. S. Wang, *J. Chem. Phys.* **107**, 16 (1997).
4. H. Wu, S. R. Desai, and L. S. Wang, *J. Phys. Chem. A* **101**, 2103 (1997).
5. X. B. Wang and L. S. Wang, *J. Chem. Phys.* **107**, 7667 (1997).

Study of Transition-Metal–Carbon Mixed Clusters

L. S. Wang, X. B. Wang,*† H. Wu,* C. F. Ding,*† X. Li,* and H. S. Cheng§

Supported by the National Science Foundation.

*Washington State University.
†Postdoctoral Research Fellow.
§Air Products and Chemicals, Inc.

The objective of this research is to study the structure and formation of metal carbide clusters (M_xC_y) in the gas phase, and the nanomaterials formed by these clusters in the condensed phase. The gas-phase study involves anion photoelectron spectroscopy, which yields electronic structure as well as vibrational information on the small M_xC_y clusters. The aims of this study are to provide fundamental understanding of the structure and bonding of the M_xC_y clusters in a wide size range, and to understand the subtle differences in bonding and structures between carbon and the transition metals across the first transition series. The gas-phase studies will lead to insight into the formation mechanisms of three classes of novel materials: endohedral metallo-fullerenes, single-shell carbon nanotubes, and metallo-carbohedrenes, because their formation all depends on the interaction between carbon and the transition metals, and exhibits certain propensity among the transition metals. The microscopic understanding of the formation of these novel materials requires a thorough characterization of the small M_xC_y clusters and how their structure and bonding evolve as the cluster size increases. Such an understanding will lead to more efficient methods to synthesize these novel materials as well as to tailor-design new cluster materials involving carbon and transition metals.

1. Growth Pathways of Metallocarbohedrene: Cage-like or Cubic?[1]

We observed new magic numbers in the anion mass spectrum of titanium carbide clusters (Fig. 4.5). A novel layer-by-layer cubic growth pathway involving C_2 dimers is suggested for large

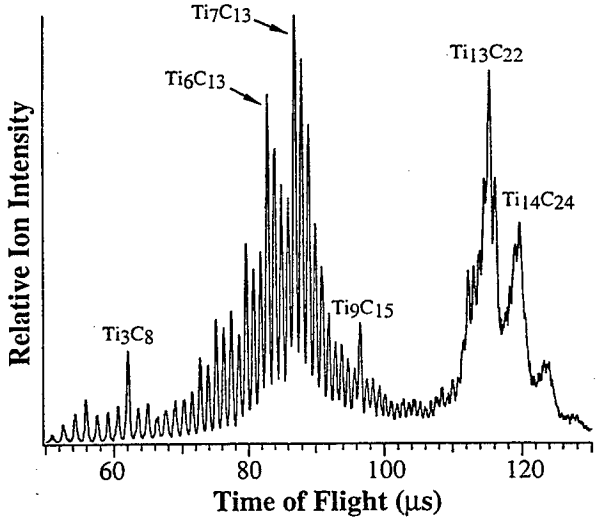

Figure 4.5. Anion mass spectrum of titanium carbide clusters. Note the absence of the $Ti_8C_{12}^-$ metcar anion and the bimodal cluster distribution. The assignment of the exact cluster compositions is ascertained by using $^{13}CH_4$ isotope substitution.

titanium carbide clusters, based on observation of new magic numbers in the anions and comparison of the measured photoelectron spectra with density functional theoretical calculations (Fig. 4.6). This growth mechanism explains all the magic numbers in a multicage growth model previously proposed for large metal carbide clusters,[2] suggesting that the cubic structures characteristic of the bulk carbide lattices dominate the growth of the large carbide clusters. Experimental and theoretical evidence indicates that the cubic layered growth with C_2 dimers can lead to new highly stable one-dimensional quantum wires (Fig. 4.7).

2. Probing the Electronic Structure of Metallocarbohedrenes: M_8C_{12} (M = Ti, V, Cr, Zr, Nb)[3]

We carried out a systematic study of the electronic structure of the five metcars in the title using anion photoelectron spectroscopy (Fig. 4.8). The electron affinities of the metcars are measured and are found to be metal-dependent and to increase from Ti_8C_{12} to Cr_8C_{12}. The electronic structure of Zr_8C_{12} and Nb_8C_{12} are found to be similar to Ti_8C_{12} and V_8C_{12}, respectively. All the spectra can be qualitatively interpreted by the molecular orbital schemes derived from a tetracapped tetrahedral M_8C_{12} cluster (Fig. 4.9). This work provides the most quantitative electronic and spectroscopic information yet about the metcars, as well as evidence supporting the tetrahedral structure for them.

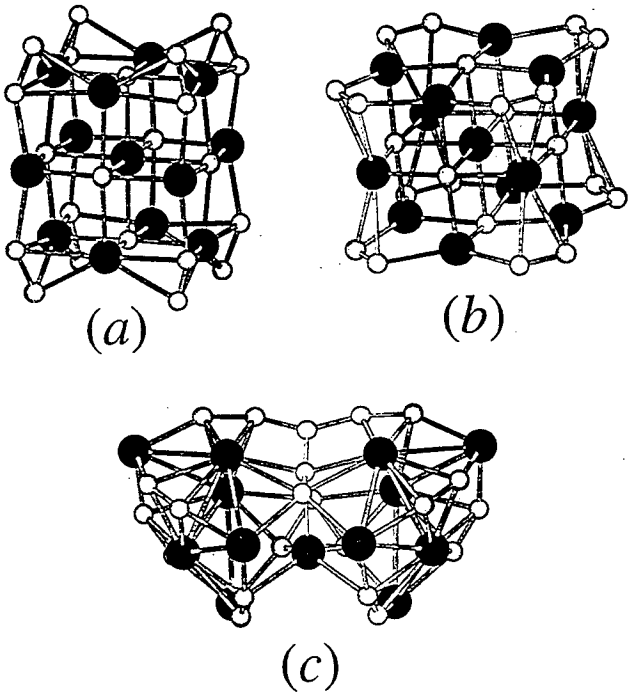

Figure 4.6. Three optimized structures for $Ti_{13}C_{22}$. (a) D_{4h}, cubic with 8 C_2 dimers at the cube corners in nearly vertical positions; (b) D_{4h}, cubic with 8 C_2 dimers at the cube corners in horizontal positions; (c) C_s, distorted structure resulting from an ideal double cage structure. Structure (a) has the lowest energy, and its calculated electron affinity and density-of-states also agree best with the experimental measurement.

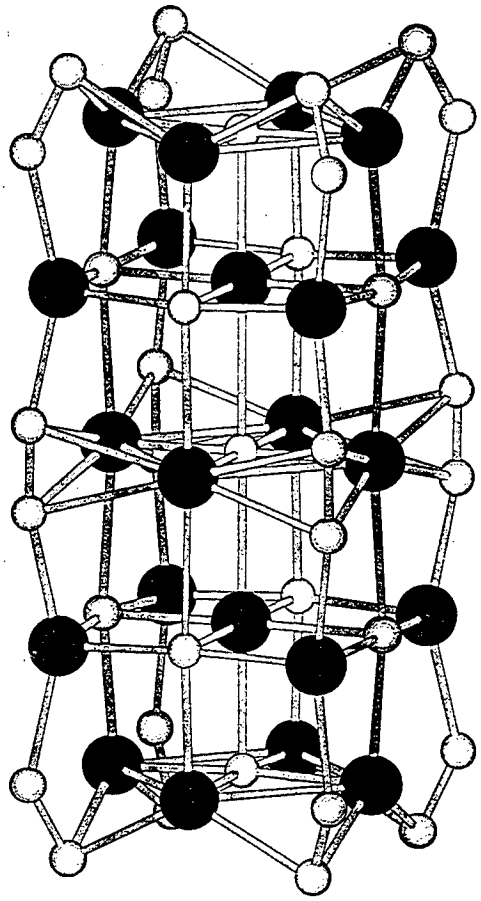

Figure 4.7. Optimized structure of a five-layer *ABABA* structure ($Ti_{22}C_{35}$) with a total binding energy of 379.72 eV (6.66 eV/atom) using density functional calculation with nonlocal correction. Further layered growth can lead to highly stable structures which form a class of novel one-dimensional quantum wires.

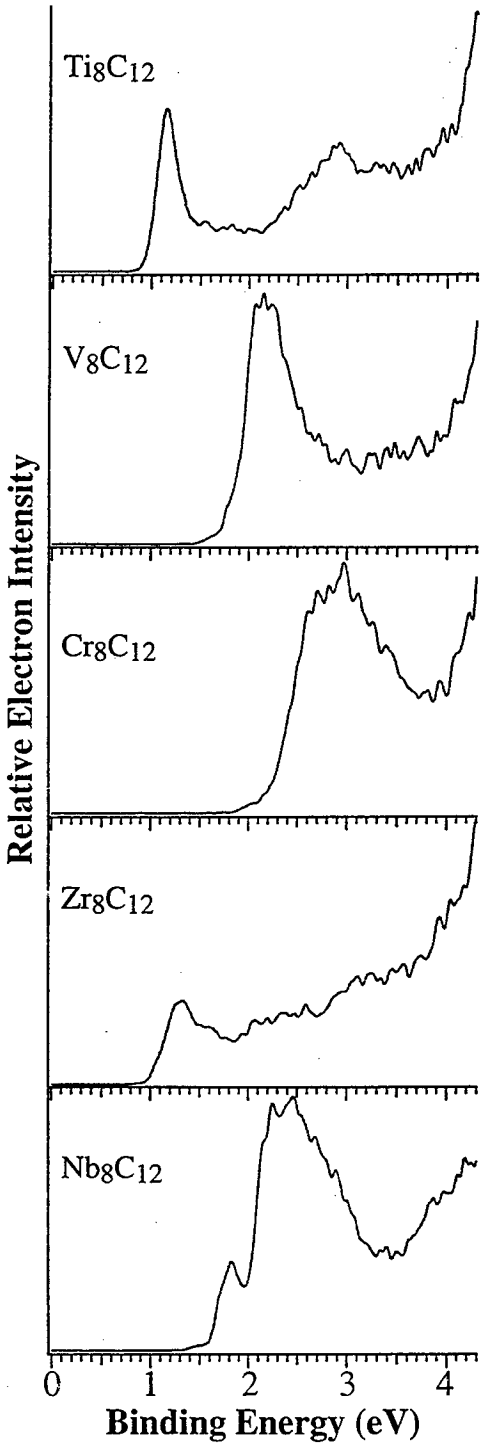

Figure 4.8. Photoelectron spectra of $Ti_8C_{12}^-$, $V_8C_{12}^-$, $Cr_8C_{12}^-$, $Zr_8C_{12}^-$, and $Nb_8C_{12}^-$ at 4.66-eV photon energy.

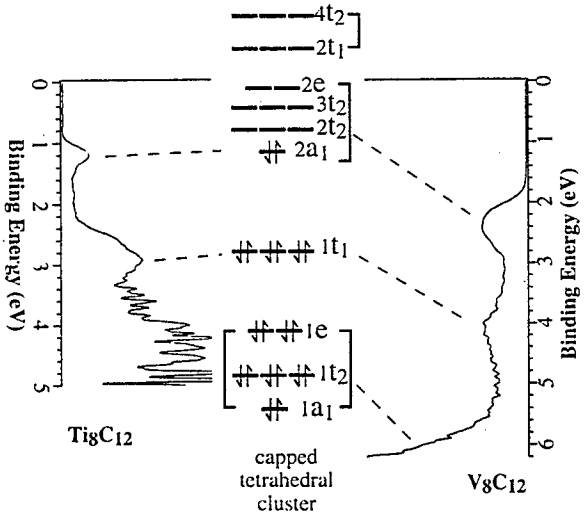

Figure 4.9. Photoelectron spectra of $Ti_8C_{12}^-$ and $V_8C_{12}^-$ at 6.42-eV photon energy, compared with the valence molecular orbitals derived from the tetracapped tetrahedral M_8C_{12} metcar (from Ref. 4). The occupation is for Ti_8C_{12}. For V_8C_{12} and Cr_8C_{12}, more orbitals above the $2a_1$ orbital will be successively occupied.

3. *Vibrationally-Resolved Photoelectron Spectra of TiC_x^- (x = 2–5) Clusters*[5]

Vibrationally-resolved photoelectron spectra are obtained for the small TiC_x^- (x = 2–5) clusters (Fig. 4.10). Adiabatic electron affinities (EAs) and low-lying electronic states are measured for the neutral TiC_x clusters. While the EAs are similar for the series of clusters, 1.542 eV for TiC_2, 1.561 eV for TiC_3, 1.494 eV for TiC_4, and 1.748 eV for TiC_5, the observed ground-state vibrational frequencies decrease for the larger clusters: 560 cm^{-1} for TiC_2, 650 cm^{-1} for TiC_3, 440 cm^{-1} for TiC_4, and 240 cm^{-1} for TiC_5. The results are interpreted using ring-type structures which are known to be the ground state structure for similar YC_x and LaC_x clusters.[6] The current results provide the first and only spectroscopic and electronic information, which will be valuable to test future theoretical calculations to understand the detailed structure and bonding of these simple titanium carbon clusters.

References

1. L. S. Wang and H. Cheng, *Phys. Rev. Lett.* **78**, 2983 (1997).
2. S. Wei, B. C. Guo, J. Purnell, S. Buzza, and A. W. Castleman Jr., *Science* **256**, 818 (1992).
3. S. Li, H. Wu, and L. S. Wang, *J. Am. Chem. Soc.* **119**, 7417 (1997).

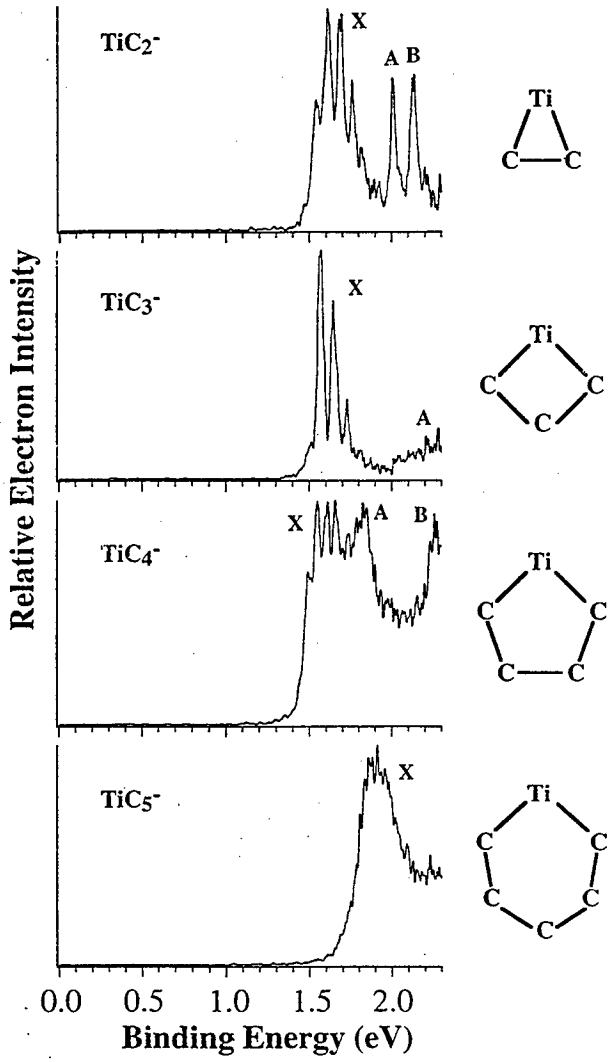

Figure 4.10. Photoelectron spectra of TiC_x^- (x = 2–5) at 532 nm (2.33 eV), showing vibrationally-resolved spectra for the ground-state features. Note the strong photon energy dependence of the A and B states of TiC_2. Schematic ring-type structures proposed for the clusters are also shown.

4. Z. Lin and M. B. Hall, *J. Am. Chem. Soc.* **115**, 11165 (1993).
5. X. B. Wang, C. F. Ding, and L. S. Wang, *J. Phys. Chem. A* **101**, 7699 (1997).
6. D. L. Strout and M. B. Hall, *J. Phys. Chem.* **100**, 18007 (1996).

Time-Resolved Spectroscopy of Solute/Solvent Clusters

D. M. Laman, A. G. Joly, and D. Ray*

Supported by DOE Office of Basic Energy Sciences.

*Postdoctoral Research Fellow.

We are developing and applying time-domain spectroscopic techniques to measure the geometric structures of solute/solvent clusters and determine suitable models for the intermolecular interactions operative in solvation in condensed phases. The methods under development are implementations of rotational coherence spectroscopy (RCS). RCS is a high-resolution, time-domain spectroscopic method for the determination of the moments of inertia of molecular species isolated in the gas phase. RCS yields the rotational constants of an absorber to an accuracy of 0.1–1% without requiring precise measurement or detailed analysis of individual eigenstates. It has become an established technique principally through the efforts of Felker and coworkers. In many cases RCS is complementary to high-resolution spectroscopy in the frequency domain. It has great utility as a method providing gross structural data, and is a particularly useful technique for species which have prohibitively dense or featureless spectra in the frequency domain.

In previous years, we have employed techniques that yielded rotational constants averaged over the ground and first electronically excited state for clusters containing chromophores that readily absorb visible and near-UV light. These techniques are adequate for clusters which absorb visible or near-UV radiation and do not undergo significant geometry changes upon electronic excitation, but inadequate for clusters that undergo photoinitiated dynamics or do not absorb light in the visible or near-UV region. In the past year we have implemented a picosecond time-resolved method to measure rotational constants of the excited state via laser-induced fluorescence and a femtosecond time-resolved method to obtain ground-state rotational constants via Raman-induced polarization spectroscopy.

Figure 4.11 shows the time-resolved fluorescence of fluorene following resonant photoexcitation to the origin of the S_1 state. In addition to the exponential decay characteristic of a fluorescence life

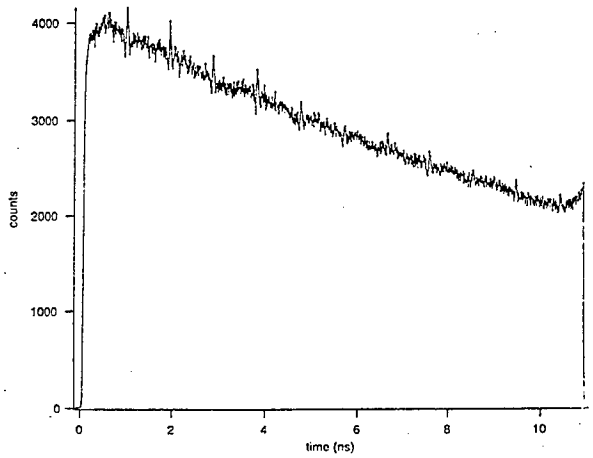

Figure 4.11. Time-resolved fluorescence of fluorene following resonant photoexcitation to the origin of the S_1 state. In addition to the exponential decay characteristic of a fluorescence lifetime of ~15 nsec, the data also exhibit a number of recurrences spaced by $\sim 2/(B + C)$ due to the rephasing of the transition moment dipoles.

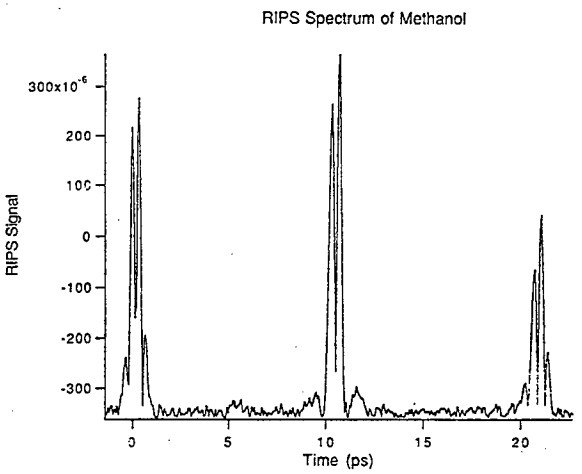

Figure 4.12. Time-resolved Raman-induced transient birefringence of several torr of CH_3OH in a gas cell. The birefringence recurs at intervals of $\sim 2/(B + C)$ and is due to rephasing of the polarizability tensor of the sample.

time of ~15 nsec, the data also exhibit a number of recurrences spaced by $\sim 2/(B + C)$ due to the rephasing of the transition moment dipoles. The fluorene was cooled to ~5 K in a continuous molecular beam and the data were collected in several minutes. This demonstrates our ability to obtain structural data on relatively large molecular species, and indicates the wide applicability of the technique to species of unknown structure. Figure 4.12 shows the Raman-induced transient birefringence of several torr of CH_3OH in a gas cell. The birefringence was induced by a 500-mJ, 150-fsec light pulse centered at 800 nm, and was probed at a later time t by monitoring the polarization rotation of a weak 150-fsec probe pulse centered at 400 nm. The birefringence recurs at intervals of $\sim 2/(B + C)$ and is due to rephasing of the polarizability tensor of the sample. This demonstrates that we can obtain ground-state structural data via a nonresonant pump, and suggests a number of important applications to clusters and ion-molecule complexes.

5. Miscellaneous

Basic and Applied Infrared Spectroscopy

S. W. Sharpe, T. A. Blake, R. L. Sams, and R. S. McDowell*

Supported by Medical Technology Initiative and DOE Office of Nonproliferation and National Security.

*Associated Western Universities Fellow.

With the exception of homonuclear diatomics such as O_2 and N_2, all molecules posses infrared (IR)-active vibrational modes. Infrared spectroscopy is one of several powerful techniques that the physical chemist can call upon for studying the behavior of matter on an atomic scale. In addition, infrared spectroscopy forms the basis for a suite of analytical techniques that are highly specific and extremely sensitive, and can be directly applied to a number of monitoring problems. Brief descriptions of several ongoing projects in these areas are summarized below.

Although our research covers both basic and applied spectroscopy, we often use experience from one project to help augment our understanding of some seemingly unrelated areas of research. For instance, we have an active program in laser-based breath analysis for the early diagnosis of certain diseases. The premise of this project is based on the ability to see trace quantities of certain biomarkers in the exhaled breath, and to correlate these markers to specific pathologies and/or abnormalities. An example is the noninvasive diagnosis of *Heliocobacter pylori*, a bacterium that lives in the mucosal lining of the stomach and is correlated to ulcers and stomach cancer. *H. pylori* is unique in that it has adapted to the highly acidic conditions of the digestive system by using urea as a primary food source and also converting it into a buffering medium:

$$O{=}C(NH_2)_2 + H^+ + 2H_2O \rightarrow HCO_3^- + 2(NH_4)^+.$$

By having a patient ingest a small amount of urea, a non-toxic amino acid, and monitoring the exhaled breath for an incremental increase in ammonia, it should be possible to detect for the presence of *H. pylori*. But how does one detect for very small changes in ammonia in the breath? Based on our previous experiences with high-resolution molecular spectroscopy, we have demonstrated that direct absorption spectroscopy utilizing near-infrared telecommunications lasers is the perfect solution to this problem. A single-mode GaAs laser is rapidly tuned through an absorption feature unique to the ammonia molecule. Even in 100% relative humidity and with 4% carbon dioxide present, trace amounts of ammonia can be detected at the parts-per-billion level. Using this technique, we have begun preclinical screening of individuals for *H. pylori*. Typical results are shown in Fig. 5.1.

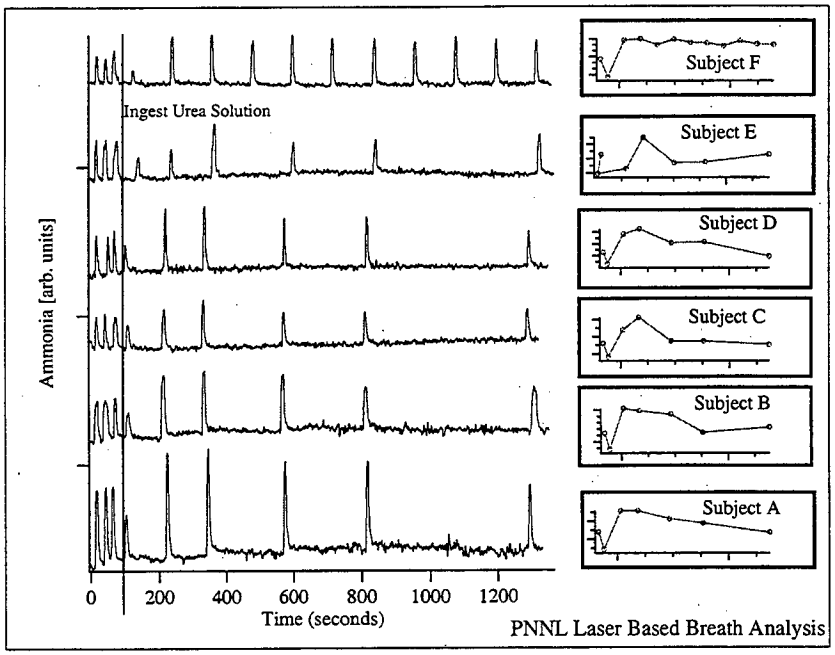

Figure 5.1. Elution profile of breath ammonia for six patients. Each "spike" on left graph represents single exhalation. Note the three base-line breaths used to normalize ammonia prior to ingesting urea solution. Of the six patients tested, only subject F had a definitive serological positive test for *H. pylori*.

In the new Wiley Laboratory, we can study extremely toxic and/or reactive species. As a government research facility involved with environmental issues, we are often asked to look at gas-phase signatures related to both nuclear and chemical weapons. This type of information is particularly important when using spectroscopic techniques to identify and locate leaking or unidentified containers. One such project involves the spectral characterization of an effusive leak of uranium hexafluoride into air.

Uranium hexafluoride (UF_6) is the starting point for gaseous diffusion isotopic enrichment of natural $^{238}U/^{235}U$ into weapon- or fuel-grade uranium. During the transportation and handling of the UF_6, it is not unusual for small amounts to leak into the surrounding air. Once released, the UF_6 undergoes an instantaneous hydrolysis reaction with atmospheric water vapor to produce a number of vapors and aerosols:

$$UF_6 + H_2O \rightarrow UOF_4 + 2HF \quad (1)$$
$$UOF_4 + H_2O \rightarrow UO_2F_2 + 2HF \quad (2)$$
$$UO_2F_2 + H_2O \rightarrow UO_3 + 2HF \quad (3)$$

Reactions (1) and (2) appear to occur spontaneously, even at extremely low temperatures (ca. 70 K). From our and previous studies, reactions (1) and (2) also appear to be diffusion-limited, based on measurements with a high-resolution Fourier-transform infrared spectrometer (FTIRS). Reaction (3) is not observed in the gas phase. Hence, the dominant room-temperature UF_6 hydrolysis products are uranyl fluoride (UO_2F_2) and its various hydrated forms ($UO_2F_2 \cdot xH_2O$).

In an excess of water, the gas-phase UF_6 hydrolysis proceeds by Eq. (4), with a release of 207 kcal/mole of UF_6. Most of this energy is associated with the hydration of the hydrogen fluoride.

$$UF_6 + 6H_2O \rightarrow UO_2F_2 \cdot 2H_2O + 4HF \cdot H_2O \quad (4)$$

The first infrared spectra of uranyl fluoride were of the solid material, collected on PVC membranes after gas-phase precipitation. From these solid samples, it was determined that UO_2F_2 had a pronounced feature at ~950 cm^{-1} (10.5 μm). Detailed gas-phase spectra of $UO_2F_2 \cdot xH_2O$ were not obtained until the early 1990s. These also exhibited a relatively intense $UO_2F_2 \cdot xH_2O$ absorption feature at 956 cm^{-1}. In addition, and as expected, HF was observed at 4100 cm^{-1}. Broad structureless features are observed under the two fundamentals of water, at 1600 and 3600 cm^{-1}; these have been attributed to the $UO_2F_2 \cdot xH_2O \cdot yHF$ complex.

In an effort to better understand the potential of spectroscopic detection for monitoring UF_6 leaks, we performed a number of experiments that augment the previous studies. From Fig. 5.2 and similar graphs we have generated accurate decay or settling curves for $UO_2F_2 \cdot H_2O$.

Molecular Beam–Fourier Transform Infrared Spectrometer
Instrumentation development supported by the EMSL Project.

High-resolution gas-phase infrared spectroscopic techniques have traditionally been plagued by a number of problems including spectral congestion, Doppler broadening, and pressure broadening. Spectral congestion is related to the number of quantum states populated at a given temperature, and is dictated by Maxwell-Boltzmann statistics. Doppler broadening is related to temperature through the kinetic energy relationship, but also involves the random three-dimensional motion of the gas molecules. Pressure broadening is related to temperature through the collisional frequency of the molecules, which depends on the density and mean molecular velocity in the sample. By cooling and reducing the pressure of a gas in specially designed cells, these three effects can be minimized, but at the expense of drastically reduced signals.

A technique that takes advantage of the properties of rapidly expanding a gaseous sample into a moderate vacuum has been used in our laboratory for the last six years. A gas sample is expanded through a slit orifice measuring 12 cm in length by 50 mm wide. The ensuing *ribbon* of gas expands at supersonic velocities, and in the process molecules entrained in this ribbon are cooled to a few degrees above absolute zero. In addition, the random three-dimensional motion of the gas molecules is changed to a two-dimensional flow with little velocity component in the plane of expansion but perpendicular to the mass flow. If infrared light is used to interrogate the gas molecules through the plane of expansion, spectral congestion, Doppler broadening, and pressure broadening are reduced significantly.

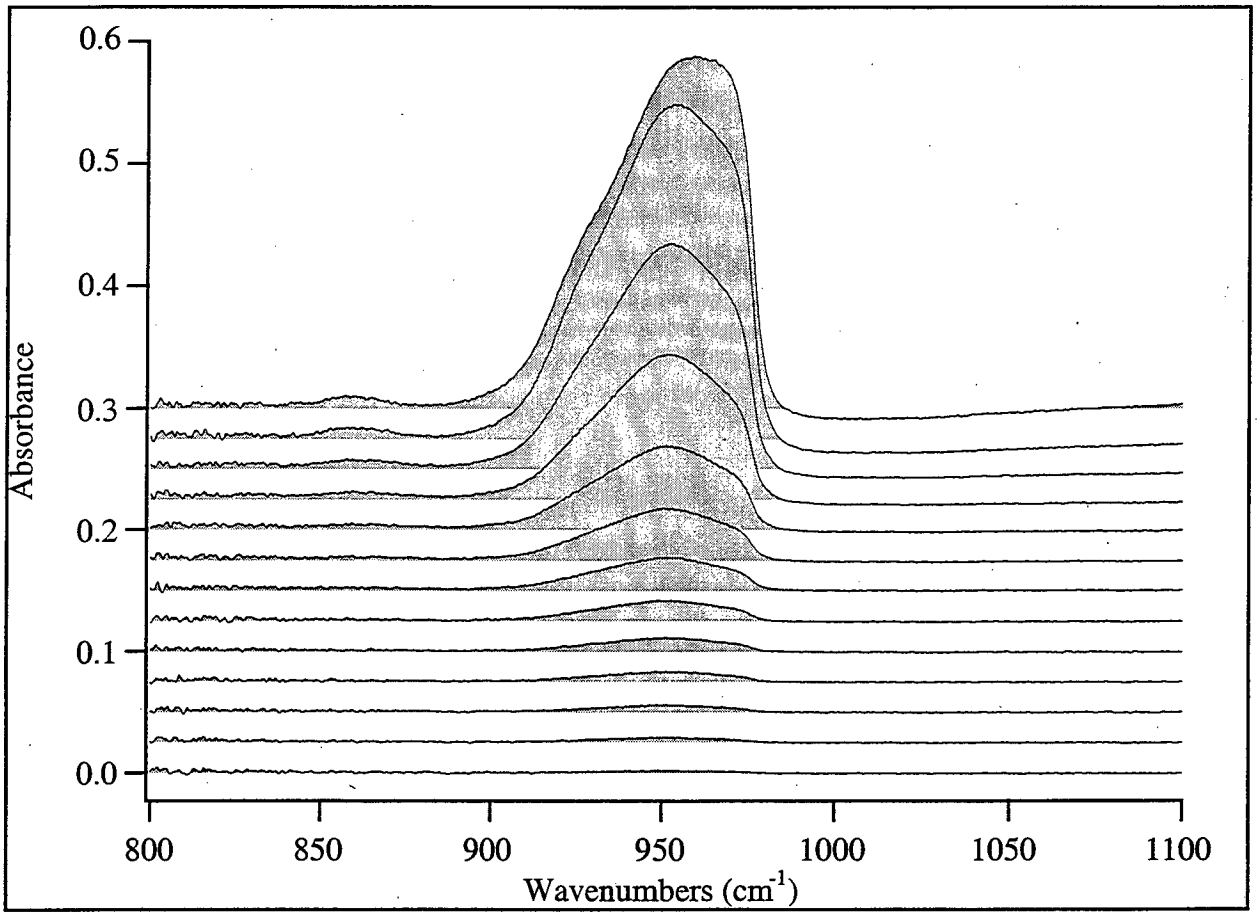

Figure 5.2. Decay of $UO_2F_2 \cdot H_2O$ aerosol feature as acquired by FTIRS. Starting from the top of the figure, each trace represents a 10-minute time interval.

In the past, we have made extensive use of tunable infrared lead-salt diode lasers to interrogate the expanding gas. While infrared lasers make ideal light sources in many respects (i.e., extremely high spectral brightness, low noise, narrow bandwidth and rapid tunability), they are severely limited by narrow spectral coverage. Often an experiment will be determined by what laser coverage is available. Recently, we have succeeded in interfacing a high-resolution FTIRS with a continuous slit expansion source. This provides an alternative to laser sources and offers continuous spectral coverage from the near to far infrared (ca. 15,000 to 10 cm^{-1}). Although FTIRS has been used to interrogate molecular beams in the past, those setups utilized a round expansion orifice at moderate spectral resolution. The PNNL FTIRS–beam machine is capable of recording high-resolution ($\Delta\nu \approx 0.0015$ cm^{-1}) spectra at rotational temperatures of 15 K anywhere in the near- to far-infrared spectral region. A schematic of this apparatus is shown in Fig. 5.3.

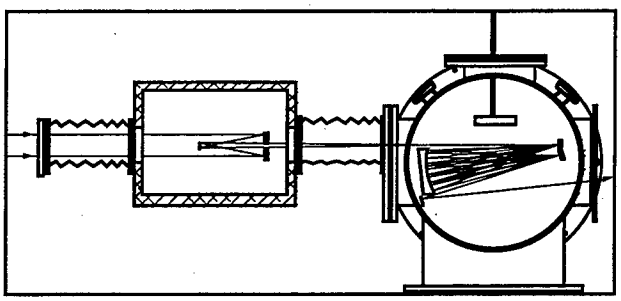

Figure 5.3. Layout of FTIR–beam machine. The box at left contains the beam-reducing optics. The supersonic molecular beam is generated at the top of the round chamber.

Fundamental Physics of Ion Cyclotron Resonance Mass Spectrometers (ICR/MS)

S. E. Barlow, A. J. Peurrung, R. T. Kouzes,† and M. D. Tinkle§*

Supported by DOE Office of Basic Energy Sciences.

*PNNL National Security Division.
†West Virginia University.
§Postdoctoral Research Fellow.

The development of ICR/MS technology, and in particular Fourier-transform ICR (FT/MS), over the past twenty years has been paralleled by developments in the non-neutral plasma community. In the realm of FT/MS, instrumental and technique developments have improved mass ranges and analytical sensitivity, while for non-neutral plasmas, physicists have made great progress in quantitatively describing and understanding this state of matter. Experimentally, the core of ICR/MS and much of the non-neutral plasma work is the Penning ion trap, which is able to trap and store ions indefinitely in a combination of *static* electric and magnetic fields. Figure 5.4 illustrates a particularly simple albeit common case of a harmonic electrostatic field superimposed on a uniform magnetic field. Ions of one charge sign or the other are trapped axially by the electrostatic potential and radially by the magnetic field. The radial electric field, which is perpendicular to the magnetic field, gives rise to azimuthal drifts which are important in understanding cloud dynamics.

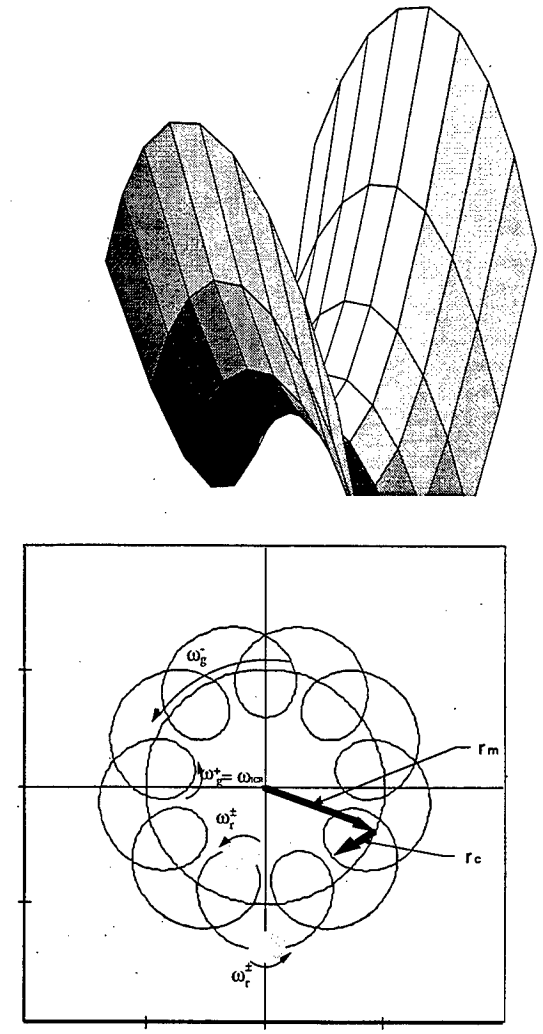

Figure 5.4. The plot in (a) shows the superposition of a harmonic electrostatic trapping potential and uniform magnetic field. The graph (b) shows the resulting cycloidal motion of an ion cloud perpendicular to the magnetic field.

In spite of the obvious connections between these two research areas, almost no communication between them occurred until very recently, for the chemists who developed ICR and the physicists who work on non-neutral plasma physics initially attacked very different problems: the chemists wished to do kinetics measurements and mass spectrometric analysis, while the physicists were attempting to study effects found in charged particle beams and fusion plasmas. Thus the developments in each field were essentially independent. Only a small amount of interfield communication occurred, mediated by the precision measurement community.

During these developments, the chemical community produced a substantial body of literature, including introductory literature for novices and students. Unfortunately, much of this literature contained physical misconceptions rather than deep insight into the fundamental processes occurring in the Penning trap. By contrast, the physical community tended to publish at a much slower rate, and attempted to maintain the highest levels of physical rigor. However, no generally readable, introductory literature was written. This meant that an outsider had almost no chance to determine whether a particular paper or research article was relevant. It is this communica-

tion barrier that we seek to overcome by a two-pronged approach to our research: first, we have begun by publishing an introductory-level invited review[1] whose outline we will describe below. Second, in our development of instrumentation techniques concomitant with BES-supported chemical research, we have opted for both chemical and physical rigor.

Equilibrium

Ions held in the static, and therefor conservative, external fields of the Penning trap interact with each other through the long-range Coulomb force. In the absence of other effects, an ensemble of ions will tend toward a Maxwell-Boltzmann speed distribution. That is, an ion cloud may be described by three conserved quantities, total energy, total canonical angular momentum, and total particle number. Arbitrary initial conditions possessing the same three values for these variables will evolve to the same final equilibrium state. This is a profound statement only recently proved by Tom O'Neal and Dan Dubin of UCSD. It means that the non-neutral state can be characterized, manipulated, and understood in much the same way as ordinary matter. Unlike a neutral plasma for instance, the stored ion cloud can be stably confined *and* possess a definite temperature.

At equilibrium in a standard trap, the ion cloud is cylindrically symmetric (or nearly so) and rotates rigidly about its axis, which is aligned with the magnetic field. An ion cloud can take on a limited variety of shapes consistent with this requirement. These form a family of shapes that are roughly spheroidal and depend on the external electric field and central ion density. Ion density varies from the center of the cloud to its edge in ways that depend on temperature. Figure 5.5 illustrates common ion cloud shapes in the limit of $T = 0$, where the density becomes uniform. Figure 5.6 shows scaled radial density profiles as the temperature increases. In the limit of high temperature, the density distribution becomes Gaussian, reflecting the fact that the thermal energy completely dominates the electrostatic energy of the ion-ion interactions.

In addition to this "standard" equilibrium picture, the ion clouds can also possess metastable transitional equilbria. The most important and widely studied of these are the $l = 0$, $m = 1$ modes known as the diocotron (or magnetron) and the cyclotron modes. These modes are nearly decoupled from the internal ion cloud motions and therefore only weakly damped. The cyclotron mode is used in ICR/MS. The fact that it is an equilibrium state explains the long transients that are routinely observed and used for high-resolution mass spectroscopy. Although readily excited and detected, this mode has been the subject of little study by the plasma community. While the picture of ion motion are relatively simple and understandable, they in fact rest upon rigorous physical foundations.

Transport

For the purpose of understanding many trap phenomena, as well as being able to properly interpret kinetic data, it is important to know just how rapidly the equilibrium will be established. This turns out to be a difficult problem. The answer is that it depends on many factors and has been a source of controversy for many years. We have succeeded in unifying the various theories; interestingly, they are all correct, but differ wildly in their predictions. The result is that now we can estimate most of the important relaxation times of ion clouds based on experimentally measurable quantities.

One area of ion transport not generally treated in the non-neutral plasma physics community is ion–neutral collisional transport. This is actually a fairly well understood and developed area in the chemical community for obvious reasons. Any general treatment of Penning trap phenomena must however include these effects.

Two outstanding and currently incompletely understood relaxation phenomena are damping of the magnetron and cyclotron modes in a ion cloud consisting of a single charge-to-mass ratio species, and the effects on both excitation and damping in ion clouds containing multiple species. Presumably, the first problem relates to the existence of nonlinear terms in the potentials. The second problem is of great importance for general purpose mass spectrometric applications and analysis.

Other Ion Cloud Modes

One of the more exciting areas of Penning-trap physics, and one having a major impact on devel-

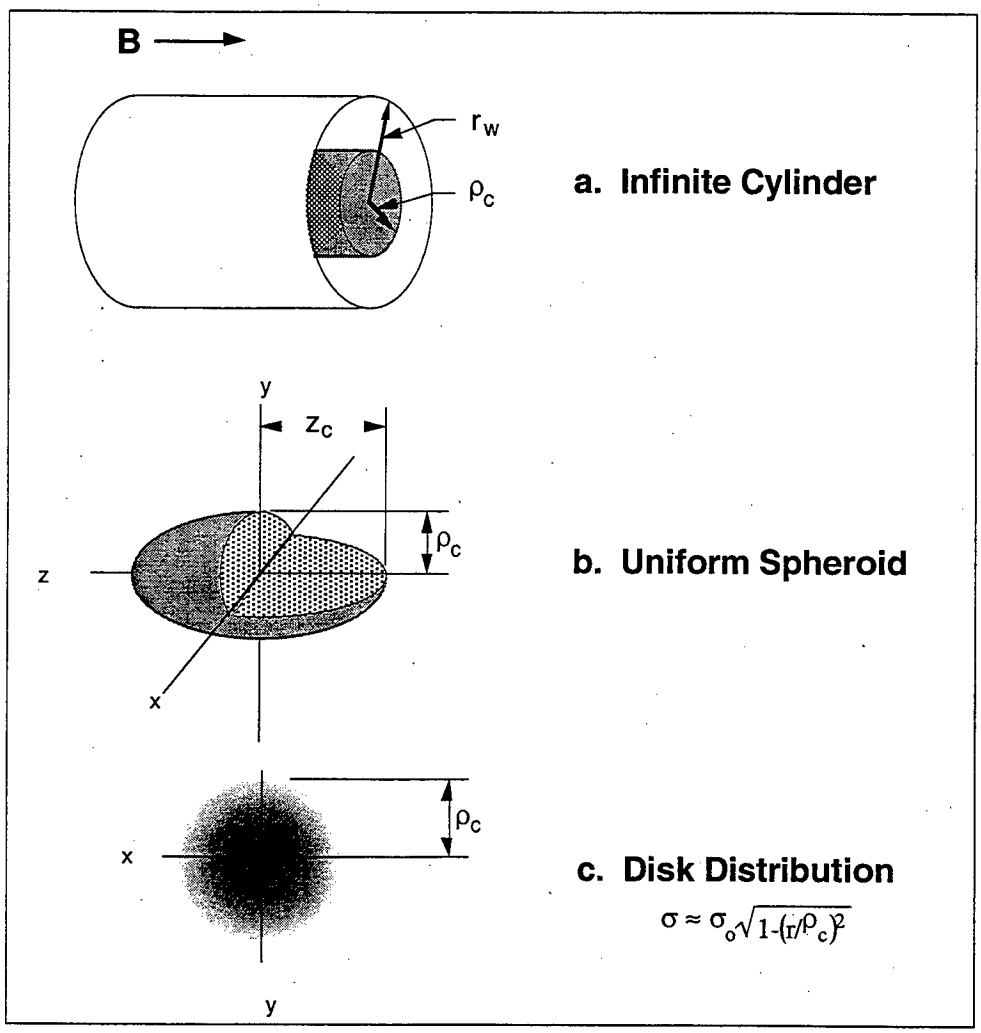

Figure 5.5. Cold ion cloud distributions.

opments in the field, concerns use of higher-order and nonlinear modes to manipulate and interrogate the ion cloud. In the ICR community, coupling of ion-neutral transport to "quadrupolar" excitation routinely allows a previously excited and dispersed ion cloud to be relaxed and recompacted for multiple measurements. Non-neutral plasma experimentalists have developed the "rotating wall" fields for the same ends. It is also possible to probe other ion cloud modes to determine the size, shape, temperature, and composition of the stored particles. These modes require very little energy and do not greatly perturb the ions, as cyclotron resonance probing does.

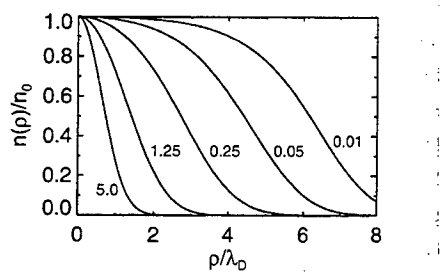

Figure 5.6. Change in radial distribution with temperature. Note that at high temperature, the distribution is essentially Gaussian, but as temperature falls, the distribtions assume a more uniform character.

The Next Steps

With our improved understand of Penning-trap phenomena, we have constructed a new Ion Cyclotron Resonance Mass Spectrometer. This trap was specifically designed in support of chemical physics research. Figure 5.7 is a sche-

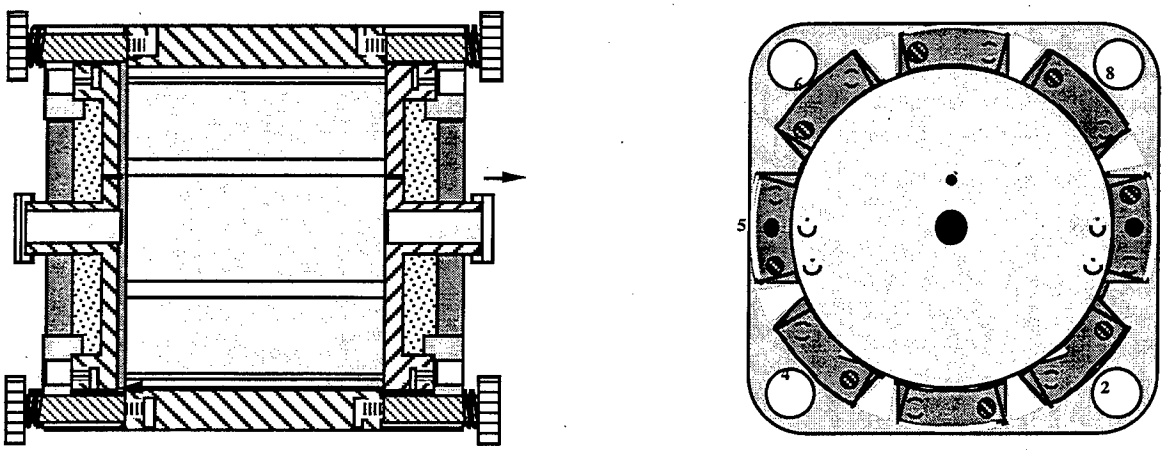

Figure 5.7. Cutaway view of new cylindrical ion trap. The ratio of length to diameter is 0.8316, whch produces a nearly pure quadrupole potential electrostatic in the center of the trap. The right-hand view shows the eight pieces of the radial electrode.

matic sketch of the new trap. The trapping fields are nearly harmonic, an arrangement not commonly used in ICR; the radial or ring electrode has been divided into eight segments. This latter feature allows us to provide the ions with precise excitation amplitudes or energies that *we can calculate from first principles*. Further, this design will allow us to directly exploit some of the new ion manipulation techniques described above.

Recent analysis of data and theoretical considerations resulting from the above developments, show that ion clouds evolve in time in a particularly simple way which depends only on the magnetic field, the trap size, and applied trapping potential. All of these are controlled and measurable quantities. This result is likely to play a key role in the further exploitation of the Penning ion trap in physical measurement. Further, this discovery opens up the possibility of new types of mass spectroscopy that can both extend the effective mass range and allow for much less intrusive mass measurements to be made.

Reference

1. A. J. Peurrung, R. T. Kouzes, and S. E. Barlow, "The Non-Neutral Plasma: an Introduction to Physics with Relevance to Cyclotron Resonance Mass Spectrometry," *Int. J. Mass Spectrom. Ion Processes* **157/158**, 39–83 (1996).

New Developments in Nonlinear Optical Imaging

E. J. Sanchez, L. Novotny,† A. Zumbusch,† D. Arnett,† G. R. Holtom, R. X. Bian,§ and X. S. Xie*

Supported by a Cooperative Research and Development Agreement (CRADA) and Laboratory Directed Research and Development (LDRD).

*Graduate Student, Portland State University.
†Postdoctoral Research Associate.
§Atmospheric Sciences Department.

Two-Photon Imaging of Single Molecules

In fluorescence microscopy, two-photon excitation of molecular fluorescence has advantages of reduced excitation volume, effective rejection of background, and easy access to UV transitions. Following fluorescence detection of single molecules in solution with two-photon excitation,[1] we obtained high-quality two-photon fluorescence images of immobilized single fluorophores by scanning the sample with respect to a diffraction limited focus of a mode-locked Ti:sapphire laser beam.[2] Figure 5.8 shows a two-photon image of single rhodamine B molecules taken in 5 minutes. Single-molecule emission spectra are also recorded with two-photon excitation. A comparison of photobleaching rates is made between one-photon and two-photon excitation.[2]

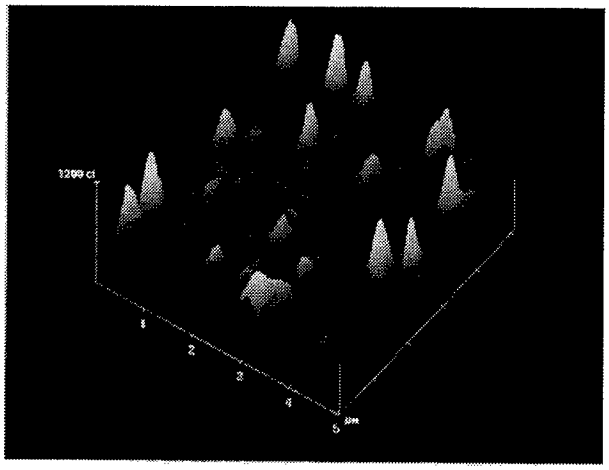

Figure 5.8. Two-photon fluorescence images of single rhodamine B molecules on a PMMA film.

Video-Rate Two-Photon Imaging

Nikon's RCM-8000 point-scan video-rate confocal microscope incorporating a resonant galvanometer[3] has been modified for two-photon fluorescence imaging. Figure 5.9 shows a 30-ms image frame from a continuous movie of single green algae *chlamydomonas* cells swimming in an aqueous solution. Natural fluorescence from chloroplast in each cell (1.5 μm diameter) is two-photon excited with a femtosecond Ti:sapphire laser. A video was taken of the swimming algae cells. Only a moderate average power (<4 mW) is needed for the video-rate imaging, and no noticeable photon bleaching was observed for 10 min of continuous imaging. The system is being used for real-time observation of biogenesis in single cells.

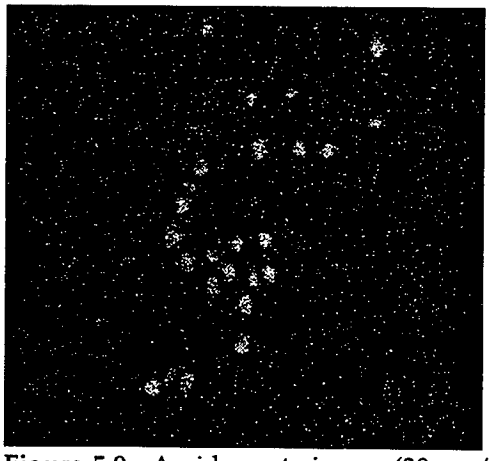

Figure 5.9. A video rate image (30 ms/frame) of single green algae cells (1.5 μm) with two-photon excitation.

Nonlinear Vibrational Imaging

With the aim of extending the high-resolution microscopy work to the infrared region, we are developing vibrational imaging in the chemically important 3-μm wavelength region by using sum-frequency mixing of femtosecond pulses from an infrared optical parametric amplifier[4] and a Ti:sapphire regenerative amplifier.

High-Resolution Near-Field Two-Photon Imaging

We are working on a new technique for high-resolution near-field imaging, using metal tips[5,6] under illumination. We have performed a rigorous electromagnetic analysis for the field enhancement at the tip end.[5] To solve Maxwell's equations in the specific geometry of the tip and its environment, we employed the multiple multipole (MMP) method. Figure 5.10 shows our three-dimensional MMP simulation of the foremost part of a gold tip (5-nm radius at the end) in water for two different monochromatic plane-wave excitations. The wavelength of the illuminating light is 810 nm (Ti:sapphire laser). In Fig. 5.10(a) a plane wave is incident from the bottom with the polarization perpendicular to the tip axis, while in

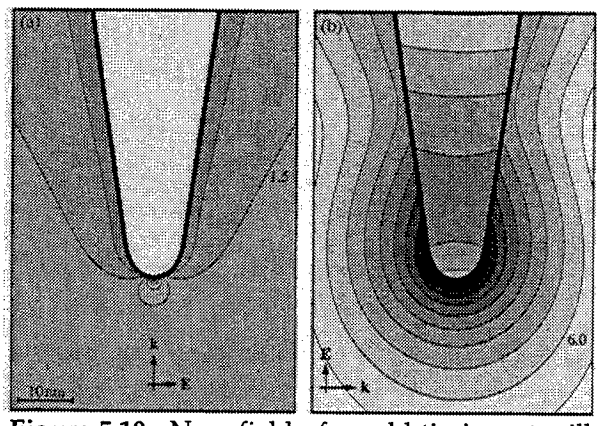

Figure 5.10. Near-field of a gold tip in water illuminated by two different monochromatic waves of 810 nm. Direction and polarization of the incident wave is indicated by the **k** and **E** vectors. The figures show contours of E^2 (factor of 2 between successive lines). The scaling is given by the numbers in the figures (multiples of the exciting field). No enhancement at the tip in (a); enhancement of 3000 in (b). The field in (b) is almost rotationally symmetric in the vicinity of the tip.

Fig. 5.10(b) the tip is illuminated from the side with the polarization parallel to the tip axis. A striking difference is seen for the two different polarizations: in (b), the intensity enhancement at the foremost part of the tip is 3000 times stronger than the illuminating intensity, whereas no enhancement beneath the tip and only moderate enhancement on the sides of the tip (factor of five) exist in (a).

Using the highly localized evanescent waves around a solid metallic tip under illumination of a mode-locked Ti:sapphire laser, we are able to obtain two-photon fluorescence images of molecular aggregates and photosynthetic membranes with a resolution that exceeds the diffraction limit.

References

1. J. Mertz, C. Xu, and W. W. Webb, *Optics Lett.* **20**, 2532 (1995).
2. E. J. Sánchez, L. Novotny, G. R. Holtom, and X. S. Xie, *J. Phys. Chem.* **101**, 7019 (1997).
3. R. Y. Tsien and B. J. Bacskai, in *Handbook of Biological Confocal Microscopy*, J.B. Pawley, ed. (1995), p. 459.
4. G. R. Holtom, R. A. Crowell, and X. S. Xie, *J. Optic. Soc. Am. B* **12**, 1723 (1995).
5. L. Novotny, R. X. Bian, and X. S. Xie, *Phys. Rev. Lett.* **79**, 645–648 (1997).
6. L. Novotny, E. J. Sánchez, and X. S. Xie, *Ultramicroscopy*, in press (1998).

The Atmospheric Water-Vapor Continuum

*S. W. Sharpe and R. L. Sams**

Supported by DOE Office of Biological and Environmental Research under the Atmospheric Radiation Measurement (ARM) Program.

*Associated Western Universities Fellow.

Atmospheric absorption of infrared radiation has been the subject of intense study since the earliest days of infrared spectroscopy, dating back to the early 1900s. The importance of accurately describing the propagation of light through the atmosphere is critical to a number of scientific and political issues. For instance, the impact of global policies based on the limiting of emissions of greenhouse gases such as carbon dioxide and certain Freons has far-ranging economic and societal ramifications. In addition, remote sensing and imaging from high-altitude platforms is critical to our national security, and this technology depends on the ability to model atmospheric spectral characteristics.

Accurate modeling of atmospheric absorbance requires that numerous effects be accounted for, including both absorbance and scattering phenomena. Absorbance effects include line-by-line absorbances of individual atmospheric vapors such as water, carbon dioxide, and methane. In addition to these individual absorbances, the continuum must also be included. As the name implies, the continuum is a featureless absorption that spans the microwave to visible regions of the spectrum. Although not nearly as strong as line transitions or as some scattering effects, the continuum can account for 15% or more solar radiation being deposited into the troposphere.

There are a number of standard models used to calculate atmospheric absorbtion, including LBLRTM, FasCode and FASE. Most of these models use the HITRAN database as a source of line-by-line molecular absorbances. The continuum is not as well understood, and is often represented phenomenologically, based on a combination of laboratory and field data. Within the last decade, quantum-based models describing the continuum have also been implemented. These quantum models are particularly important in that they tell us the origin of the continuum is due to the far-

wing absorbance of water vapor. Previous speculation attributed the continuum effect to hydrated ions or water dimers.

Historically, Fourier-transform infrared spectroscopy (FTIRS) has been used to map out the line-by-line transitions of atmospheric gases. A number of optical techniques have been used to monitor the continuum, with most measurements performed in the field. The bulk of the continuum measurements in the laboratory have been performed in hot cells or through super-heated steam. With the advent of reliable, commercially available lasers and new optical materials, it is now possible to perform both line-by-line and continuum measurements under highly-controlled conditions in the laboratory. We have recently built a laboratory system for re-mapping the line-by-line transitions and studying the continuum effect. The research apparatus is based on a tunable near-infrared laser system and a 100-meter folded optical cell. In operation, this cell is allowed to come to equilibrium with a salt-water solution. Depending on the specific salt used (e.g. NaCl, LiCl, KCl) a highly reproducible relative humidity can be created above the solution, at a specific temperature. In addition, a dual-channel humidity sensor is used to verify the water concentration. Zero humidity conditions are created by replacing the salt solutions with anhydrous phosphorous pentoxide. A collimated, tunable, near-infrared laser is propagated through the cell and undergoes 182 reflections from the two end mirrors for a total optical path length of 100 meters. Absolute intensity spectra are recorded as a function of relative humidity.

During the course of mapping out the water vapor spectrum in the 1.5-μm region, we have observed numerous errors in the HITRAN database. These errors not only include missing lines but also incorrect intensity and broadening information; see Table I and Figs. 5.11 and 5.12. Work on the continuum measurements in the 1.5-μm region is also progressing with preliminary results indicating some deviation from previous findings. Most notably, we see a continuum absorbance approximately 10 times greater than many previous researchers. We are performing several critical experiments to confirm that we are not observing some artifact due to mirror reflectivity change as a function of humidity.

Table I. Comparison of Air-Broadened Halfwidths for Some Water Transitions Belonging to the 021–000 Band.

HITRAN Position		Halfwidth (HWHH), cm^{-1}		
(cm^{-1})	Transition	Present	Benedict	HITRAN
6658.38102	$9_{1,9}$–$10_{1,10}$	0.0301	0.0388	0.0617
6658.65180	$9_{0,9}$–$10_{0,10}$	0.0372	0.0388	0.0617
6726.24882	$6_{0,6}$–$7_{0,7}$	0.0651	0.0649	0.0737
6727.23199	$6_{1,6}$–$7_{1,7}$	0.0681	0.0642	0.0758
2746.94764	$5_{0,5}$–$6_{0,6}$	0.0681	0.0775	0.0823
6753.57764	$5_{2,4}$–$6_{6,5}$	0.0737	0.0818	0.0833
6755.02083	$4_{1,3}$–$5_{1,4}$	0.0812	0.0926	0.0925
6746.57188	$6_{3,4}$–$7_{3,5}$	0.0795	0.0771	0.0785

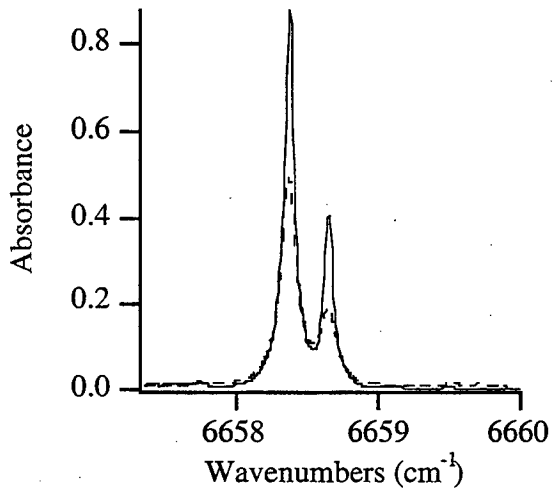

Figure 5.11. Spectrum of 61.5% RH water vapor at 20.2°C and 100-m optical path. Solid line is experimental; dashed line is based on HITRAN. Note significant differences.

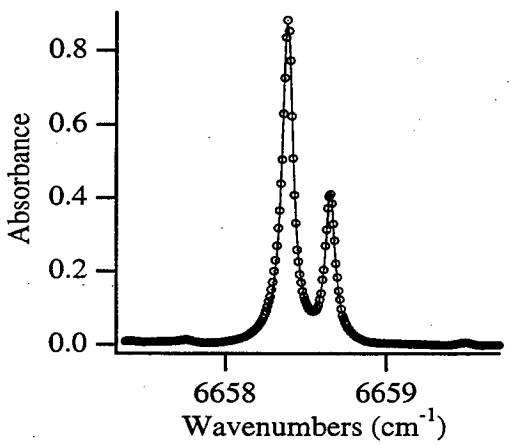

Figure 5.12. Line-width parameters are obtained from experimental data by fitting to a multi-peak Lorentzian profile. Circles represent experimental data and line is best fit.

6. Appendix

Chemical Structure and Dynamics Staff

Associate Director, EMSL

Steven D. Colson

B.S. Utah State University 1963; Ph.D. California Institute of Technology 1968; Postdoctoral Fellow, National Research Council (Ottawa) 1968; Assistant Professor to Professor of Chemistry, Yale University, 1968–1989; joined PNNL as Associate Director for Chemical Structure and Dynamics June 1989. Research interests: photochemistry, photophysics, and molecular dynamics; electronic structures of molecules; processes at the molecule/surface interface.

(509) 376-4598 sd_colson@pnl.gov

Program Manager

Robin S. (Rod) McDowell

B.A. Haverford College 1956; Ph.D. M.I.T. 1960; Staff Member, Assistant Group Leader, and Laboratory Fellow, Los Alamos National Laboratory, 1960–1991; joined PNNL as Program Manager for Chemical Structure and Dynamics April 1991. Research interests: high-resolution infrared and Raman spectroscopy applied to molecular structure and bonding; molecular dynamics and force fields; statistical mechanics; infrared analytical techniques.

(509) 376-1421 rs.mcdowell@pnl.gov

Staff

Stephan E. Barlow

B.A. Southern Oregon State College 1976; Ph.D. University of Colorado 1984, Postdoctoral Fellow 1984–1989; Senior Instructor in Chemistry, University of Denver 1989–1991; joined PNNL June 1991. Research interests: development and application of mass spectrometric techniques to gas-phase chemical kinetics, reaction mechanisms, and structure.

(509) 376-9051 se_barlow@pnl.gov

James P. Cowin

B.S. Case Western Reserve University 1974; Ph.D. University of Chicago 1981; Postdoctoral Fellow, University of Toronto 1981–1983; Assistant Professor of Chemistry, University of California, Santa Barbara, 1983–1990; joined PNNL July 1990. Research interests: molecular motions at interfaces, especially energy and charge transfer, bond formation dynamics, and light-stimulated surface reactions.

(509) 376-6330 jp_cowin@pnl.gov

Wayne P. Hess

B.A. University of Colorado 1981; M.S. University of Oregon 1983; Ph.D. University of Colorado 1988; Postdoctoral Fellow, Sandia Livermore Combustion Research Facility 1988–1990; joined PNNL January 1990. Research interests: modeling condensed phase chemistry through the study of energetic reactive processes in molecular solids and thin films (dissociation and fragmentation, electronic and vibrational energy transfer), using laser-induced desorption and ablation of adsorbed molecules and solid surfaces.

(509) 376-9907 wp_hess@pnl.gov

Gary R. Holtom

B.A. Pfeiffer College 1969; Ph.D. University of California, Berkeley, 1978; Postdoctoral Fellow, Wesleyan University 1978–1979; Head of Laser Operations, University of Pennsylvania Regional Laser and Biotechnology Laboratory, 1979–1989; joined PNNL September 1989. Research interests: short-pulse laser spectroscopy; condensed-phase photochemistry, in particular the dynamics of electronically-excited organic molecules.

(509) 376-5331 gr_holtom@pnl.gov

Stephen A. Joyce

B.S. Boston College 1982; Ph.D. M.I.T. 1987; Postdoctoral Fellow, National Institute of Standards and Technology 1987–1989; Sandia National Laboratories 1989–1991; joined PNNL October 1991. Research interests: scanning probe microscopies for studying molecularly-resolved chemistry on solid surfaces.

(509) 376-3532 sa_joyce@pnl.gov

Bruce D. Kay

B.S. University of Illinois 1976; Ph.D. University of Colorado 1982; Senior Member of the Technical Staff, Sandia National Laboratories, 1982–1991; joined PNNL November 1991. Research interests: chemical dynamics and kinetics of molecular processes occurring at the gas-surface interface; dissociative chemisorption of halogenated hydrocarbons on model oxide surfaces; quantum-resolved H-atom reactive scattering from halogenated surfaces;

trapping and "solvation" of ions and molecules on multilayer ice surfaces.
(509) 376-0028 bd_kay@pnl.gov

Thomas M. Orlando
B.S. Southampton College 1982; Ph.D. State University of New York at Stony Brook 1988; Postdoctoral Fellow, Universität Basel 1988–1989, Sandia National Laboratory 1990–1991; joined PNNL September 1991. Research interests: non-thermal interfacial reaction dynamics; electron- and photon-induced surface chemistry; liquid interfaces; low-temperature plasmas; dissociative electron attachment; laser spectroscopy.
(509) 376-9420 tm_orlando@pnl.gov

Douglas Ray
B.A. Kalamazoo College 1979; Ph.D. University of California, Berkeley, 1985; Postdoctoral Fellow, Joint Institute for Laboratory Astrophysics 1985–1990; joined PNNL June 1990. Research interests: the experimental study of dynamical processes in clusters and at liquid interfaces using techniques of laser spectroscopy and mass spectrometry.
(509) 376-8069 d_ray@pnl.gov

Steven W. Sharpe
B.S. University of Bridgeport 1979; Ph.D. State University of New York at Stony Brook 1986; Postdoctoral Fellow, University of Southern California 1987–1990; joined PNNL May 1990. Research interests: high-resolution molecular spectroscopy.
(509) 376-7769 sw_sharpe@pnl.gov

Lai-Sheng Wang
B.S. Wuhan University 1982; Ph.D. University of California, Berkeley, 1989; Postdoctoral Fellow, Rice University 1990–1992; joint Washington State University/PNNL appointment January 1993. Research interests: clusters of metals, semiconductors, and insulators important as model systems for catalysis, interfaces, and surface chemistry; photoelectron spectroscopy and pulsed laser-vaporization techniques; novel gas-phase molecules involving metal atoms with oxygen, carbon, and nitrogen and the nature of M–O, M–C, and M–N chemical bonding; electrospray and solvation of singly- and multiply-charged anions.
(509) 376-8709 ls_wang@pnl.gov

Xiaoliang (Sunney) Xie
B.S. Peking University 1984; Ph.D. University of California at San Diego 1990; Postdoctoral Fellow, University of Chicago 1990–1991; joined PNNL January 1992. Research interests: single-molecule spectroscopy and dynamics, near-field microscopy, chemical physics in biological systems.
(509) 376-5709 xs_xie@pnl.gov

Research Scientists

Kenneth M. Beck
B.A. Northwestern University 1972; M.S. University of Chicago 1985, Ph.D. 1988; Postdoctoral Fellow University of Pennsylvania 1988–1990, PNNL 1990–1991; Asst. Professor, University of Central Florida 1991–1995; PNNL 1996; joined PNNL staff September 1996.
(509) 376-9152 km_beck@pnl.gov

Thomas A. Blake
B.S. University of Bridgeport 1981; Ph.D. Wesleyan University 1989; Postdoctoral Fellow, University of Washington 1988–1991; NRC Research Associate, NASA Ames Research Center 1991–1994; joined PNNL September 1994.
(509) 376-8974 ta_blake@pnl.gov

Martin J. Iedema
B.S. University of Southern California 1988; Technician, Mt. Wilson Observatory 1987–1990; joined PNNL September 1990.
(509) 376-6039 mj_iedema@pnl.gov

Alan G. Joly
B.S. University of Rochester 1985; Ph.D. M.I.T. 1990; Postdoctoral Fellow, PNNL 1990–1993; joined PNNL staff June 1993.
(509) 376-7707 ag_joly@pnl.gov

Gregory A. Kimmel
B.S. Cornell University 1984, Ph.D. 1992; Postdoctoral Fellow PNNL, 1992–1995; joined PNNL staff September 1995.
(509) 376-2501 ga_kimmel@pnl.gov

Hong (Peter) Lu
B.A. Beijing University 1982, M.Sc. 1984; M. Phil. Columbia 1987, Ph.D. 1991; Postdoctoral Fellow, Northwestern 1991–1995; Postdoctoral Fellow, PNNL, 1995–1996; joined PNNL staff November 1996.
(509) 376-3897 h_lu@pnl.gov

R. Scott Smith
B.S. Northern Arizona University 1983; Ph.D. University of Utah 1988; Postdoctoral Fellow, University of Arizona 1988–1989, PNNL 1990–1992; joined PNNL staff October 1992.
(509) 376-0907 rs_smith@pnl.gov

Russell G. Tonkyn
B.A. Reed College 1978; Ph.D. University of Wisconsin 1988; Postdoctoral Fellow, Brookhaven National Laboratory 1988–1991, PNNL 1991–1992; joined PNNL staff November 1992.
(509) 376-8817 rg_tonkyn@pnl.gov

Visiting Scientists

Ulrike Diebold
Assistant Professor of Physics, Tulane University; PNNL Affiliate Staff Scientist (PASS) with Steve Joyce, July–Sept. 1997.

Carey K. Johnson
B.S., B.A. Tabor College 1973; Ph.D. Iowa State University 1981; Postdoctoral Fellow, University of Pennsylvania 1982–1984; Associate Professor of Chemistry, University of Kansas; AWU Visiting Scientist Fellowship at PNNL with Sunney Xie, June–July 1996, 1997– .

Hannes Jonsson
B.S. University of Iceland 1970; Ph.D. University of California, San Diego, 1985; Postdoctoral Fellow, Stanford 1986–1988; Assistant Professor of Chemistry, University of Washington; PNNL Affiliate Staff Scientist (PASS) with Bruce Kay, 1997.

Nikolai G. Petrik
M.S. Technical University of Leningrad 1977, Ph.D. 1980; D.Sc. Research Institute of Complex Power Technology (VNIPIET), Leningrad, 1984; Senior Scientist with VNIPIET, St. Petersburg; SABIT (Special American Business Internship Training Program) appointment at PNNL with Thom Orlando, April–Sept. 1996, 1997– .
(509) 376-5379

Bobbi J. Roop
B.S. Tulane University 1979; Ph.D. M.I.T. 1985; Postdoctoral Fellow, University of Texas at Austin 1985–1988; Chemist, National Institute of Standards and Technology 1988–1989; Research Chemist/Consultant Argonne National Laboratory 1989–1991; Roop Scientific Research 1992–1994; AWU Visiting Scientist Fellowship at PNNL with Jim Cowin, April 1996 – July 1997.

Robert L. Sams
B.A. Western Washington University 1962; M.S. University of Washington 1967; National Bureau of Standards/National Institute of Standards and Technology 1967–1995; AWU Visiting Scientist Fellowship at PNNL with Steve Sharpe from December 1995.
(509) 376-8995 rl_sams@pnl.gov

Athanassios A. Tsekouras
B.S. National University of Athens 1987; Ph.D. Stanford University 1992; Postdoctoral Fellow M.I.T. 1992–1996; AWU Visiting Scientist at PNNL with Jim Cowin, July 1996 – Aug. 1997; now at University of Athens.

Operations Administrator

Denise A. Motsenbocker (to May 1997)
Cynthia A. Irwin (from June 1997)

Office Support

Jayme R. Crow
Debra M. Hinton

Postdoctoral Fellows

James Chesko
B.Sc. University of British Columbia 1987; Ph.D. University of California, Berkeley, 1995, Postdoctoral Fellow 1995–1996; Postdoctoral Fellow, CS&D, with Sunney Xie, 1996– 1997.

Chuan-Fan Ding
B.S. University of Science and Technology of China 1984; Ph.D. Fudan University, Shanghai; Research Fellow, Institute of Chemistry, Chinese Academy of Sciences 1991–1995; Postdoctoral Fellow with Lai-Sheng Wang, 1996– .

Zdenek Dohnalek
B.S. Institute of Chemical Engineering, Prague, 1989, M.S. 1991; Ph.D. University of Pittsburgh 1997; Postdoctoral Fellow, CS&D, with Bruce Kay, 1997– .

David S. Karpovich
B.S. Saginaw Valley (Mich.) State University 1992; Ph.D. Michigan State University 1996; Postdoctoral Fellow, CS&D, with Doug Ray, 1996– .

Karen Knutsen
B.A. Linfield College 1981; Ph.D. University of Colorado 1992; Postdoctoral Fellow, CS&D, with Thom Orlando, 1994–1997.

David M. Laman
B.S. Florida International University 1986; M.S. Syracuse University 1988; Ph.D. University of Maryland 1997; Postdoctoral Fellow, CS&D, with Doug Ray, 1997– .

San (Sam) Li
B.S. Nankai University, Tianjin, 1983; Ph.D. Memphis State University 1991; Postdoctoral Fellow, University of Florida, 1991–1996; Postdoctoral Fellow with Lai-Sheng Wang, 1996–1997.

Lukas Novotny
Dipl.El.-Eng. Swiss Federal Institute of Technology (ETH) 1992, Dr.Sc.Nat. 1996; Postdoctoral Fellow, CS&D, with Sunney Xie, 1996– .

James Bradley Rowland
B.S. Southeastern Oklahoma State University 1990; Ph.D. Oklahoma State University 1995; Postdoctoral Fellow, CS&D, with Wayne Hess, 1996– .

Matthew T. Sieger
B.S. University of Missouri at Rolla 1990; M.S. University of Illinois 1991, Ph.D. 1995; Postdoctoral Fellow, CS&D, with Thom Orlando, 1996–.

William C. Simpson
B.S. Willamette University 1990; Ohio State University 1990–1991; M.S. University of California, Riverside, 1992, Ph.D. 1995; Postdoctoral Fellow, CS&D, with Thom Orlando, 1996– .

Kip Stevenson
B.S. University of Puget Sound 1989; Ph.D. University of Washington 1997; Postdoctoral Fellow, CS&D, with Bruce Kay, 1997– .

David P. Taylor
B.A. Concordia College 1979; Analytical Chemist, Wyeth Laboratories 1980–1982; Merck and Co. 1982–1985; Smith Kline and French Laboratories 1985–1987; M.S. Drexel University 1987; Ph.D. SUNY Stony Brook 1993; Postdoctoral Fellow, Colorado State University 1993–1996; Postdoctoral Fellow, CS&D, with Thom Orlando, 1996–1997; now with Aerospace Corp., Los Angeles.

Mark D. Tinkle
B.S. California Institute of Technology 1984; M.S. California State University, Fullerton 1987; M.S. University of California, San Diego 1989, Ph.D. 1994; Postdoctoral Fellow, CS&D, with Steve Barlow, 1996– .

Xue-Bin Wang
B.S. University of Science and Technology of China 1988; Ph.D. Institute of Chemistry, Chinese Academy of Sciences 1995; Postdoctoral Fellow Columbia 1995–1996; Postdoctoral Fellow, CS&D, with Lai-Sheng Wang, 1997– .

Richard M. Williams
B.S. University of Idaho 1991; Ph.D. University of Colorado/JILA, 1997; Postdoctoral Fellow, CS&D, with Wayne Hess, 1997– .

Andreas Zumbusch
Ph.D. University of Karlsruhe 1996; Postdoctoral Fellow, CS&D, with Sunney Xie, 1996– .

Graduate Students

Margaret S. Fyfield
Portland State University, working with Jim Cowin.

Xi Li
B.S. Northwest University, Lanzhou, China, 1986; M.S. Institute of Applied Physics, Chengdu University of Science and Technology, 1991; Researcher and Lecturer, Gansu United University, Lanzhou, 1992–1995; Washington State University, working with Lai-Sheng Wang, 1996– .

Erik D. Sanchez
Portland State University, working with Sunney Xie, 1995– .

Paul R. Winter
University of Colorado, working with Wayne Hess, 1997 .

Hongbin Wu
Washington State University, working with Lai-Sheng Wang, 1994–1997.

Liming Ying
Peking University, working with Sunney Xie, 1997– .

Undergraduate Students

Kimberly Briggman
Northwestern University, worked with Thom Orlando, summer 1997.

Ryan Ciolli
University of Oklahoma, worked with Bruce Kay, summer 1997.

Chris J. Fuller
Columbia Basin College, working with Wayne Hess, 1997– .

Jeremiah Lehman
Department of Physics and Environmental Engineering, Tulane University, worked with Steve Joyce, summer 1997.

Bradley Ornstein
University of Washington, worked with Sunney Xie, summer 1997.

Kati Shiels
M.I.T., worked with Doug Ray, summer 1997.

Rebecca Washenfelder
Pomona College, worked with Doug Ray, summer 1997.

Publications and Presentations

Publications

K. M. Beck, M. I. McCarthy, and W. P. Hess, "Atomic and Molecular Photostimulated Desorption from Complex Ionic Crystals," *J. Electronic Materials* **26**, 1335–1341 (1997). (BES)

K. M. Beck, D. P. Taylor, and W. P. Hess, "Photostimulated Desorption of CO from Geologic Calcite Following 193-nm Irradiation," *Phys. Rev. B* **55**, 13253–13262 (1997). (BES, SERDP)

J. P. Biesecker, G. B. Ellison, H. Wang, M. J. Iedema, A. A. Tsekouras, and J. P. Cowin, "Ion Beam Source for Soft-Landing Deposition," *Rev. Sci. Instr.* **69**, 485–495 (1998). (BES)

R. G. Clemmer, J. F. Kelly, S. W. Martin, G. M. Mong, and S. W. Sharpe, "Laser Based Detection of Chemical Contraband," *Proc. SPIE* **2937**, 46–56 (1997) (*Facilitating Technologies for Law Enforcement*). (NN-20)

S. R. Desai, H. Wu, C. M. Rohlfing, and L. S. Wang, "A Study of the Structure and Bonding of Small Aluminum Oxide Clusters by Photoelectron Spectroscopy: $Al_xO_y^-$ (x = 1–2, y = 1–5)," *J. Chem. Phys.* **106**, 1309–1317 (1997). (BES)

S. C. Goheen, K. L. Wahl, J. A. Campbell, and W. P. Hess, "Mass Spectrometry of Low Molecular Mass Solids by Matrix-Assisted Laser Desorption/Ionization," *J. Mass. Spectrom.* **32**, 820–828 (1997). (BES, SERDP)

B. Hecht, H. Bielefeldt, Y. Inouye, D. W. Pohl, and L. Novotny, "Facts and Artifacts in Near-Field Optical Microscopy," *J. Appl. Phys.* **81**, 2492–2498 (1997).

W. P. Hess, B. A. Bushaw, M. I. McCarthy, J. A. Campbell, S. D. Colson, and J. T. Dickinson, "Laser Ablation/Ionization Characterization of Solids: Second Interim Progress Report of the Strategic Environmental Research Development Program," PNNL-11420 (1997).

J. F. Kelly, B. D. Cannon, S. W. Sharpe, R. L. Sams, and T. A. Blake, "Applications of Wideband FM Spectroscopy to Environmental and Industrial Process Monitoring," *Proc. SPIE* **3127**, 64–102 (1997) (*Application of Lidar to Current Atmospheric Topics II*).

G. A. Kimmel, T. M. Orlando, P. Cloutier, and L. Sanche, "Low-Energy (5–40 eV) Electron-Stimulated Desorption of Atomic Hydrogen and Metastable Emission from Amorphous Ice," *J. Phys. Chem. B* **101**, 6301–6303 (1997). (BES)

N. Kizhakevariam, M. J. Iedema, and J. P. Cowin, "Mixed Oxide Surfaces: Ultrathin Films of $Ca_xMg_{1-x}O$," *J. Phys. Chem B* **102**, 693–700 (1998). (BES)

K. Knutsen and T. M. Orlando, "Photon-Stimulated Desorption of $O(^3P)$ and $NO(^2\Pi)$ from $NaNO_3$ Single Crystals," *Phys. Rev. B* **55**, 13246–13252 (1997). (BES)

S. Li, H. Wu, and L. S. Wang, , "Probing the Electronic Structure of Metallocarbohedrenes: M_8C_{12} (M = Ti, V, Cr, Zr, Nb)," *J. Am. Chem. Soc.* **119**, 7417–7422 (1997). (NSF)

H. P. Lu and X. S. Xie, "Single-Molecule Spectral Fluctuations at Room Temperature," *Nature* **385**, 143–146 (1997). (BES)

H. P. Lu and X. S. Xie, "Single-Molecule Kinetics of Interfacial Electron Transfer," *J. Phys. Chem. B* **101**, 2753–2757 (1997). (BES)

R. S. McDowell, "Infrared Spectroscopy" and (in part) "Molecular Structure and Spectra," *McGraw-Hill Encyclopedia of Science & Technology*, 8th ed. (McGraw Hill Book Co., 1997), **9**, 184–191; **11**, 405–406.

R. S. McDowell and J. F. Kelly, "Spectroscopy, Optical," *Kirk-Othmer Encyclopedia of Chemical Technology*, 4th ed. (John Wiley & Sons, New York, 1991–) **22**, 627–670 (1997). (BES)

D. Meisel, A. Cook, D. Camaioni, and T. M. Orlando, "Chemistry, Radiation, and Interfaces in Suspensions of Nuclear Waste Simulants," in K. Rajeshwar, L. M. Peter, A. Fujishima, D. Meissner, and M. Tomkiewicz, eds., *Photoelectrochemistry* (Electrochemical Society Publications, **97-20**), pp. 350-357. (EMSP)

M. B. More, D. Ray, and P. B. Armentrout, "Cation–Ether Complexes in the Gas Phase: Bond Dissociation Energies of Na^+(dimethyl ether)$_x$ (x = 1–4), Na^+(dimethoxyethane)$_x$ (x = 1 and 2) and Na^+(12-crown-4)," *J. Phys. Chem. A* **101**, 831–839 (1997). (BES)

M. B. More, D. Ray, and P. B. Armentrout, "Cation–Ether Complexes in the Gas Phase: Bond Dissociation Energies of M^+(dimethyl ether)$_x$, x = 1–3, M^+(1,2-dimethoxyethane)$_x$, x = 1 and 2, and M^+(12-crown-4) where M = Rb and Cs," *J. Chem. Phys. A* **101**, 7007–7017 (1997). (BES)

M. B. More, D. Ray, and P. B. Armentrout, "Cation–Ether Complexes in the Gas Phase: Bond Dissociation Energies of K^+(dimethyl ether)$_x$, x = 1–4; K^+(1,2-dimethoxyethane)$_x$, x = 1 and 2; and K^+(12-crown-4)," *J. Phys. Chem. A* **101**, 4254–4262 (1997). (BES)

L. Novotny, R. X. Bian, and X. S. Xie, "Theory of Nanometric Optical Tweezers," *Phys. Rev. Lett.* **79**, 645–648 (1997). (BES)

T. M. Orlando and G. A Kimmel, "The Role of Excitons and Substrate Temperature in Low-Energy (5–50 eV) Electron-Stimulated Dissociation of Amorphous D_2O Ice," *Surf. Sci.* **390**, 79–85 (1997). (BES)

B. Rowland and W. P. Hess, "UV Photochemistry of Thin Film and Matrix-Isolated Acetyl Chloride by Polarized FTIR," *J. Phys. Chem.* A **101**, 8049–8056 (1997). (BES)

E. J. Sánchez, L. Novotny, G. R. Holtom, and X. S. Xie, "Room-Temperature Fluorescence Imaging and Spectroscopy of Single Molecules by Two-Photon Excitation," *J. Phys. Chem. A* **101**, 7019–7023 (1997). (CRADA)

M. T. Sieger and T. M. Orlando, "Effect of Surface Roughness on the Electron-Stimulated Desorption of D^+ from Microporous D_2O Ice," *Surf. Sci.* **390**, 92–96 (1997). (BES)

M. T. Sieger, W. C. Simpson, and T. M. Orlando, "Electron-Stimulated Desorption of D^+ from D_2O Ice: Surface Structure and Electronic Excitations," *Phys. Rev. B* **56**, 4925–4937 (1997). (BES)

W. C. Simpson, L. Parenteau, R. S. Smith, L. Sanche, and T. M. Orlando, "Electron Stimulated Desorption of D^- (H^-) from Condensed D_2O (H_2O) Films," *Surf. Sci.* **390**, 86–91 (1997). (BES)

W. C. Simpson, M. T. Sieger, G. A. Kimmel, L. Parenteau, L. Sanche, and T. M. Orlando, "Dissociative Electron Attachment Resonances in Nanoscale Water Films," *Radiat. Res.* **148**, 491–492 (1997) (extended abstract). (BES)

W. C. Simpson, M. T. Sieger, T. M. Orlando, L. Parenteau, K. Nagesha, and L. Sanche, "Dissociative Electron Attachment in Nanoscale Ice Films: Temperature and Morphology Effects," *J. Chem. Phys* **107**, 8668–8677 (1997). (BES)

R. S. Smith, C. Huang, and B. D. Kay, "Evidence for Molecular Translational Diffusion During the Crystallization of Amorphous Solid Water," *J. Phys. Chem. B* **101**, 6123–6126 (1997). (BES)

R. S. Smith, C. Huang, E. K. L. Wong, and B. D. Kay, "The Molecular Volcano: Abrupt CCl_4 Desorption Driven by the Crystallization of Amorphous Solid Water," *Phys. Rev. Lett.* **79**, 909–912 (1997). (BES)

R. S. Smith and B. D. Kay, "Adsorption, Desorption, and Crystallization Kinetics in Nanoscale Water Films," *Recent Res. Devel. Phys. Chem.* **1**, 209–219 (1997). (BES)

R. S. Smith and B. D. Kay, "Molecular Beam Studies of Kinetic Processes in Nanoscale Water Films," *Surf. Rev. Lett.* **4**, 781–797 (1997). (BES)

D. P. Taylor, W. P. Hess, and M. I. McCarthy, "Structure and Energetics of the Water/NaCl Interface," *J. Phys. Chem. B* **101**, 7455–7463 (1997). (BES)

R. S. Taylor, D. Ray, and B. C. Garrett, "Understanding the Mechanism for the Mass Accommodation of Ethanol by a Water Droplet," *J. Phys. Chem. B* **101**, 5473–5476 (1997). (BES)

R. Tonkyn, S. Barlow, M. L. Balmer, T. Orlando, J. Hoard, and D. Goulette, "Vehicle Exhaust Treatment Using Electrical Discharge Methods," *SAE Technical Paper Series*, No. 971716, 1–6 (1997) (International Spring Fuels & Lubricants Meeting, Dearborn, Mich., May 5–8, 1997). (USCAR CRADA)

S. H. Tseng, D. F. Eggers, T. A. Blake, R. D. Beck, R. O. Watts, F. J. Lovas, and N. Zobov, "Infrared and Microwave Spectra of the N_2–Propyne van der Waals Cluster," *J. Mol. Spectrosc.* **182**, 132–147 (1997).

V. A. Venturo, A. G. Joly, and D. Ray, "Pulse Compression with a High-Energy Nd:YAG Regenerative Amplifier System," *Appl. Opt.* **36**, 5048–5052 (1997). (BES)

H. Wang, J. P. Biesecker, M. J. Iedema, G. B. Ellison, and J. P. Cowin, "Low-Energy Deposition and Collision-Induced Dissociation of Water on Pt(111)," *Surf. Sci.* **381**, 142–156 (1997). (BES)

L. S. Wang, "Study of Iron Carbon Mixed Clusters, FeC_n (n = 2–5): A Possible Linear to Cyclic Transition from FeC_3 to FeC_4," *Surf. Rev. Lett.* **3**, 423–427 (1997). (NSF)

L. S. Wang and H. Cheng, "Growth Pathways of Metallocarbohedrenes: Cagelike or Cubic?" *Phys. Rev. Lett.* **78**, 2983–2986 (1997). (NSF)

L. S. Wang, S. R. Desai, H. Wu, and J. B. Nicholas, "Small Silicon Oxide Clusters: Chains and Rings," *Z. Phys. D: Atoms, Mols., Clusters* **40**, 36–39 (1997). (BES)

L. S. Wang, J. B. Nicholas, M. Dupuis, H. Wu, and S. D. Colson, "Si_3O_y (y = 1–6) Clusters: Models for Oxidation of Silicon Surfaces and Defect Sites in Bulk Oxide Materials," *Phys. Rev. Lett.* **78**, 4450–4453 (1997). (BES)

L. S. Wang and H. Wu, "Photoelectron Spectroscopy of Transition Metal Clusters," *Z. Phys. Chem.* **203**, 45–55 (1998). (NSF)

L. S. Wang and H. Wu, "Probing the Electronic Structure of Transition Metal Clusters from Molecular to Bulk-Like Using Photoelectron Spectroscopy," *Advances in Metal and Semiconductor Clusters*, M. A. Duncan, ed., vol. **4**, pp. 299–343 (1997). (NSF)

L. S. Wang, H. Wu, and H. Cheng, "Photoelectron Spectroscopy of Small Chromium Clusters: Observation of Even–Odd Alternations and Theoretical Interpretation," *Phys. Rev. B* **55**, 12884–12887 (1997). (NSF)

X.-B. Wang, C.-F. Ding, and L. S. Wang, "Vibrationally Resolved Photoelectron Spectra of TiC_x^- (x = 2–5) Clusters," *J. Phys. Chem. A* **101**, 7699–7701 (1997). (NSF)

X.-B. Wang and L. S. Wang, "Electronic Structure and Photoelectron Spectroscopy of AlSi Mixed Dimer," *J. Chem. Phys.* **107**, 7667–7672 (1997). (NSF)

H. Wu, S. R. Desai, and L. S. Wang, "Chemical Bonding Between Cu and Oxygen–Copper Oxides vs. O_2 Complexes: A Study of CuO_x (x = 0–6) Species by Anion Photoelectron Spectroscopy," *J. Phys. Chem. A* **101**, 2103–2111 (1997). (NSF)

H. Wu and L. S. Wang, "A Study of Nickel Monooxide (NiO), Nickel Dioxide (ONiO), and $Ni(O_2)$ Complex by Anion Photoelectron Spectroscopy," *J. Chem. Phys.* **107**, 16–21 (1997). (NSF)

H. Wu and L. S. Wang, "Electronic Structure of Titanium Oxide Clusters: TiO_x (x = 1–3) and $(TiO_2)_x$ (x = 1–4)," *J. Chem. Phys.* **107**, 8221–8228 (1997). (BES)

X. S. Xie, H. P. Lu, L. Novotny, and E. Sanchez, "Single Molecule Imaging, Spectroscopy and Dynamics at Room Temperature," *Cell Vision* **4**, 188–189 (1997). (BES)

In Press and Submitted

C. C. Ainsworth, D. M. Friedrich, P. L. Gassman, Z. Wang, and A. G. Joly, "Characterization of Salicylate–Aluminum Oxide Surface Complexes by Polarized Fluorescence Spectroscopy," *Geochim. Cosmochim. Acta*, in press.

A. Al-Kahtani, D. L. Williams, J. W. Nibler, and S. W. Sharpe, "High Resolution Infrared Studies of $Al(BH_4)_3$ and $Al(BD_4)_3$," *J. Chem. Phys.*, submitted. (BES)

A. H. Bahnmaier, A. G. Joly, J. M. Price, and D. Ray, "Rotational Coherence Spectroscopy of Mass-Selected Fluorene–Ar Heterodimers by Time-Resolved Ionization Depletion," *Chem. Phys. Lett.*, submitted. (BES)

K. M. Beck and W. P. Hess, "Quantum-State Resolved Products via Vacuum Ultraviolet Photostimulated Desorption from Geologic Calcite," *Appl. Surf. Sci.*, in press.

S. D. Colson, R. E. Gephart, V. L. Hunter, J. Janata, and L. G. Morgan, "A Risk and Outcome Based Strategy for Justifying Characterization to Resolve Tank Waste," in *Science and Technology for Disposal of Radioactive Tank Wastes* (Plenum Publishing, New York), in press.

M. V. Gorshkov, J. A. Mack, S. E. Barlow, D. Ray, and J. M. Price, "Frequency-Sweep Radiofrequency Ion Trap Mass Spectrometry," *J. Am. Soc. Mass. Spectrom.*, submitted. (BES, LDRD)

W. P. Hess, S. Deshmukh, B. Rowland, P. R. Winter, and G. B. Ellison, "The Gas and Condensed Phase Ultraviolet Photochemistry of Organic Acid Chlorides," *Recent Research Developments in Photochemistry and Photobiology*, in press. (BES)

W. P. Hess, H. K. Park, O. Yavas, and R. F. Haglund Jr., "IR-MALDI of Low Molecular Weight Compounds Using a Free Electron Laser," *Appl. Surf. Sci.*, in press. (BES)

Th. Huser, L. Novotny, Th. Lacoste, R. Eckert, and H. Heinzelmann, "Observation and Analysis of Near-Field Optical Diffraction," *J. Opt. Soc. Am. A*, submitted.

K. Knutsen and T. M. Orlando, "Low-Energy (5–100 eV) Electron and Ultraviolet (6.4 eV) Photon-Stimulated Degradation of Neutral Fragments from $NaNO_3$ Single Crystals," *Appl. Surf. Sci.*, in press. (BES)

O. Kornienko, S. Brynjelsen, L. Hanley, and T. M. Orlando, "Analysis of Ethylenediaminetetraacetic acid (EDTA) by Laser Desorption Ion Trap Mass Spectrometry," *Proc. 42nd ASMS Conf. Mass Spectrom. Allied Topics*, in press. (LDRD)

L. Novotny, B. Hecht, and D. W. Pohl, "Implications of High Resolution to Near-Field Optical Microscopy," *Ultramicroscopy*, in press. (BES)

L. Novotny, E. J. Sanchez, and X. S. Xie, "Near-Field Optical Imaging Using Metal Tips Illuminated by Higher-Order Hermite-Gaussian Beams," *Ultramicroscopy*, in press. (BES)

C. H. F. Peden, G. S. Herman, I. Z. Ismagilov, B. D. Kay, M. A. Henderson, Y. J. Kim, and S. A. Chambers, "Model Catalyst Studies with Single Crystals and Epitaxial Thin Oxide Films," *Catalysis Today*, submitted. (BES)

R. L. Sams, T. A. Blake, S. W. Sharpe, J.-M. Flaud, and W. J. Lafferty, "High Resolution Infrared Study of the ν_{14}, ν_{17}, and ν_{18} Bands of $^{11}B_2H_6$ and $^{10}B^{11}BH_6$," *J. Mol. Spectrosc.*, submitted.

M. T. Sieger, T. M. Orlando, G. A. Kimmel, and W. C. Simpson, "On the Origin of O_2 in Planetary Ices," *Nature*, submitted. (BES)

W. C. Simpson, T. M. Orlando, L. Parenteau, K. Nagesha, and L. Sanche, "Dissociative Electron Attachment in Nanoscale Ice Films: Thickness and Charge Trapping Effects," *J. Chem. Phys.*, in press. (BES)

S. C. Stone, L. A. Philips, G. T. Fraser, F. J. Lovas, L.-H. Xu, and S. W. Sharpe, "High-Resolution Microwave and Infrared Molecular Beam Studies of the Conformers of 1,1,2,2-Tetrafluoroethane," *J. Mol. Spectrosc.*, submitted. (BES)

D. P. Taylor, W. C. Simpson, K. Knutsen, M. A. Henderson, and T. M. Orlando, "Photon Stimulated Desorption of Cations from Yttria-Stabilized Cubic $ZrO_2(100)$," *Appl. Surf. Sci.*, in press. (LDRD)

R. G. Tonkyn, M. Balmer, S. Barlow, T. M. Orlando, J. Hoard, and D. Goulette, "Vehicle Exhaust Treatment Using Electrical Discharge and Materials Chemistry," *Proc. 1997 Diesel Exhaust Reductions Workshop*, in press. (USCAR CRADA)

A. A. Tsekouras, M. K. Iedema, G. B. Ellison, and J. P. Cowin, "Assembling Ionic Interfaces via Soft-Landed Ions," *Science*, submitted. (BES)

A. A. Tsekouras, M. J. Iedema, G. B. Ellison, and J. P. Cowin, "Soft-Landed Ions: A Route to Ionic Solution Studies," *J. Mass Spectrom. Ion Processes*, in press. (BES, SERDP)

A. A. Tsekouras, N. Kizhakevariam, and J. P. Cowin, "Amorphous Water Ice Relaxations Measured with Soft-Landed Ions," *Phys. Rev. Lett.*, submitted. (BES)

X. B. Wang, H. Cheng, H. Wu, and L. S. Wang, "New Magic Numbers in $Ti_xC_y^-$ and $V_xC_y^-$ Anion Clusters: Implications for Met-Car Growth Pathways," *J. Am. Chem. Soc.*, submitted.

P. R. Winter, B. Rowland, W. P. Hess, J. G. Radziszewski, M. R. Nimlos, and G. B. Ellison, "The UV Photodissociation of Matrix Isolated Propionyl Chloride," *J. Phys. Chem.*, submitted. (BES)

H. Wu and L. S. Wang, "A Photoelectron Spectroscopic Study of Monovanadium Oxide Anions: VO_x^- (x = 1–4)," *J. Chem. Phys.*, in press. (NSF)

X. S. Xie, R. X. Bian, and R. C. Dunn, "Near-Field Microscopy and Spectroscopy of Single Molecules, Single Proteins, and Biological Membranes," in *Focus on Multidimensional Microscopy*, P. C. Cheng, P. P. Hwang, J. L. Wu, G. Wang, and H. Kim, eds. (World Scientific Publ. Co.), in press. (BES)

Patents

S. E. Barlow, M. L. Alexander, and J. C. Follansbee, "Asymmetric Ion Trap," U.S. Patent 5,693,941, issued Dec. 2, 1997. (BES)

S. E. Barlow, T. M. Orlando, and R. G. Tonkyn, "Design for Monolithic Dielectric Packing Discharge Reactor," patent pending. (USCAR CRADA)

S. E. Barlow, R. G. Tonkyn, and T. M Orlando, "Method and Apparatus for Processing Exhaust Gas with Corona Discharge," patent pending. (USCAR CRADA)

K. M. Beck, "Photoacoustic Touch-Off Probe," patent pending.

A. J. Peurrung and S. E. Barlow, "Confinement of Weakly Ionized Gas in the Presence of a Neutral Gas," patent pending.

Presentations *(Presenter underlined)*

C. C. Ainsworth, Z. Wang, D. M. Friedrich, P. L. Gassman, and A. G. Joly, "Kinetics of Salicylate Surface Complexation in Aqueous Alumina Suspensions," Symposium on Environmental Chemistry at Soil Mineral Surfaces, Soil Science Society of America National Meeting, Anaheim, Cal., Oct. 30, 1997. (LDRD)

M. A. Alexander and S. E. Barlow, "Asymmetric Quadrupole Ion Trap Design for Simultaneous Ejection of Positive and Negative Ions Trapped from Laser Desorption," Sanibel Conference on Quadrupole Ion Traps, Sanibel I., Fla., Jan. 1997.

K. M. Beck and W. P. Hess, "Quantum-State Resolved Products via Vacuum Ultraviolet Photostimulated Desorption from Geologic Calcite," Fourth International Conference on Laser Ablation, Asilomar, Cal., July 21, 1997.

K. M. Beck, M. I. McCarthy, and W. P. Hess, "Atomic and Molecular Photostimulated Desorption from Complex Ionic Crystals," 1997 Symposium on Low Energy Processes in Electronic Materials: Energetic Beam, Deposition, and Synthesis, Orlando, Fla., Feb. 8–12, 1997.

R. X. Bian, L. Novotny, and X. S. Xie, "FDTD Simulations of the Nanometric Optical Near-Field Tip," International Conference on Computational Physics, Santa Cruz, Cal., Aug. 25–28, 1997 [abstract: *Bull. Amer. Phys. Soc.* **42**, 1563 (1997)].

R. X. Bian, X. S. Xie, and P. Leung, "Applications of the Finite Difference Time Domain Method to Near-Field Microscopy and Spectroscopy," Fourth International Conference on Near-Field Optics, Jerusalem, Israel, Feb. 9–13, 1997.

J. D. Chesko, H. P. Lu, and X. S. Xie, "Slow Dynamics of Single Molecules in a Room Temperature Polymer Matrix," 213th American Chemical Society National Meeting, San Francisco, April 13–17, 1997.

S. D. Colson, "Risk and Outcome-Based Strategy for Justifying Characterization to Resolve Tank Waste Safety Issues," 214th American Chemical Society National Meeting, Las Vegas, Sept. 8–11, 1997.

J. P. Cowin, "Mixed Oxide Surfaces: Ultrathin Films of $Ca_xMg_{(1-x)}O$," Washington State University, Pullman, Feb. 14, 1997.

J. P. Cowin, "REALLY Building the Electrochemical Double Layer in Ultra-High Vacuum," Phys-

ics Department Seminar, Washington State University, Pullman, April 9, 1997.

J. P. Cowin, "Soft-Landing Ions for Recreating Solution–Solid Interfaces," Chemistry Department Seminar, Notre Dame University, Notre Dame, Ind., May 19, 997.

J. P. Cowin, "Soft-Landing Ions for Recreating Solution–Solid Interfaces," Chemistry Department Seminar, Purdue University, West Lafayette, Ind., May 20, 1997.

J. P. Cowin, "Soft-Landing Ions for Recreating Solution–Solid Interfaces," University of Illinois, Chicago, May 21, 1997.

J. P. Cowin, "Soft-Landing Ions for Recreating Solution–Solid Interfaces," Fifth Annual Conference on Physical Electronics, Eugene, Ore., June 18–21, 1997.

J. P. Cowin, "Recreating the Solution/Solid Interface via Epitaxy with a 1-eV Ion Beam," Chemistry Department Seminar, Oklahoma State University, Stillwater, Aug. 27, 1997.

J. P. Cowin, "Soft-Landing Ions to Recreate Aqueous–Solid Interfaces," American Vacuum Society National Symposium, San Jose, Cal., Oct. 20–24, 1997.

J. P. Cowin, M. J. Iedema, and A. A. Tsekouras, "Soft Landing of Ions to Recreate Aqueous–Solid Interfaces" (poster), 214th American Chemical Society National Meeting, Las Vegas, Sept. 8–11, 1997.

J. P. Cowin and A. A. Tsekouras, "Soft Landing and Mobility of Cs^+ Ions on Hexane Ice" (poster), Conference on the Dynamics of Molecular Collisions, Gull Lake, Minn., July 20–25, 1997.

J. P. Cowin and A. A. Tsekouras, "Soft-Landed Cs^+ and D_3O^+ Ion Studies on D_2O Ice" (poster) Gordon Research Conference on Dynamics at Surfaces, Andover, N.H., Aug. 10–15, 1997.

D. M. Friedrich, C.C. Ainsworth, Z. Wang, A. G. Joly, and P L. Gassman, "Speciation and Kinetics of the Surface Complexation of Salicylate Anion in Aqueous Alumina Suspensions," invited presentation at the Humic Materials Symposium, American Chemical Society Northwest Regional Meeting, Moscow, Idaho, June 20,1997. (LDRD)

D. M. Friedrich, Z. Wang, C. C. Ainsworth, P. L. Gassman, and A. G. Joly, "Characterization of Salicylate–Alumina Surface Complexes by Polarized Fluorescence Spectroscopy," Symposium on Environmental Chemistry at Soil Mineral Surfaces, Soil Science Society of America National Meeting, Anaheim, Cal., Oct. 27, 1997. (LDRD)

W. P. Hess, "Laser Desorption in Molecular Speciation," Los Alamos National Laboratory, Jan. 1997.

W. P. Hess, "Molecular Desorption from Ionic Molecular Crystals Following Resonant UV Excitation," 213th American Chemical Society National Meeting, San Francisco, April 13–17, 1997.

W. P. Hess, "Development of Laser Ablation for Characterization of Hazardous Waste and Contaminated Soils," 213th American Chemical Society National Meeting, San Francisco, April 13–17, 1997.

W. P. Hess, "IR MALDI of Low Molecular Weight Compounds Using a Free-Electron Laser," Fourth International Conference on Laser Ablation (COLA), Pacific Grove, Cal., July 21–25, 1997.

S. A. Joyce, "Structural Studies of Thin-Film Oxide Surfaces by STM and LEED," Texas Superconductor Center, University of Houston, Feb. 1, 1997.

D. S. Karpovich, A. G. Joly, and D. Ray, "Receptors for Ionic Guests at Liquid/Liquid Interfaces Studied by Nonlinear Laser Spectroscopy," 213th American Chemical Society National Meeting, San Francisco, April 13–17, 1997.

D. S. Karpovich, A. G. Joly, and D. Ray, "Metal Ion Complexants at Liquid Interfaces," 214th American Chemical Society National Meeting, Las Vegas, Sept. 8–11, 1997.

D. S. Karpovich and D. Ray, "Thermochemistry of DMSO Transport Across the Liquid/Vapor Interface of Water," 214th American Chemical Society National Meeting, Las Vegas, Sept. 8–11, 1997.

B. D. Kay, "Molecular Beam Studies of Kinetic Processes in Nanoscale Films of Amorphous Ice,", Physical Chemistry Seminar, University of Washington, Seattle, Jan. 22, 1997.

B. D. Kay, "State-to-State Inelastic and Reactive Gas–Surface Scattering," Fourth European Summer School in Surface Science: Surface Reactivity, Humlebaek, Denmark, Aug. 17–22, 1997.

B. D. Kay, "Beam Studies of Adsorption, Desorption, Diffusion, and Phase Transformation Kinetics," Joint Physics and Chemistry Seminar, Washington State University, Pullman, Nov. 18, 1997.

B. D. Kay, R. Smith, and C. Huang, "Adsorption, Desorption, Phase Transformation, Diffusion and Reaction Dynamics (Kinetics) in Nanoscale Ice Films," Gordon Research Conference on Dynamics at Surfaces, Andover, N.H., Aug. 10–15, 1977.

B. D. Kay, R. Smith, and C. Huang, "Beam Studies of Adsorption, Desorption, Diffusion, and Phase Transformation Kinetics," Fourth European Summer School in Surface Science: Surface Reactivity, Humlebaek, Denmark, Aug. 17–22, 1997.

G. A. Kimmel, R. S. Smith, M. A. Covert, and B. D. Kay, "Next Generation Molecular Beam Scattering Machines," Ninth Annual Pacific Northwest Symposium, American Vacuum Society, Troutdale, Ore., Sept. 18–19, 1997.

M. W. Kimmel, M. S. Johnson, S. E. Bisson, P. J. Hargis Jr., T. J. Kulp, T. A. Blake, J. F. Kelly, and S. W. Sharpe, "UV Fluorescence Detection of Particles Generated by Gas Hydrolysis" (poster), CALIOPE Program Fourth Technical Review, Livermore, Cal., February 25–27 1997.

K. Knutsen and T. M. Orlando, "Free Radical Reactions at $NaNO_3$–Organic Interfaces," 214th American Chemical Society National Meeting, Las Vegas, Sept. 8–11, 1997.

S. Li, H. Wu, X. Li, C. Ding, and L. S. Wang, "Photoelectron Spectroscopy of Metallocarbohedrenes $M_8C_{12}^-$ (M = Ti, V, Cr, Zr, Nb)," 213th American Chemical Society National Meeting, San Francisco, April 13–17, 1997.

H. P. Lu and X. S. Xie, "Spectral Fluctuations and Chemical Dynamics of Single Molecules and Single Proteins," 213th American Chemical Society National Meeting, San Francisco, April 13–17, 1997.

H. P. Lu, X. S. Xie, and L. Xun, "Conformational Fluctuations and Chemical Dynamics of Single Molecules and Single Proteins," Gordon Research Conference on Proteins, Holderness, N.H., June 15–20, 1997.

C. R. Mahon, C. Chackerian Jr., L. P. Giver, and T. A. Blake, " Zeeman Tuning Rates in the ν_3 Band of NO_2," 52nd Ohio State University International Symposium on Molecular Spectroscopy, Columbus, June 16–20, 1997.

M. B. More, P. B. Armentrout, and D. Ray, "Determination of the Alkali Metal Ion Binding Affinities of Crown Ethers by Guided Ion Beam Mass Spectrometry," Ion Chemistry Conference, Lake Arrowhead, Cal., January 24–26, 1997.

L. Novotny, "Light Propagation and Confinement in Near-Field Optics," Seminar, Photophysics Laboratory, University of Dresden, Germany, March 1997.

L. Novotny, "Theoretical Aspects of Near-Field Optics," Workshop on Near-Field Scanning Optical Microscopy, Marburg, Germany, April 1997.

L. Novotny, "Light Propagation and Confinement in Near-Field Optics," Seminar, Experimental Physics Dept., University of Chemnitz, Germany, April 1997.

L. Novotny, E. J. Sanchez, and X. S. Xie, "Is Near-Field Fluorescence Imaging with 10-nm Resolution Possible?" Fourth International Conference on Near-Field Optics, Jerusalem, Israel, Feb. 9–13, 1997.

T. M. Orlando, "Quantum-Resolved Studies of Low-Energy (5–150 eV) Electron-Stimulated Interactions in Molecular Solids," 7th International Workshop on Desorption Induced by Electronic Transition (DIET VII), Ambleside, England, April 8–11, 1997.

T. M. Orlando, "Dissociative Electron Attachment Resonances in Nanoscale Water Films," 5th International Workshop on Radiation Damage to DNA: Techniques, Quantitation and Mechanisms, Bowness-on-Windermere, England, April 19–24, 1997.

T. M. Orlando, "UV Photon and Low-Energy (5–150 eV) Electron-Stimulated Processes at Environmental Interfaces," 24th IEEE International Conference on Plasma Science (ICOPS '97), San Diego, May 19–22, 1997. (BES)

T. M. Orlando, "A Comparison Between UV-Photon and Low-Energy Electron-Stimulated Desorption Processes from Wide Band-Gap Materials," Fourth International Conference on Laser Ablation (COLA), Pacific Grove, Cal., July 21–25, 1997. (BES, LDRD)

T. M. Orlando, "Photon Stimulated Desorption of Cubic Zirconia," Fourth International Conference

on Laser Ablation (COLA), Pacific Grove, Cal., July 21–25, 1997.

T. M. Orlando, "Quantum State Resolved Stimulated Desorption Studies of Wide Band-Gap Materials," Fourth International Conference on Laser Ablation (COLA), Pacific Grove, Cal., July 21–25, 1997.

T. M. Orlando and G. A. Kimmel, "The Role of Excitons and Substrate Temperature in Low-Energy (5–50 eV) Electron-Stimulated Dissociation of Amorphous D_2O Ice," 7th International Workshop on Desorption Induced by Electronic Transitions (DIET VII), Ambleside, England, April 8–11, 1997.

N. G. Petrik, D. P. Taylor, W. C. Simpson, M. T. Sieger, and T. M. Orlando, "Laser-Stimulated Luminescence of Yttria-Stabilized Cubic Zirconia Crystals," Northwest Regional Meeting, American Vacuum Society, Troutdale, Ore, Sept. 25–28, 1997.

N. G. Petrik, R. G. Tonkyn, W. C. Simpson, S. E. Barlow, and T. M. Orlando, "A Liquid Beam Source Ultrahigh Vacuum System for Liquid Interface Studies," Northwest Regional Meeting, American Vacuum Society, Troutdale, Ore, Sept. 25–28, 1997.

D. Ray, "Transport of Molecules Across the Liquid Water/Vapor Interface Probed by Surface Nonlinear Optical Spectroscopy," Department of Chemistry, University of Nevada, Reno, March 1997.

D. Ray, "Metal Ion Complexants at Liquid Interfaces," Northwest Regional Meeting, American Vacuum Society, Troutdale, Ore, Sept. 25–28, 1997.

D. Ray and D. S. Karpovich, "Crown Ethers at Liquid/Liquid Interfaces Studied by Nonlinear Laser Spectroscopy: Toward a Molecular-Level Understanding of Solvent Extraction," Tenth Symposium on Separation Science and Technology for Energy, Gatlinburg, Tenn., Oct. 1997.

B. Rowland and W. Hess, "Ultraviolet Photolysis of Condensed-Phase Acetyl Chloride: Verification of a Concerted Elimination Reaction," 52nd Ohio State University International Symposium on Molecular Spectroscopy, Columbus, June 16–20, 1997.

B. Rowland and W. Hess, "IR Polarization Study of the UV Photolysis of Acetyl Chloride," 52nd Ohio State University International Symposium on Molecular Spectroscopy, Columbus, June 16–20, 1997.

B. Rowland and W. Hess, "IR Polarization Study of the UV Photodissociation of Acetyl Chloride: Alignment of Photoproducts in the Condensed Phase," 214th American Chemical Society National Meeting, Las Vegas, Sept. 8–11, 1997.

R. L. Sams, T. A. Blake, S. W. Sharpe, J.-M. Flaud, and W. J. Lafferty, "The High-Resolution Infrared Spectrum of Diborane," 52nd Ohio State University International Symposium on Molecular Spectroscopy, Columbus, June 16 - 20, 1997.

E. J. Sanchez, L. Novotny, and X. S. Xie, "Fluorescence Imaging of Single Molecules and Photosynthetic Membranes with Two-Photon Excitation," 213th American Chemical Society National Meeting, San Francisco, April 13–17, 1997.

E. J. Sanchez and X. S. Xie, "Towards High-Resolution Spectroscopic Imaging," Fifth Annual Conference on Physical Electronics, Eugene, Ore., June 25–28, 1997.

M. T. Sieger, T. M. Orlando, and G. K. Schenter, "The Role of Diffraction in Electron-Stimulated Desorption," Fifth Annual Conference on Physical Electronics, Eugene, Ore., June 25–28, 1997.

M. T. Sieger, G. Schenter, and T. M. Orlando, "Electron Standing Wave Stimulated Desorption of H^+ from Si(100)," Fifth Annual Conference on Physical Electronics, Eugene, Ore., June 25–28, 1997.

M. T. Sieger, W. C. Simpson, and T. M. Orlando, "Effect of Surface Roughness on the Electron-Stimulated Desorption of D^+ from Microporous D_2O Ice," 7th International Workshop on Desorption Induced by Electronic Transitions (DIET VII), Ambleside, England, April 8–11, 1997.

W. C. Simpson, L. Parenteau, R. S. Smith, L. Sanche, and T. M. Orlando, "Electron-Stimulated Desorption of D^- (H^-) from D_2O (H_2O) Films," 7th International Workshop on Desorption Induced by Electronic Transitions (DIET VII), Ambleside, England, April 7–11, 1997.

W. C. Simpson, M. T. Sieger, G. A. Kimmel, T. M. Orlando, L. Parenteau, and L. Sanche, "Dissociative Electron Attachment in Condensed D_2O Films: The Effects of Film Thickness, Temperature and Morphology," Gordon Research Confer-

ence on Chemical Reactions at Surfaces, Ventura, Cal., Feb. 16–21, 1997.

W. C. Simpson, W. Wang, J. Yarrmoff, and T. M. Orlando, "The Photon- and Electron-Stimulated Desorption of O^+ from Zirconium Oxide Surfaces," Northwest Regional Meeting, American Vacuum Society, Troutdale, Ore, Sept. 25–28, 1997.

R. S. Smith, "The Adsorption, Desorption, Phase Transformation, and Diffusion Kinetics in Nanoscale Amorphous Ice Films," Physical Chemistry Seminar, University of Utah, Salt Lake City, Nov. 10, 1997.

R. S. Smith, C. Huang, E. Wong, and B. D. Kay, "Thermodynamic Continuity and Mobility in Amorphous Solid Water: Evidence for the Existence of Supercooled Liquid Water," Fifth Annual Conference on Physical Electronics, Eugene, Ore., June 25–28, 1997.

R. S. Smith, C. Huang, E. Wong, and B. D. Kay, "Thermodynamic Continuity and Mobility in Amorphous Solid Water: Evidence for the Existence of Supercooled Liquid Water," Gordon Research Conference on the Chemistry and Physics of Liquids, Plymouth, N.H., August 1997.

R. S. Smith, C. Huang, E. Wong, and B. D. Kay, "Thermodynamic Continuity and Mobility in Amorphous Solid Water: Evidence for the Existence of Supercooled Liquid Water," Ninth Annual Pacific Northwest Symposium, American Vacuum Society, Troutdale, Ore., Sept. 18–19, 1997.

D. P. Taylor, W. C. Simpson, K. Knutsen, M. A. Henderson, and T. M. Orlando, "Photon-Stimulated Desorption and Laser Ablation of Yttria-Stabilized $ZrO_2(100)$ Crystals," Fourth International Conference on Laser Ablation (COLA), Pacific Grove, Cal., July 21–25, 1997.

R. S. Taylor, D. S. Karpovich, J. L. Daschbach, B. C. Garrett, and D. Ray, "Transport of Small Molecules Across the Liquid/Vapor Interface of Water," 214th American Chemical Society National Meeting, Las Vegas, Sept. 8–11, 1997.

M. D. Tinkle, G. A. Anderson, and S. E. Barlow, "An FT/ICR for Chemical Physics Experimentation," 45th American Society for Mass Spectrometry Conference on Mass Spectrometry and Allied Topics, Palm Springs, Cal., June 1997.

M. D. Tinkle and S. E. Barlow, "Preliminary Results from a ICR Mass Spectrometer," Fourth Workshop on Non-Neutral Plasma Physics, Boulder, Col., Aug. 1997.

A. A. Tsekouras, M. J. Iedema, and J. P. Cowin, "Soft Landing and Mobility of Cs^+ Ions on Hexane Ice Multilayers," Northwest Regional Meeting, American Vacuum Society, Troutdale, Ore, Sept. 25–28, 1997.

L. S. Wang, "Probing the Electronic Structures of Metals and Metal Oxide Clusters Using Anion Photoelectron Spectroscopy," Lawrence Livermore National Laboratory, Livermore, Cal., Aug. 1997.

L. S. Wang, "Gas-Phase Studies of Novel Nanoclusters Using Laser Ablation and Anion Photoelectron Spectroscopy," University of Idaho, Moscow, Oct. 1997.

L. S. Wang, "Experimental Studies of the Electronic Structure of Nanoclusters," Symposium on Frontiers of Chemistry, The Hong Kong University of Science and Technology, Dec. 20–23, 1997.

L. S. Wang and H. Cheng, "Growth Pathways of Metallocarbohedrenes (Metcars): Cage-Like or Cubic?" 214th American Chemical Society National Meeting, Las Vegas, Sept. 8–11, 1997.

L. S. Wang, J. B. Nicholas, M. Dupuis, H. Wu, and S. D. Colson, "Si_3O_y (y = 1–6) Clusters: Models for Oxidation of Silicon Surfaces and Defect Sites in Bulk Oxide Materials," 213th American Chemical Society National Meeting, San Francisco, April 13–17, 1997.

L. S. Wang and H. Wu, "Probing the Electronic Structure Evolution of Transition Metal Clusters from Atom to Bulk," 213th American Chemical Society National Meeting, San Francisco, April 13–17, 1997.

L. S. Wang and H. Wu, "Electronic Structure of Titanium Oxide Clusters: TiO_x (x = 1–3) and $(TiO_2)_x$ (x = 1–4)," 214th American Chemical Society National Meeting, Las Vegas, Sept. 8–11, 1997.

Z. Wang, C. C. Ainsworth, D. M. Friedrich, A. G. Joly, and P. L. Gassman, "The Surface Reaction Kinetics of Salicylate on Alumina," 213th American Chemical Society National Meeting, San Francisco, April 13–17, 1997. (LDRD)

H. Wu and L. S. Wang, "An Experimental Study of the Electronic Structures of the First-Row Transition Metal Monoxides and Dioxides by Anion Photoelectron Spectroscopy," 213th American

Chemical Society National Meeting, San Francisco, April 13–17, 1997.

X. S. Xie, "Probing Single-Molecule Behaviors," AMSIE '97, Seattle, Feb. 1997.

X. S. Xie, "Imaging, Spectroscopy, and Dynamics of Single Molecules, Single Enzymes, and Biological Membranes," Department of Physics, University of Alberta, Edmonton, Mar. 7, 1997.

X. S. Xie, "Imaging, Spectroscopy, and Dynamics of Single Molecules, Single Enzymes, and Biological Membranes," Department of Chemistry, University of Kansas, Lawrence, Mar. 10, 1997.

X. S. Xie, "Imaging, Spectroscopy, and Dynamics of Single Molecules, Single Enzymes, and Biological Membranes," Department of Chemistry, Iowa State University, Ames, May 2, 1997.

X. S. Xie, "Single-Molecule Spectroscopy and Dynamics at Room Temperature," Gordon Research Conference on Molecular Electronic Spectroscopy and Dynamics, Oxford, Engl., Aug. 1997.

X. S. Xie, "Imaging, Spectroscopy, and Dynamics of Single Molecules, Single Enzymes, and Biological Membranes," Department of Chemistry, Stanford University, Stanford, Cal., Sept. 29, 1997.

X. S. Xie, "Imaging, Spectroscopy, and Dynamics of Single Molecules, Single Enzymes, and Biological Membranes," Department of Chemistry, University of California, Berkeley, Sept. 30, 1997.

X. S. Xie, "Imaging, Spectroscopy, and Dynamics of Single Molecules, Single Enzymes, and Biological Membranes," Department of Chemistry, University of Illinois at Urbana–Champaign, Nov. 12, 1997.

X. S. Xie, "Imaging, Spectroscopy, and Dynamics of Single Molecules, Single Enzymes, and Biological Membranes," Department of Chemistry, University of Pittsburgh, Nov. 13, 1997.

X. S. Xie, "Imaging, Spectroscopy, and Dynamics of Single Molecules, Single Enzymes, and Biological Membranes," Department of Chemistry, Pennsylvania State University, State College, Nov. 14, 1997.

X. S. Xie, "Imaging, Spectroscopy, and Dynamics of Single Molecules, Single Enzymes, and Biological Membranes," Department of Chemistry, Massachusetts Institute of Technology, Cambridge, Dec. 8, 1997.

X. S. Xie, "Imaging, Spectroscopy, and Dynamics of Single Molecules, Single Enzymes, and Biological Membranes," Department of Chemistry, Georgia Institute of Technology, Atlanta, Dec. 10, 1997.

X. S. Xie, H. P. Lu, L. Novotny, and E. J. Sanchez, "Single Molecule Imaging, Spectroscopy, and Dynamics at Room Temperature," Focus on Multidimensional Spectroscopy '97, Buffalo, N.Y., Apr. 27–30, 1997.

X. S. Xie, H. P. Lu, E. J. Sanchez, and L. Novotny, "Imaging, Spectroscopy, and Dynamics of Single Molecules, Single Proteins, and Biological Membranes," 1997 Quantum Electronics and Laser Science Conference on Nonlinear Optical Phenomena, Baltimore, May 1997.

X. S. Xie, H. P. Lu, and L. Xun, "Probing Dynamics of Single Enzyme Molecules," Symposium on Frontiers of Chemistry, Hong Kong, Dec. 21–23, 1997.

X. S. Xie, H. P. Lu, and L. Ying, "Single-Molecule Studies of Spectral Diffusion, Interfacial Electron Transfer, and Exciton Dynamics," 21st Solar Photochemistry Research Conference, Copper Mountain, Col., June 1997.

L. Ying, H. P. Lu, X. S. Xie, and N. Hunter, "Single-Molecule Studies of Light-Harvesting Complexes (LH2) from Photosynthetic Bacteria," 213th American Chemical Society National Meeting, San Francisco, April 13–17, 1997.

Honors and Recognition

Ken Beck was nominated by NSF for a Japanese Science Technology Agency short-term fellowship for a research collaboration at Tsukuba Science City, based on a proposal entitled "The Preparation and Characterization of Functional Nanocomposite Films by Laser Ablation."

Tom Blake was promoted to Research Scientist III, January 1997.

Wayne Hess was promoted to Chief Scientist IV, December 1997.

Alan Joly was promoted to Research Scientist III, January 1997.

Steve Joyce assumed the chair of the Pacific Northwest Section, American Vacuum Society, in January 1997. He also serves on the AVS Surface Science Executive Committee.

Bruce Kay was appointed Affiliate Professor of Chemistry, University of Washington, December 1997.

Greg Kimmel was promoted to Research Scientist III, December 1997.

Rod McDowell was appointed to a four-year term as a Titular Member of the International Union of Pure and Applied Chemistry's Commission I.5 (Physical Chemistry Division, Commission on Molecular Structure and Spectroscopy) starting January 1998. He is responsible for preparing for publication a IUPAC Recommendations document, *Notations and Conventions in Molecular Spectroscopy: Part 4. Vibrational-Rotational Spectroscopy.*

Lukas Novotny received the 1997 M. T. Thomas Award for Outstanding Postdoctoral Achievement, recognizing significant scientific contributions to projects relevant to the EMSL mission. He received a cash prize and his name has been added to a plaque in the EMSL lobby. The citation reads, "For his contributions to the theoretical understanding of near-field optical microscopy, especially in demonstrating the feasibility of optical trapping and manipulation at a nanometer scale."

Thom Orlando received a Young Investigator Award to attend the 5th International Workshop on Radiation Damage to DNA: Techniques, Quantitation and Mechanisms, Bowness-on-Windermere, England, April 19–24, 1997.

Steve Sharpe was promoted to Chief Scientist IV, March 1997.

The paper by **R. S. Smith, C. Huang, E. K. L. Wong,** and **B. D. Kay**, "The Molecular Volcano: Abrupt CCl_4 Desorption Driven by the Crystallization of Amorphous Solid Water," *Phys. Rev. Lett.* **79**, 909–912 (1997), received significant attention in the popular scientific press:

Physics News Update (http://www.aip.org/news/physnews/), No. 330, July 17, 1997.

Science Now (http://www.sciencenow.org), July 25, 1997.

Science News **152**, 103 (Aug. 16, 1997).

Physics Today, "Physics Update," p. 9 (Sept. 1997).

Natur und Wissenschaft, Sept. 3, 1997.

Lai-Sheng Wang was selected as an Alfred P. Sloan Research Fellow in February 1997. This highly competitive award included an unrestricted research grant.

Lai-Sheng Wang was awarded the Washington State University Westinghouse Distinguished Professorship in Materials Science and Engineering for the 1997–1998 academic year, in recognition of his pioneering work in the synthesis and characterization of novel clusters of oxide materials.

Hongbin Wu received a travel award from Washington State University to present a paper at the 213th American Chemical Society National Meeting, San Francisco, April 13–17, 1997.

Hongbin Wu successfully defended his thesis, "Photoelectron Spectroscopic Studies on the Electronic Structures of Transition Metal Clusters and Transition Metal Oxide Clusters," done under the supervision of Lai-Sheng Wang, and was awarded the Ph.D. degree by Washington State University, Dec. 1997.

Andreas Zumbusch was awarded a Feodor Lynen Fellowship by the Alexander von Humboldt Foundation. Lynen fellowships are awarded to German postdoctoral students for research abroad in collaboration with a former Humboldt Fellow, in this case **Steve Colson**, Humboldt Fellow 1991–92.

Collaborations

External Collaborations

Type of collaborator:
(1) = non-visiting;
(2) = short-term (<1 month);
(3) = long-term (≥1 month).

K. M. Beck
University of Central Florida (R. Peale, PASS Affiliated Scientist) (3)
Optically Detected Magnetic Resonance (ODMR) and Time-Resolved FTIR of Immobilized Heavy Metals on Calcite Surfaces

K. M. Beck
National Institute of Materials and Chemical Research, Japan (T. Sasaki) (2)
Preparation and Characterization of Pt/SiO_2 and Pt/MgO Functional Nanocomposite Films by Laser Ablation

J. P. Cowin
University of Colorado (G. B. Ellison) (2)
Soft-Landing Ions

J. P. Cowin
Washington State University (M. Dresser) and Associated Western Universities (D. Doering) (2)
Ferroelectric Ice

J. P. Cowin
Arrowhead University (M. C. Gallagher) (1)
Thin-Film Al_2O_3

J. P. Cowin
Washington State University (B. Pate) (2)
Soft-Landing Ion Studies

W. P. Hess
Vanderbilt University (R. F. Haglund, Jr.) (1)
Studies of Laser/Solids Interactions

W. P. Hess
University of Colorado (G. B. Ellison) (1,2)
Photochemistry of Thin Molecular Films

W. P. Hess
Washington State University (J. T. Dickinson) (1)
Laser Ablation Characterization of Solids

S. A. Joyce
Tulane University (U. Diebold) (2)
Structure and Chemistry of Metal Oxides

B. D. Kay
Chalmers University, Göteborg, Sweden (B. Kasemo) (1)
Desorption and Phase Transformation Kinetics in Amorphous Ice

B. D. Kay
University of Wellington, N.Z. (R. J. Speedy) and Princeton University (P. G. Debenedetti) (1)
Metastability of Glassy Water and its Relation to Liquid Water

T. M. Orlando
Argonne National Laboratory (D. Meisel) (1)
Radiation Chemistry

T. M. Orlando
Lawrence Livermore National Laboratory (J. N. Bardsley and B. M. Penetrante) (1)
Development of Plasma Processing Techniques

T. M. Orlando
University of Sherbrooke (L. Sanche) (1)
Low-Energy Electron-Stimulated Processes in Water Overlayers

T. M. Orlando
Istituto di Struttura della Materia, CNR, Frascati, Rome (N. Zema) and University of Rome (M. Piancentini) (1)
Investigation of Surface Excitations in Low-Energy Electron- and Photon-Stimulated Desorption

T. M. Orlando
Research Institute of Complex Power Technology (VNIPIET), St. Petersburg (N. G. Petrik) (3)
Laser-Stimulated Luminescence

T. M. Orlando and J. P. Cowin
Rutgers University (T. E. Madey) and Brookhaven National Laboratory (P. E. Haustein) (1)
Radiolytic and Thermal Processes Relevant to Dry Storage of Spent Nuclear Fuels

T. M. Orlando, R. G. Tonkyn, and S. E. Barlow
Ford Motor Company (J. Hoard) and General Motors Company (M. Hemingway and G. Fischer) (1)
Vehicle Exhaust Treatment Using Electrical Discharge and Materials Chemistry

D. Ray
University of Utah (P. B. Armentrout) (1)
Gas-Phase Cation–Ether Complexes

S. W. Sharpe
Oregon State University (J. W. Nibler) (2)
Jet Spectroscopy of Metal Borohydrides

S. W. Sharpe
State University of New York at Stony Brook (P. Varanasi) (1)
High-Resolution Infrared Spectroscopy of Atmospheric Interest

S. W. Sharpe
University of Colorado (V. Vaida) (2)
Spectroscopy of Water Clusters and Small Droplets: Relevance to Atmospheric Radiative Transfer

S. W. Sharpe
Sandia National Laboratory (P. Hargis) (2)
Atmospheric Hydrolysis Chemistry

S. W. Sharpe
Wesleyan University (S. E. Novick) (1)
High-Resolution Spectroscopy of Hydrogen-Bonded Dimers

S. W. Sharpe and T. A. Blake
National Institute for Standards and Technology (G. T. Fraser and W. J. Lafferty) (1)
Rovibrational Spectral Analysis of Molecules and Molecular Clusters

R. G. Tonkyn
Delphi Energy and Engine Management Systems, Flint, Mich. (M. Hemingway) (1)
Vehicle Exhaust Treatment

L. S. Wang
Air Products and Chemicals, Inc., Allentown, Pa. (H. S. Chen) (1)
Theoretical Studies of Atomic Clusters

L. S. Wang
Sandia National Laboratory, Livermore, Cal. (C. M. Rohlfing) (1)
Theoretical Study of Small Aluminum Oxide Clusters

L. S. Wang
Washington State University (X. Li) (3)
Photoelectron Spectroscopy of Clusters

L. S. Wang
Washington State University (C.-F. Ding) (3)
Study of Solvated Clusters

L. S. Wang
Washington State University (X. B. Wang) (3)
Photoelectron Spectroscopy of Met-Cars

L. S. Wang
Washington State University (H. Wu) (3)
Electronic Structure of Transition-Metal Clusters

X. S. Xie
University of Sheffield, Engfland (N. Hunter) (1)
Single-Molecule Studies of Light-Harvesting Complexes and Single-Cell Studies of Biogenesis

X. S. Xie
Washington State University (L. Xun) (1)
Single-Molecule Studies of Biodegrading Enzymes

X. S. Xie
University of Kansas (C. Johnson) (3)
Single-Molecule Studies of Protein Conformational Motions

X. S. Xie
University of Kalsruhe (A. Zumbusch) (3)
Nonlinear Optical Imaging

Collaborations within PNNL

S. E. Barlow
EHSD Materials and Chemical Sciences Department, Nuclear Chemistry Section (A. J. Peurrung)
Stabilization of Nonneutral Plasmas

S. D. Colson
Staff throughout PNNL (L. G. Morgan, J. Janata, J. G. Hill, M. S. Hanson, and R. E. Gephart)
Hanford Tank Characterization and Safety Issue Resolution Project

S. D. Colson and R. S. McDowell
Energy Division, Engineering and Analytical Sciences Department, Sensors and Measurement Systems Section (J. S. Hartman); and EHSD Materials and Chemical Sciences Department, Atomic and Molecular Chemistry Section (M. L. Alexander)
Waste Tank Speciation Methods

J. P. Cowin
Atmospheric Sciences Department (R. S. Disselkamp, C. M. Berkowitz); Battelle Columbus (C. W. Spicer); Atmospheric and Environmental Research, Inc., Boston (Y. Zhang); Argonne National Laboratory (C. Bishop)
Effects of Heterogeneous Chemistry on NO_y in the Troposphere

J. P. Cowin and T. M. Orlando
Environment, Safety and Health Division, Radiological Control Group (S. C. Marschman)
Dehydration and Radiolysis of Spent Nuclear Fuels

W. P. Hess
EHSD Analytical Chemistry Resources, Advanced Organic & Analytical Methods (J. A. Campbell and S. C. Goheen)
Laser Ablation Characterization of Solids

W. P. Hess
EMSL Theory, Modeling, and Simulation (M. I. McCarthy, S. S. Xantheas, and J. D. Myers)
Studies of Laser/Solid Interactions

S. A. Joyce
EMSL Interfacial and Processing Science (B. C. Bunker)
Physics and Chemistry of Ceramic Surfaces

S. A. Joyce
EMSL Interfacial and Processing Science (M. A. Henderson); and EHSD Earth Systems Sciences Department, Thermodynamic and Molecular Geochemistry Group (J. R. Rustad)
Surface Chemistry of Iron Oxides

S. A. Joyce
EMSL Interfacial and Processing Science (S. A. Chambers)
Contaminant Interactions with Iron and Manganese Oxides

B. D. Kay
EMSL Interfacial and Processing Science (B. C. Bunker)
Physics and Chemistry of Ceramic Surfaces

T. M. Orlando
EHSD Materials and Chemical Sciences Department, Atomic and Molecular Chemistry Section (D. M. Camaioni)
Tank Waste Chemistry

T. M. Orlando
Environmental Technology Division, Process Technology Department, Electrical and Chemical Processes Group (W. O. Heath)
Low-Temperature Plasma Destruction Techniques

T. M. Orlando
Environmental and Health Sciences Division, Materials Group (M. L. Balmer)
Plasma-Activated Surface Catalysis

D. Ray
EMSL Theory, Modeling, and Simulation (D. F. Feller)
Gas-Phase Cation–Ether Complexes

D. Ray
EMSL Theory, Modeling, and Simulation (B. C. Garrett, G. K. Schenter) and Interfacial and Processing Science (J. L. Daschbach)
Transport Across Liquid Interfaces

S. W. Sharpe
National Security Division (R. G. Clemmer and S. W. Martin)
Standoff Infrared Sensors for Detection of Clandestine Methamphetamine Production

S. W. Sharpe
Energy Division, Engineering and Analytical Sciences Department, Sensors and Measurement Systems Section (J. S. Hartman) (1)
Development of Infrared Sniffer System

S. W. Sharpe
Energy Division, Engineering and Analytical Sciences Department, Sensors and Measurement Systems Section (J. W. Griffin)
Infrared Analysis in Head-Space Sampling for Paper and Pulp Digesters

S. W. Sharpe
Energy Division, Engineering and Analytical Sciences Department, Sensors and Measurement Systems Section (J. S. Hartman and M. A. Khaleel)
Sensors and Modeling for Auto Glass Production

S. W. Sharpe
Energy Division, Engineering and Analytical Sciences Department, Sensors and Measurement Systems Group (J. F. Kelly)
Spectroscopic Techniques for Atmospheric Monitoring

R. G. Tonkyn
Environmental Technology Division, Process Technology Department (W. O. Heath)
Vehicle Exhaust Treatment

L. S. Wang and S. D. Colson
EMSL Theory, Modeling, and Simulation (J. B. Nicholas)
Cluster Model Studies of Environmentally-Important Oxide Clusters

X. S. Xie
Atmospheric Sciences Department (R. X. Bian)
Near-Field Optical Tweezers Manipulation of Enzymatic Reactions on Biological Membranes.

Acronyms and Abbreviations

AES	Auger electron spectrometer
APC	allophycocyanin
ARM	Atmospheric Radiation Measurement Program
ASMS	American Society for Mass Spectrometry
ASW	amorphous solid water
AVS	American Vacuum Society
AWU	Associated Western Universities
BDE	bond dissociation energy
BES	DOE Office of Basic Energy Sciences
BET	Brunauer-Emmett-Teller
BSK	Beam Surface Kinetics instrument
CALIOPE	Chemical Analysis by Laser Interrogation of Proliferant Effluents
COLA	Conference on Laser Ablation
CRADA	Cooperative Research and Development Agreement
CS&D	Chemical Structure and Dynamics
DEA	dissociative electron attachment
DIET	Desorption Induced by Electronic Transition
DMSO	dimethyl sulfoxide
DNA	deoxyribonucleic acid
DOE	U. S. Department of Energy
EA	electron affinity
EDS	Environmental Dynamics and Simulation Group.
EDTA	ethylenediaminetetraacetic acid
EHSD	Environmental and Health Sciences Division
EMSL	William R. Wiley Environmental Molecular Sciences Laboratory
EMSP	DOE Environmental Management Science Program
EPR	electron paramagnetic resonance
ESD	electron-stimulated desorption
ESDIAD	electron-stimulated desorption ion angular distributions
ETH	Swiss Federal Institute of Technology
FAD	flavin adenine dinucleotide
FASE	FasCode for the Environment
FDTD	finite difference time domain
FEL	free-electron laser
FM	frequency modulated
FROG	frequency-resolved optical gating
FT	Fourier transform
FTIR	Fourier-transform infrared
FTIRS	Fourier-transform infrared spectrometer/spectroscopy
FY	fiscal year
HITRAN	Air Force molecular transition database
HOMO	highest occupied molecular orbital
HWHH	half width at half height
ICOPS	International Conference on Plasma Science
ICR	ion cyclotron resonance
ICS	Instrumentation for Clusters and Surfaces
IEEE	Institute of Electrical and Electronics Engineers
IPS	Interfacial and Processing Science Group
IR	infrared
IUPAC	International Union of Pure and Applied Chemistry
JILA	Joint Institute for Laboratory Astrophysics, Boulder
KE	kinetic energy
LAMS	laser ablation mass spectrometry
LBLRTM	line-by-line radiative transfer model
LDRD	Laboratory Directed Research and Development
LDS	liquid droplet source
LEED	low-energy electron diffraction
LEET	low-energy electron transmission
LSL	laser-stimulated luminescence
LUMO	lowest unoccupied molecular orbital
MALDI	matrix-assisted laser desorption–ionization
MBE	molecular beam epitaxy
MD	molecular dynamics
ML	monolayer
MMP	multiple multipole
MS	mass spectrometry
NASA	National Aeronautics and Space Administration
NMR	nuclear magnetic resonance
NN	DOE Office of Nonproliferation and National Security
NRC	National Research Council
NSF	National Science Foundation
ODMR	optically detected magnetic resonance
PASS	PNNL Affiliate Staff Scientist
PED	photoelectron diffraction
PES	photoelectron spectroscopy/spectrometer
PES	potential energy surface
PMMA	polymethyl methacrylate
PNNL	Pacific Northwest National Laboratory
PSD	photon-stimulated desorption
PVC	polyvinyl chloride
QMS	quadrupole mass spectrometer
RCS	rotational coherence spectroscopy

REELS	reflection electron energy-loss spectroscopy
REMPI	resonance-enhanced multiphoton ionization
RH	relative humidity
SABIT	Special American Business Internship Training Program
SAE	Society of Automotive Engineers
SERDP	Strategic Environmental Research and Development Program
SHG	second harmonic generation
SIMS	secondary-ion mass spectrometer/spectrometry
SPIE	Society of Photo-Optical and Instrumentation Engineers
STM	scanning tunneling microscope/microscopy
SUNY	State University of New York
TOF	time-of-flight
TPD	temperature-programmed desorption
UCSD	University of California at San Diego
UHV	ultra high vacuum
USCAR	U.S. Council for Automotive Research
UV	ultraviolet
VFT	Vogel-Fulcher-Tammann
VNIPIET	Russian Research Institute of Complex Power Technology
VUV	vacuum ultraviolet
WSU	Washington State University
XPS	X-ray photoelectron spectrometer
YAG	yttrium aluminum garnet
YSZ	yttria-stabilized zirconia

Where CS&D Fits in PNNL

Pacific Northwest National Laboratory (W. J. Madia, *Director*)
- Energy Division (G. L. Work, *Associate Laboratory Director*)
- **Environmental and Health Sciences Division** (G. M. Stokes, *Associate Laboratory Director*)
  - Analytical Chemistry Resources (D. W. Koppenaal)
  - Atmospheric Sciences and Global Change Resources (W. T. Pennell)
  - Biogeochemistry Resources (H. Bolton Jr.)
  - Materials Resources (M. L. Thompson)
  - Molecular Biosciences Resources (J. D. Saffer)
  - Statistics Resources (B. A. Pulsipher)
  - **William R. Wiley Environmental Molecular Sciences Laboratory (EMSL)** (T. R. Fryberger, *Interim Director*)
    - **Chemical Structure and Dynamics (CS&D)** (S. D. Colson)
    - Interfacial and Processing Science (IPS) (W. L. Kuhn, *acting*)
    - Macromolecular Structure and Dynamics (MS&D) (P. D. Ellis)
    - Theory, Modeling, and Simulation (TM&S) (D. A. Dixon)
    - Environmental Dynamics and Simulation (ED&S) (J. M. Zachara)
    - Computing and Information Sciences (C&IS) (R. A. Bair)
- Environmental Technology Division (B. D. Shipp, *Associate Laboratory Director*)
- National Security Division (M. Kluse, *Associate Laboratory Director*)

Report Number (14) PNNL--11863

Publ. Date (11) 199803

Sponsor Code (18) DOE/ER, XF

UC Category (19) UC-400, DOE/ER